(2)

ESL-TR-87-72

DEVELOPMENT OF VAPOR DISPERSION MODELS FOR NONNEUTRALLY BUOYANT GAS MIXTURES-ANALYSIS OF TFI/NH_3 TEST DATA

T.O. SPICER, J. HAVENS

UNIVERSITY OF ARKANSAS
CHEMICAL ENGINEERING DEPARTMENT
FAYETTEVILLE AR 72701

OCTOBER 1988

FINAL REPORT

MARCH 1986 - MARCH 1987

AFESC

ENGINEERING & SERVICES LABORATORY
AIR FORCE ENGINEERING & SERVICES CENTER
TYNDALL AIR FORCE BASE, FLORIDA 32403

NOTICE

PLEASE DO NOT REQUEST COPIES OF THIS REPORT FROM HQ AFESC/RD (ENGINEERING AND SERVICES LABORATORY). ADDITIONAL COPIES MAY BE PURCHASED FROM:

NATIONAL TECHNICAL INFORMATION SERVICE
5285 PORT ROYAL ROAD
SPRINGFIELD, VIRGINIA 22161

FEDERAL GOVERNMENT AGENCIES AND THEIR CONTRACTORS REGISTERED WITH DEFENSE TECHNICAL INFORMATION CENTER SHOULD DIRECT REQUESTS FOR COPIES OF THIS REPORT TO:

DEFENSE TECHNICAL INFORMATION CENTER
CAMERON STATION
ALEXANDRIA, VIRGINIA 22314

UNCLASSIFIED
SECURITY CLASSIFICATION OF THIS PAGE

REPORT DOCUMENTATION PAGE

1a. REPORT SECURITY CLASSIFICATION Unclassified	1b. RESTRICTIVE MARKINGS N/A
2a. SECURITY CLASSIFICATION AUTHORITY N/A	3. DISTRIBUTION/AVAILABILITY OF REPORT Approved for public release Distribution unlimited
2b. DECLASSIFICATION/DOWNGRADING SCHEDULE N/A	
4. PERFORMING ORGANIZATION REPORT NUMBER(S) N/A	5. MONITORING ORGANIZATION REPORT NUMBER(S) ESL-TR-87-72
6a. NAME OF PERFORMING ORGANIZATION University of Arkansas Chemical Engineering Dept. 6b. OFFICE SYMBOL (If applicable) N/A	7a. NAME OF MONITORING ORGANIZATION U.S. Air Force Engineering and Services Center
6c. ADDRESS (City, State, and ZIP Code) Fayetteville AR 72701	7b. ADDRESS (City, State, and ZIP Code) Air Force Engineering and Services Center/RDVS Tyndall AFB FL 32403-6001
8a. NAME OF FUNDING/SPONSORING ORGANIZATION U.S. Air Force 8b. OFFICE SYMBOL (If applicable) N/A	9. PROCUREMENT INSTRUMENT IDENTIFICATION NUMBER DTCG23-80-C-20029
8c. ADDRESS (City, State, and ZIP Code) U.S. Coast Guard Headquarters 2100 2d Street SW Washington DC 20593	10. SOURCE OF FUNDING NUMBERS PROGRAM ELEMENT NO.: 63723F PROJECT NO.: 2103 TASK NO.: 50 WORK UNIT ACCESSION NO.: 04

11. TITLE (Include Security Classification)
DEVELOPMENT OF VAPOR DISPERSION MODELS FOR NONNEUTRALLY BUOYANT GAS MIXTURES--ANALYSIS OF TFI/NH_3 TEST DATA

12. PERSONAL AUTHOR(S)
Thomas O. Spicer; Jerry Havens

13a. TYPE OF REPORT	13b. TIME COVERED	14. DATE OF REPORT (Year, Month, Day)	15. PAGE COUNT
Final	FROM Mar 86 TO Mar 87	October 1988	138

16. SUPPLEMENTARY NOTATION
Availability of this report is specified on reverse of front cover.

17. COSATI CODES		
FIELD	GROUP	SUB-GROUP

18. SUBJECT TERMS (Continue on reverse if necessary and identify by block number)
Dense Gas; DEGADIS; Heavier-than-Air Gas; Model Evaluation; Dispersion Modeling; Release Richardson Number; Jet Release; Ammonia Aerosol Release

19. ABSTRACT (Continue on reverse if necessary and identify by block number)

Field-scale releases of pressurized anhydrous ammonia were performed by the Lawrence Livermore National Laboratories in 1983 for the U.S. Coast Guard, the Fertilizer Institute, and Environment Canada. Release rates for the four experiments ranged between 80 and 130 kilograms per second. The pressurized liquid ammonia jet formed a denser-than-air aerosol cloud. A method of determining the relative importance of jet and nonjet dispersion processes is discussed.

The data from these experiments were analyzed to determine the mass flux of ammonia and the lateral and vertical concentration profile parameters for the cloud (σ_y and σ_z for the Gaussian plume model and S_y and S_z for DEGADIS) at 800 meters downwind. These observed values of maximum concentration and concentration profile parameters were compared with

20. DISTRIBUTION/AVAILABILITY OF ABSTRACT ☒ UNCLASSIFIED/UNLIMITED ☒ SAME AS RPT ☐ DTIC USERS	21. ABSTRACT SECURITY CLASSIFICATION UNCLASSIFIED
22a. NAME OF RESPONSIBLE INDIVIDUAL Capt. Larry Key	22b. TELEPHONE (Include Area Code) 904 233-4234 22c. OFFICE SYMBOL HQ AFESC/RDVS

DD FORM 1473, 84 MAR 83 APR edition may be used until exhausted. All other editions are obsolete.

SECURITY CLASSIFICATION OF THIS PAGE

19. (Concluded)

DEGADIS and Gaussian plume model predictions. (DEGADIS is an atmospheric dispersion model designed to account for the influences of denser-than-air gases.) In addition, analysis of the experimental data indicated heat transfer to the aerosol cloud was insignificant although the cloud temperature was as low as -60 centigrade.

Several simplifying assumptions were tried when determining the aerosol density as a function of cloud concentration including: (1) a pseudobinary mixture of ammonia and air/water which ignored water phase changes; (2) ideal ammonia/water liquid solution behavior; and (3) assumption of a linear relationship between ammonia concentration and mixture density. Based on calculations with DEGADIS, the assumption of a pseudobinary mixture of ammonia and air/water proved to be inadequate. The DEGADIS-predicted distance to given concentration levels were calculated assuming ideal solutions in the liquid phase for the ammonia/water system; these computations reproduced the DEGADIS-predicted distances using the unsimplified thermodynamics treatment. Finally, the DEGADIS-predicted distance to given concentration levels were calculated assuming a linear relationship between mixture density and contaminant concentration; these computations reproduced the DEGADIS-predicted distances using the unsimplified thermodynamics treatment to within about 20 percent. In the absence of heat transfer, this last assumption may be useful as a screening technique for hazard assessment.

PREFACE

This report was prepared by the Chemical Engineering Department, University of Arkansas, Fayetteville, Arkansas 72701, under Contract Number DTCG23-80-C-20029, for the U.S. Coast Guard Headquarters, Washington DC 20593, and for the Air Force Engineering and Services Center, Air Force Engineering and Services Laboratory (AFESC/RDVS), Tyndall Air Force Base, Florida 32403-6001.

This report summarizes the work done between 31 March 1986 and 15 March 1987. HQ AFESC/RDVS program manager was Captain Lawrence E. Key, and the USCG HQ program manager was Lieutenant Commander Peter Tebeau.

This report has been reviewed by the Public Affairs Office (PA) and is releasable to the National Technical Information Service (NTIS). At NTIS, it will be available to the general public, including foreign nationals.

This report has been reviewed and is approved for public release.

MICHAEL T. MOSS, Capt, USAF
Chief, Modeling Systems

THOMAS J. WALKER, Lt Col, USAF, BSC
Chief, Environics Division

KENNETH T. DENBLEYKER, Maj, USAF
Chief, Environmental Sciences Branch

LAWRENCE D. HOKANSON, Colonel, USAF
Director, Engineering and Services Laboratory

(The reverse of this page is blank)

TABLE OF CONTENTS

TABLE OF CONTENTS
(Concluded)

LIST OF FIGURES

LIST OF TABLES

LIST OF TABLES
(Concluded)

LIST OF SYMBOLS

a_v	dimensionless empirical constant, 1.3, in Equation (B-5)
B_{EFF}	effective width of gas plume (m)
$2B'$	local half width of source seen by observer i (m)
b	half width of horizontally homogeneous central section of gas plume (m)
b_v	dimensionless empirical constant, 1.2, in Equation (B-21)
C_E	dimensionless constant, 1.15, in density intrusion (spreading) relation
C_p	heat capacity (J/kg K)
C_{p_a}	heat capacity of air (J/kg K)
C_{p_c}	heat capacity of contaminant (J/kg K)
C_{p_w}	heat capacity of water (liquid phase) (J/kg K)
c	concentration (kg/m^3)
c_c	centerline, ground-level concentration (kg/m^3)
$c_{c,L}$	vertically averaged layer concentration (kg/m^3)
c_f	friction coefficient
c'_c	centerline, ground-level concentration corrected for x-direction dispersion (kg/m^3)
$c_{max}(x;t)$	maximum concentration associated with averaging time t (kg/m^3)
D	diameter of the area release (m)
D_h	added enthalpy (J/kg)
$\mathcal{D}$	diffusivity (m^2/s)
d_v	dimensionless empirical constant, 0.64, in Equation (B-5)
E	plume strength (kg/s)
$E(t)$	source rate (kg/s)
e_v	dimensionless empirical constant, 20., in Equation (B-8)

LIST OF SYMBOLS
(Continued)

F	overall mass transfer coefficient (kg/m^2 s)
F_f	mass transfer coefficient due to forced convection (kg/m^2 s)
F_n	mass transfer coefficient due to natural convection (kg/m^2 s)
Gr	Grashoff number
g	acceleration due to gravity (m/s^2)
H	vertical length scale of the release (m)
H_a	ambient absolute humidity (kg water/kg dry air)
H_{EFF}	effective cloud depth (m)
H_h	height of head in density-driven flow (m)
H_L	gas layer depth (m)
H_t	height of tail in density-driven flow (m)
H_1	average depth of gravity current head (m)
H_4	depth of inward internal flow in a gravity current head (m)
h	enthalpy of source blanket (J/kg)
h_a	enthalpy of ambient humid air (J/kg)
h_E	enthalpy associated with primary source mass rate (J/kg)
h_f	heat transfer coefficient due to forced convection (J/m^2 s K)
h_L	enthalpy of vertically averaged layer (J/kg)
h_n	heat transfer coefficient due to natural convection (J/m^2 s K)
h_0	overall heat transfer coefficient (J/m^2 s K)
h_w	enthalpy associated with mass flux of water from surface (J/kg)
K_0	constant in Equation (B-96) ($m^{1-\gamma_1}$)

LIST OF SYMBOLS
(Continued)

K_y	horizontal turbulent diffusivity (m^2/s)
K_z	vertical turbulent diffusivity (m^2/s)
k	von Karman's constant, 0.35
k_1	dimensionless constant in Equation (B-6)
k_2	dimensionless constant in Equation (B-71)
L	source length (m)
L_B	buoyancy length scale (m)
M	total cloud mass (kg)
M_a	rate of air moving downwind in the contaminant/air mixture (kg/s) or total mass of air in the cloud (kg)
M_c	total mass of contaminant in the cloud (kg)
M_i	initial cloud mass (kg)
MW	molecular weight
$\dot{M}_a$	mass rate of air entrainment into the cloud (kg/s)
$\dot{M}_{w,s}$	mass rate of water transfer to the cloud from the water surface under the source (kg/s)
$\dot{m}$	source mass rate (kg/s)
N	number of observers
Nu	Nusselt number
P	cloud momentum (kg m/s)
P_h	momentum of head in density-driven flow (kg m/s)
P_t	momentum of tail in density-driven flow (kg m/s)
P_v	virtual momentum due to acceleration reaction (kg m/s)
Pr	Prandtl number
p	atmospheric pressure (atm) or power in power law dependence of c_{max} with averaging time

LIST OF SYMBOLS
(Continued)

$p_{w,c}$	partial pressure of water in the cloud (atm)
$p^*_{w,s}$	vapor pressure of water at the surface temperature (atm)
Q	volumetric release rate (m^3/s)
Q_E	source mass flux (kg/m^2 s)
Q_e	volumetric entrainment flux (m/s)
Q	flux of ambient fluid into front of gravity current head (m/s)
$\dot{Q}_s$	rate of heat transfer from the surface (J/s)
Q_*	atmospheric takeup flux (kg/m^2 s)
Q_{*max}	maximum atmospheric takeup flux of contaminant (kg/m^2 s)
q_s	surface heat flux (J/m^2 s)
R	jet radius (m) or gas source cloud radius (m)
R_h	inner radius of head in density-drive flow (m)
R_m	value of R when ($\pi R^2 Q_*$) is a maximum (m)
R_{max}	maximum radius of the cloud (m)
R_p	ground-level source radius (m)
Ri_c	continuous release Richardson number
Ri_f	Richardson number associated with the front velocity, Equation (B-11)
Ri_T	Richardson number associated with temperature differences, Equation (B-88)
Ri'_*	Richardson number associated with density differences corrected for convective scale velocity
Ri_*	Richardson number associated with density differences, Equation (B-78)
Sc	Schmidt number
Sh	Sherwood number
St_H	Stanton number for heat transfer

St_M	Stanton number for mass transfer
S_y	horizontal concentration scaling parameter (m)
S_z	vertical concentration scaling parameter (m)
S_{z0}	S_z at the downwind edge of the source ($x = L/2$) (m)
S_{z0_m}	value of S_{z0} when ($\pi R^2 Q_*$) is a maximum (m)
T	temperature associated with source blanket enthalpy (K)
T_{AM}	adiabatic mixing temperature for a given concentration level (°C)
$T_{c,L}$	temperature associated with layer-averaged enthalpy (K)
T_{OBS}	observed temperature (°C)
T_s	surface temperature (K)
t	time (s)
t_{av}	averaging time (s)
t_s	specified time (s)
t_{dn_i}	time when observer i encounters downwind edge (s)
t_{up_i}	time when observer i encounters upwind edge (s)
u	wind velocity at about 10 m (m/s) or characteristic wind tunnel velocity (m/s)
u_a	ambient average velocity (m/s)
u_e	frontal entrainment velocity (m/s)
u_{EFF}	effective cloud advection velocity (m/s)
u_f	cloud front velocity (m/s)
u_i	velocity of observer i (m/s)
u_L	gas mean advection speed (m/s)
u_x	downwind velocity (m/s)
u_0	wind velocity measured at $z = z_0$ (m/s)

u_3	internal flow out of gravity current head (m/s)
u_4	internal flow into gravity current head (m/s)
u_*	friction velocity in the absence of any contaminant (m/s)
$\bar{u}$	characteristic average velocity (m/s)
V	velocity of the material leaving the spill pipe (m/s)
V_H	heat transfer velocity (0.0125 m/s) in Equation (B-38) (m/s)
V_j	jet velocity (m/s)
w_a	mass fraction of air
w_c	mass fraction of contaminant
w_e	vertical entrainment velocity associated with H_L (m/s)
w'_e	entrainment velocity associated with H_{EFF} (m/s)
w_*	convective scale velocity (m/s)
$x_i(t)$	x position of observer i at time t (m)
x_{pi}	position of puff center due to observer i (m)
x_t	downwind distance where gravity spreading terminates (m)
x_v	virtual point source distance (m)
x_{dn_i}	x position of downwind edge of source for observer i
x_{up_i}	x position of upwind edge of source for observer i
x,y,z	Cartesian coordinates (m)
x_0	downwind edge of the gas source (m)
y_v	contaminant mole fraction
z_R	surface roughness (m)
z_0	reference height in wind velocity profile (m)

Greek Letters

α	constant in power law wind profile

LIST OF SYMBOLS
(Continued)

β	power in power law parameterization of σ_y
Γ	gamma function
γ	ratio of $(\rho - \rho_a)/c_c$
γ_1	constant in Equation (B-96)
Δ	ratio of $(\rho - \rho_a)/\rho$
ΔT	temperature driving force (K) $(T_s - T_{c,L})$ or $(T_s - T)$
Δ'	ratio of $(\rho - \rho_a)/\rho_a$
δ	constant power law parameterization of $\sigma_y(m^{1-\beta})$
δ_L	constant (2.15)
δ_v	constant (0.20) in Equation (B-25)
ϵ	frontal entrainment coefficient (0.59) in Equation (B-33)
ζ	collection of terms defined by Equation (B-62) $(m^{-1/(1+\alpha)})$
λ	Monin-Obukhov length (m)
μ	viscosity (kg/m s)
ρ	density of gas-air mixture (kg/m^3)
ρ_a	ambient density (kg/m^3)
ρ_c	cloud density (kg/m^3)
ρ_E	initial contaminant density (kg/m^3)
ρ_L	averaged gas layer density (kg/m^3)
ρ_0	density of contaminant's saturated vapor at initial temperature (kg/m^3)
σ_x	Pasquill-Gifford x-direction dispersion coefficient (m)
σ_y	Pasquill-Gifford y-direction dispersion coefficient (m)
$\sigma_y(x;t)$	lateral dispersion coefficient based on averaging time t (m)

LIST OF SYMBOLS
(Concluded)

σ_z	Pasquill-Gifford z-direction dispersion coefficient (m)
ϕ	function describing influence of stable density stratification on vertical diffusion, Equation (B-76)
$\phi(Ri_*)$	air-entrainment function from DEGADIS
$\hat{\phi}$	integrated source entrainment function
ψ	logarithmic velocity profile correction function

(The reverse of this page is blank.)

SECTION I
INTRODUCTION

A. OBJECTIVE

The objective of this project was to calculate the release Richardson number for four field-scale releases of liquid anhydrous ammonia to determine the importance of cloud density in the atmospheric dispersion of toxic clouds resulting from these test spills. After calculating the release Richardson number, the DEGADIS model was used to simulate the atmospheric dispersion of the toxic clouds. The model results were compared to field measurements to determine the suitability of DEGADIS to simulate these types of releases.

B. BACKGROUND

The U. S. Air Force (USAF) has been taking steps to improve the safety procedures available during operations involving hazardous chemicals and fuels. In support of this effort, the Air Force Engineering and Services Laboratory (AFESC/RDV) has sponsored research on the dispersion of denser-than-air gas clouds resulting from accidental releases of toxic chemicals. This study examines four field-scale releases of liquid anhydrous ammonia from the "Desert Tortoise" (DT) series (Reference 1).

Denser-than-air gases are of particular interest because current (passive) dispersion models used to predict concentrations (and safety limits) may be inappropriate. Models currently used for safety assessment assume that the dispersing contaminant does not affect the atmospheric flow field. This may not be true for denser-than-air gases; dispersion rates may be considerably reduced for denser-than-air gases due to the stable stratification which may be present. The release Richardson number has been used successfully as a

criterion for determining whether a particular release of material can be adequately modeled using passive dispersion techniques or whether denser-than-air gas effects must be considered. (The release Richardson number is a dimensionless number relating the effects of the type of material released, the ambient wind profile, and characteristics of the release itself.) This study examines the applicability of the release Richardson number to the DT tests. The liquid anhydrous ammonia was released as a pressurized liquid jet in the DT tests; this study also attempts to quantify the effect of the jet behavior on the relative importance of the denser-than-air gas effects present in the releases.

C. SCOPE/APPROACH

Because the liquid anhydrous ammonia was released as a pressurized jet, the ammonia formed a cold ammonia aerosol as it moved downwind. Upon mixing it with the ambient air, some of the ambient humidity condensed to form a nonideal liquid phase composed of ammonia and water. This study examines the influence on the dispersion processes by the aerosol formation, the nonideal liquid solution behavior of the ammonia and water, and the heat transfer to the cold aerosol; potential simplifications are discussed.

Finally, this study examines the consistency of model predictions using the Gaussian plume model and DEGADIS (a computer model designed to account for the influences of denser-than-air gases) with the results of the DT tests. The importance of such factors as the aerosol behavior, heat transfer to the ammonia cloud, and initial jet behavior on the model predictions are discussed. The sensitivity of DEGADIS to uncertainty in input parameters not routinely available at operational USAF sites is also assessed.

SECTION II
METHODOLOGY

Four field-scale releases of liquid anhydrous ammonia (the "Desert Tortoise" (DT) series) were performed in 1983 by Lawrence Livermore National Laboratories (LLNL) for the U.S. Coast Guard, the Fertilizer Institute, and Environment Canada (Reference 1). The releases were conducted on Frenchman Flat, a dry lake bed approximately 6 kilometers long and 3 kilometers wide, at the Nevada Test Site. Although the area is normally very dry, unusually heavy rains had occurred before the test period. Water was standing on the test site during the first three tests, but the lake bed was dry during Test 4. A summary of the release conditions for the tests is presented in Table 1. A surface roughness of 0.003 meters was used for the site (Reference 1). Pressurized storage resulted in rapid expansion of the ammonia as it exited through an orifice at the end of the spill pipe. This section summarizes important aspects of this type of release specifically dealing with the initial properties of the ammonia aerosol which was formed. Also, the dispersion processes downwind of the source are discussed. The succeeding sections address the analysis of the DT test data to yield information suitable for model

TABLE 1. SUMMARY OF RELEASE CONDITIONS FOR THE DESERT TORTOISE SERIES

	DT1	DT2	DT3	DT4
Spill rate (kg/s)	81.	117.	133.	108.
Windspeed at 5.83 m (m/s)	8.33	6.01	8.16	4.99
Friction velocity (m/s)	0.442	0.339	0.448	0.286
Ambient temperature (°C)	28.7	30.9	33.8	33.2
Ambient pressure (bar)	0.909	0.910	0.907	0.903
Relative humidity (%)	13.2	17.5	14.8	21.3
Monin-Obukhov length (m)	92.7	94.7	570.7	45.2
Pasquill stability class	D	D	D	E

comparison, a method of determining the relative importance of the various flow and dispersion processes present, and the comparison of the results from the DT test data with a Gaussian plume model and DEGADIS.

A. AMMONIA AEROSOL FORMATION AND SUBSEQUENT MIXING WITH AIR

The release of anhydrous ammonia from storage at elevated pressure and ambient temperature results in the formation of a denser-than-air ammonia aerosol if the release is from the liquid phase; such releases are typically violent jets. The DT release conditions represent this type of release. (A general discussion of the behavior of the early phases of ammonia releases is presented by Wheatley (References 2 and 3); for this report, only the conditions of the DT releases are discussed.) The behavior of the flashing liquid jet can be described (approximately) as either isenthalpic or isentropic. (Isenthalpic behavior implies that all of the energy of the liquid jet goes into the energy of the resulting aerosol, ignoring any kinetic energy; isentropic behavior implies that the flow is adiabatic, frictionless, and ignores other irreversibilities such as shocks.) For storage temperatures below about 50°C, the mass fraction of liquid ammonia in the resulting aerosol is approximately the same regardless of whether the flow is assumed to be isenthalpic or isentropic. Assuming isenthalpic flow, the aerosol was estimated to have (initially) a temperature of -36°C with about 81 percent (by mass) of ammonia in the liquid phase. For hazard assessment purposes, the distance required for the flashing liquid jet to regain thermal equilibrium and form the aerosol is insignificant (on the order of 1 meter).

Since dispersion depends on the density of the air/ammonia mixture, it is necessary to estimate the mixture density as a function of ammonia mole fraction. Some of the ambient humidity will condense when air is entrained into the aerosol. Since ammonia and water form nonideal solutions in the liquid phase, consideration of the nonideal behavior of the liquid phase may be important under some circumstances. For the ammonia/water system, Wheatley (References 4 and 5) has investigated these interactions and incorporated them into a computer code, TRAUMA, which was used to estimate the ammonia/air/water mixture density as a function of ammonia concentration for the DT releases. Figure 1 shows the mixture density and mixture

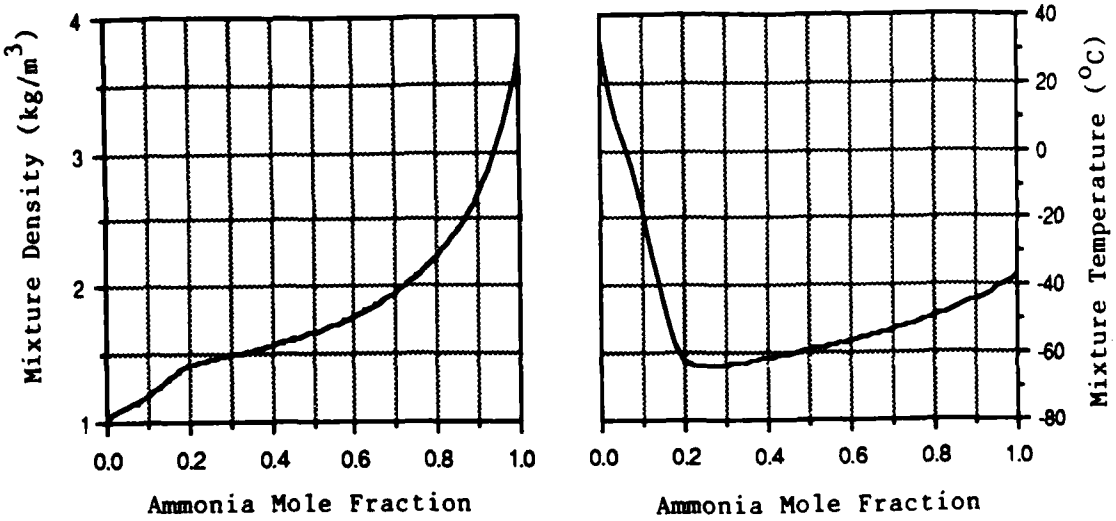

Figure 1. Ammonia/Air/Water Mixture Temperature and Density as Functions of Ammonia Mole Fraction for DT4 Conditions Calculated using TRAUMA.

temperature as functions of ammonia mole fraction for DT4 which is typical of all of the releases calculated using TRAUMA version 1.0. (The equilibrium mixture temperature decreases with the addition of air.)

Three simplifying assumptions can be made to describe the ammonia/air/water mixture density: (1) a pseudobinary mixture of ammonia and air/water; (2) ideal ammonia/water liquid solution behavior; and (3) assumption of a linear relationship between ammonia concentration (in kg/m^3) and mixture density. To determine whether these assumptions are appropriate, the effect on DEGADIS predictions of the DT4 release conditions was examined. TRAUMA was used to determine the mixture density of a pseudobinary mixture of air/water and ammonia; water phase changes were ignored, greatly simplifying the calculation procedure required (since the partial pressure of ammonia is then equal to its vapor pressure). Ammonia phase changes were taken into account. (For details of the capabilities of TRAUMA, see Wheatley (Reference 6).) Comparing simulations made with this simplified density specification and the density specification of Figure 1, substantial differences were noted in the DEGADIS dispersion calculation for

ammonia concentrations below on the order of 1 percent for the release conditions of DT4. TRAUMA was also used to determine the ammonia/air/water mixture density assuming ideal liquid solution behavior; this assumption also simplifies the calculation procedure required (since the partial pressure of ammonia is then equal to its vapor pressure times its liquid phase mole fraction). Heat of mixing effects between the ammonia and water in the liquid phase were ignored. The assumption of ideal liquid-phase solution behavior adequately described the mixture density so that no difference was noted in the DEGADIS dispersion calculations based on the release conditions of DT4 (for relative humidities ranging from 0 to 100 percent). Finally, a linear relationship between ammonia concentration (in kg/m^3) and mixture density was used directly in DEGADIS; the endpoints were represented by the released ammonia aerosol and the ambient air. Upon comparison, the DEGADIS-predicted distances using this simplified scheme were within about $\pm$20 percent of the DEGADIS-predicted distance to a given concentration level using the density specification of Figure 1; this agreement was checked to about 100 ppm for the conditions of DT4.

B. JET AND NONJET FLOW PHASES

The initial growth of a turbulent jet is characterized by large-scale turbulent motions which entrap air in the jet flow (Reference 7). This initial near-jet region was estimated to persist on the order of 10 meters for the DT series. As a result of air entrainment and expansion of the jet, the momentum of the jet decreases, and the jet is well described by self-similar velocity and concentration profiles in the absence of interaction with the ground (Reference 8). The jet velocity decreases (due to air entrainment) and approaches the ambient wind velocity. For the DT series, the ammonia was released 0.79 meters above ground level, and the jet struck the ground within one meter or so. Therefore, the DT releases would be expected to behave like a ground-level (jet) release due to the interaction with the solid boundary. In contrast to nonaerosol jets, the aerosol jets in the DT releases may be subject to rainout (deposition of some of the liquid phase on the ground). Wheatley (Reference 5) has examined the possibilities of rainout for ammonia aerosols and found that rainout is not expected for pressurized releases in the absence of solid boundary interactions. For the DT series, Goldwire et al. (Reference 1)

reported that some of the ammonia was deposited on the ground and formed a liquid pool, probably because the release was near ground level.

After the contaminant/air mixture jet velocity has diminished, nonjet flow phases become important including: (1) negative buoyancy-dominated flow; (2) stably stratified shear flow; and (3) passive dispersion due to atmospheric flow. The theory underlying the dispersion prediction of trace contaminants (passive dispersion) generally assumes that the dispersion is the result of atmospheric turbulence. Although characterization of the atmospheric flow suffers from the limits of understanding of turbulent fluid motion, there is a fairly well-developed theoretical basis for prediction of passive atmospheric dispersion, along with an extensive experimental data base derived from atmospheric flow measurements (Reference 9). In contrast to passive dispersion, the release of large quantities of a denser-than-air gas (DTAG) into the atmosphere can significantly alter the atmospheric flow in the vicinity of the release. For some releases, this negative buoyancy-dominated (gravity-driven) flow and the resulting interaction with the atmospheric flow can have an important effect on the distance needed to reduce the concentration to a given level. Between these two extremes, the stably stratified shear flow phase differs from neutrally buoyant flow and is characterized by the following: (1) a crosswind gravity-driven flow due to the negative buoyancy of the flow is present; (2) because of this gravity-driven spreading, these plumes tend to be wider and shallower than a neutrally buoyant plume under the same conditions; and (3) because of stable vertical density stratification, the vertical mixing rate is reduced. (A detailed discussion of each of these nonjet flow phases is found in Havens and Spicer (Reference 10); see Section III and Appendix A for a method to estimate the relative importance of the jet and nonjet flow phases.)

SECTION III

ANALYSIS OF DESERT TORTOISE DATA FOR MODEL COMPARISON

For the DT releases, two sensor arrays were used to measure the downwind ammonia concentrations. The mass flux array consisted of a row of seven gas sensor masts located 100 meters downwind of the release area. The primary gas concentration sensors in this array were Mine Safety Appliance (MSA) nondispersive IR gas sensors which were heated to vaporize the aerosol so that the total ammonia concentration could be determined. (The velocity of gas through the 100-meter array was to be measured with anemometers to determine the mass flux of gas through the array, but corrosion caused by the ammonia made these instruments unreliable.) At 800 meters downwind of the release area, the instrument array consisted of five sensor masts spaced 100 meters apart; each mast had three gas sensors and three thermocouples. The sensors were located at 1.0, 3.5, and 8.5 meter heights on each sensor mast. The primary gas sensors in this array were International Sensor Technology (IST) solid-state gas sensors. In addition to these sensor arrays, eight portable IST gas sensors were located at 1-meter elevations from 1.4 to 5.5 kilometers downwind.

To facilitate the comparison of model simulations and reported concentration and temperature measurements, the reported concentrations and temperatures along with reported wind trajectories and mass rates at 800 meters were analyzed to determine the best representation of steady-state concentrations and temperatures. (The reported wind trajectories did not correspond exactly with the plume centerline due to the momentum of the release.) The mass rate passing the 800-meter array was reported by LLNL on the basis of the observed concentration and temperature profiles at the 800-meter array and velocity profiles interpolated from other meteorological towers. The mass rate passing the 800-meter array for each of the tests during the time period when the concentration and temperature profiles were examined are summarized in Table 2. Most of the released mass is accounted for at the 800-meter array (67 percent to 89 percent) for all tests except DT3 (42 percent). Ignoring the uncertainty in the estimated ammonia mass rate at 800 meters, the unaccounted ammonia mass at the 800-meter array could have been deposited on the ground by rainout or could

have been absorbed by the water on the ground in DT1 - DT3. Tables 3-6 summarize the reported concentration and temperature for the time reflecting these (approximate) steady-state conditions.

TABLE 2. REPORTED AMMONIA MASS RATES AT 800-METER SENSOR ARRAY AT THE SPECIFIED TIMES

Release	Integrated Contaminant Mass Rate at 800 m (kg/s)*	Time from Start of Release (s)
DT1	66.5	~240.
DT2	104.6	~270.
DT3	56.0	~200.
DT4	72.1	~340 to 390

*from Reference 1.

TABLE 3. REPORTED CONCENTRATION AND TEMPERATURE FOR DT1 AT 800 METERS AND 240 SECONDS REFLECTING (APPROXIMATE) STEADY-STATE CONDITIONS

	Concentration (%) / Temperature (°C)				
Sensor Elevation (m)	Sensor Station G24	Sensor Station G23	Sensor Station G22	Sensor Station G21	Sensor Station G20
8.5	0.0/29.1	0.07/27.4	0.02/28.6	0.0/29.6	0.0/29.6
3.5	0.0/28.9	0.88/22.7	0.88/22.7	0.0/29.3	0.0/29.3
1.0	0.0/28.8	1.00/24.0	1.00/24.0	0.0/29.4	0.0/29.4

Note: The plume centerline was approximately midway between G22 and G23.

TABLE 4. REPORTED CONCENTRATION AND TEMPERATURE FOR DT2 AT 800 METERS AND 270 SECONDS REFLECTING (APPROXIMATE) STEADY-STATE CONDITIONS

Sensor Elevation (m)	Concentration (%) / Temperature (°C)				
	Sensor Station G24	Sensor Station G23	Sensor Station G22	Sensor Station G21	Sensor Station G20
8.5	0.0/30.3	0.14/28.0	0.23/26.7	0.0/30.4	0.0/30.4
3.5	0.0/30.3	1.08/25.7	1.70/21.7	0.91/23.3	0.0/30.7
1.0	0.0/30.0	1.67/25.0	1.86/22.5	1.71/22.2	0.0/30.7

Note: The plume centerline was approximately over G22.

TABLE 5. REPORTED CONCENTRATION AND TEMPERATURE FOR DT3 AT 800 METERS AND 200 SECONDS REFLECTING (APPROXIMATE) STEADY-STATE CONDITIONS

Sensor Elevation (m)	Concentration (%) / Temperature (°C)				
	Sensor Station G24	Sensor Station G23	Sensor Station G22	Sensor Station G21	Sensor Station G20
8.5	0.0/32.7	*	0.0/33.4	0.0/33.3	0.0/33.1
3.5	0.58/29.2	*	0.78/29.2	0.0/33.3	0.0/33.3
1.0	0.87/28.1	*	1.00/28.1	0.0/32.9	0.0/32.9

Note: The plume centerline was approximately over G23.

*G23 failed to record any data due to instrument failure.

TABLE 6. REPORTED CONCENTRATION AND TEMPERATURE FOR DT4 AT 800 METERS AND 350 SECONDS REFLECTING (APPROXIMATE) STEADY-STATE CONDITIONS

Sensor Elevation (m)	Concentration (%) / Temperature (°C)				
	Sensor Station G24	Sensor Station G23	Sensor Station G22	Sensor Station G21	Sensor Station G20
8.5	0.0/32.9	0.0/32.0	0.0/32.0	0.0/32.2	0.0/32.2
3.5	0.0/32.2	0.77/25.9	1.26/23.9	0.80/24.8	0.47/27.4
1.0	0.0/31.4	1.29/26.3	1.94/23.9	1.90/23.3	0.83/27.3

Note: The plume centerline was approximately midway between G21 and G22.

For model comparison purposes, the measured concentrations were fitted to two similarity profiles:

$$c = c_c \exp \left\{ - \frac{1}{2} \left(\frac{y}{\sigma_y} \right)^2 - \frac{1}{2} \left(\frac{z}{\sigma_z} \right)^2 \right\} \quad (1)$$

and

$$c = c_c \exp \left\{ - \left(\frac{y}{S_y} \right)^2 - \left(\frac{z}{S_z} \right)^{1+\alpha} \right\} \quad (2)$$

where c_c represents the maximum centerline contaminant concentration, z represents the height above ground, y represents the lateral distance from the centerline, σ_y and σ_z are Gaussian (Pasquill-Gifford) dispersion coefficients, S_y and S_z are distribution coefficients used in the DEGADIS model, and α is the power-law wind profile parameter. The concentration profiles of Equations (1) and (2) were integrated, along with a (typical) velocity profile of the form

$$u_x = u_0 \left(\frac{z}{z_0} \right)^{\alpha} \quad (3)$$

to give the mass rate passing a plane downwind:

$$\dot{m} = \int_{-\infty}^{\infty} \int_{0}^{\infty} cu_x dz dy \qquad (4)$$

Using Equation (4) and the reported mass rates passing the 800-meter array, σ_y, σ_z, S_y, and S_z were then determined by a weighted nonlinear least-squares technique from the reported concentrations and temperatures of Tables 3-6. The values of σ_y, σ_z, and c_c for Equation (1) and S_y, S_z, and c_c for Equation (2) are summarized in Tables 7 and 8, respectively. Notice that the maximum centerline concentration is different for the different profiles. Furthermore, notice that $\sigma_y \simeq S_y/\sqrt{2}$ and $\sigma_z \simeq S_z$ (to within about 10 percent).

TABLE 7. ESTIMATES OF σ_y AND σ_z FOR THE DESERT TORTOISE SERIES AT 800 METERS

	σ_y (m)	σ_z (m)	c_c (kg/m^3)
DT1	31.2	3.42	0.0267
DT2	65.7	3.60	0.0241
DT3	66.0	2.50	0.0155
DT4	86.7	2.80	0.0218

TABLE 8. ESTIMATES OF S_y AND S_z FOR THE DESERT TORTOISE SERIES AT 800 METERS

	S_y (m)	S_z (m)	c_c (kg/m^3)
DT1	43.8	3.78	0.0323
DT2	105.0	4.80	0.0205
DT3	106.2	2.66	0.0171
DT4	143.5	3.11	0.0222

SECTION IV

RELEASE RICHARDSON NUMBER

The purpose of this section is to examine one way of determining whether the ground-level jet dominates a release or whether the other nonjet phases of a ground-level release (including the negative buoyancy-dominated dispersion phase, the stably stratified shear flow phase, and the passive dispersion phase) are the only important dispersion phases. (The derivation of these criteria is discussed in Appendix A.)

From Havens and Spicer (Reference 10) and Spicer and Havens (Reference 11), the previous criteria for determining which phase of the dispersion process dominates a particular ground-level, low initial momentum (nonjet) release was based on water tunnel experiments reported by Britter (Reference 12). In that set of experiments, a salt/water solution was released at floor level, and the lateral and upwind extent of the plume was recorded. Analysis of Britter's releases showed the following criteria of a release Richardson number were obtained for ground-level, nonjet releases:

If $Ri_c \gtrsim 30$	negative buoyancy-dominated phase
If $1 \lesssim Ri_c \lesssim 30$	stably stratified shear flow phase
If $Ri_c \lesssim 1$	passive dispersion phase

where $Ri_c = g(\rho_E - \rho_a)H/(\rho_a u_*^2)$. The vertical length scale H is approximated as $H \cong Q/uD$ for these ground-level, nonjet releases. (For Britter's releases, the ground-level release was directed upward so that, in the absence of entrainment and gravity spreading at the source, the depth of material moving downstream (H) would just be Q/uD for a uniform approach velocity u.) Ri_c represents a ratio of the potential energy characteristic of the release to a measure of the ambient turbulent kinetic energy. For the DT series, this approximation for H is not appropriate. To best approximate the potential energy characteristic of the release as used in Ri_c, the value of H used herein for the DT releases is 2.0 meters for all the releases based on observation of the photographic records of the tests as well as the height of the release pipe outlet (0.79 meters). Using this value for H, the values of Ri_c for the DT series are shown in Table 9. (For estimation of Ri_c, values of u_* were taken from Goldwire et al. (Reference 1), and values of the initial aerosol density were estimated

TABLE 9. VALUES OF Ri_c AND $(V/u_*)^2$ FOR THE DT SERIES

Test	Ri_c	$(V/u_*)^2$
DT1	280	2300
DT2	490	5000
DT3	270	3700
DT4	630	6100

using TRAUMA as discussed in Section I.) As indicated by Ri_c, all of the DT releases would be in the negative buoyancy-dominated flow phase at the release in the absence of any jet effects.

After criteria of domination of a particular nonjet dispersion phase have been established, it can be determined whether a particular release is dominated by jet effects. Of course, jet effects would dominate a release in the absence of wind for a horizontal release. Goldwire et al. (Reference 1) suggest that jet effects were important in the DT series to over 100 meters downwind of the release because agreement between the position of the vapor cloud and wind trajectories was only fair. For this analysis, a release will be considered dominated by jet effects associated with the release if the rate of air entrainment due to the jet dominates the rate of air entrainment due to the dominant nonjet dispersion phase of the release. Based on the analysis in Appendix A, ground-level, horizontal jet effects dominate the dominant nonjet flow phase when:

$V/u \lesssim 0.8$ for passive dispersion phase

$V/u \lesssim 16/(19+Ri_c)$ for stably stratified shear flow phase

$(V/u_*)^2 \lesssim 10\ Ri_c$ for negative buoyancy-dominated phase

where V is the velocity of the material leaving the pipe. For the DT series, the appropriate condition to check is $(V/u_*)^2 \lesssim 10\ Ri_c$ since the dominant nonjet flow phase is the negative buoyancy-dominated flow phase. Ratios of $(V/u_*)^2$ are also shown in Table 9. Based on this criteria, the only release which would be clearly dominated by jet effects is DT3, and

the remaining tests should be adequately predicted by a model which properly takes into account the ground-level, nonjet flow phases discussed above.

SECTION V

COMPARISON OF THE PASQUILL-HANNA GAUSSIAN PLUME MODEL AND DEGADIS WITH THE DESERT TORTOISE DATA

The Pasquill-Hanna Gaussian plume model has proven to be applicable to atmospheric dispersion problems when the dispersion of the contaminant is only a function of the atmospheric turbulence and the plume does not perturb the ambient flow field (passive dispersion). The steady-state Gaussian plume model for ground-level releases is given by

$$y_v = \frac{Q}{\pi \sigma_y \sigma_z u} \exp\left[-\frac{1}{2}\left(\frac{y}{\sigma_y}\right)^2 - \frac{1}{2}\left(\frac{z}{\sigma_z}\right)^2 \right] \qquad (5)$$

where y_v is the contaminant mole fraction, Q is the volumetric source evolution rate, and σ_y and σ_z are the standard deviation of the lateral and vertical concentration distributions, respectively. Values of σ_y were taken from Hanna et al. (Reference 13), and values for σ_z which take into account surface roughness effects were taken from Pasquill and Smith (Reference 9).

The DEGADIS (DEnse GAs DISpersion) model was developed for the U.S. Coast Guard and the Gas Research Institute and was designed to model the atmospheric dispersion of DTAG's (References 10, 11). DEGADIS is an adaptation of the Shell HEGADAS model described by Colenbrander (Reference 14) and Colenbrander and Puttock (Reference 15); DEGADIS also incorporates some techniques used by van Ulden (Reference 16). The model was developed to predict the dispersion of gas from a ground-level area source (such as a boiling liquid pool), and describes three phases of dispersion which typically occur following nonjet, ground-level DTAG releases discussed in Section II. The near-field, buoyancy-dominated dispersion phase is modeled using a lumped parameter model of a denser-than-air "secondary source" cloud which incorporates air entrainment at the gravity-spreading front using a frontal entrainment velocity; this description is based on laboratory data reported in Havens and Spicer (Reference 10). The downwind dispersion phase of the calculation assumes a power law concentration distribution in the vertical direction and a modified Gaussian profile in the horizontal direction with a power law wind profile (Figure 2). The

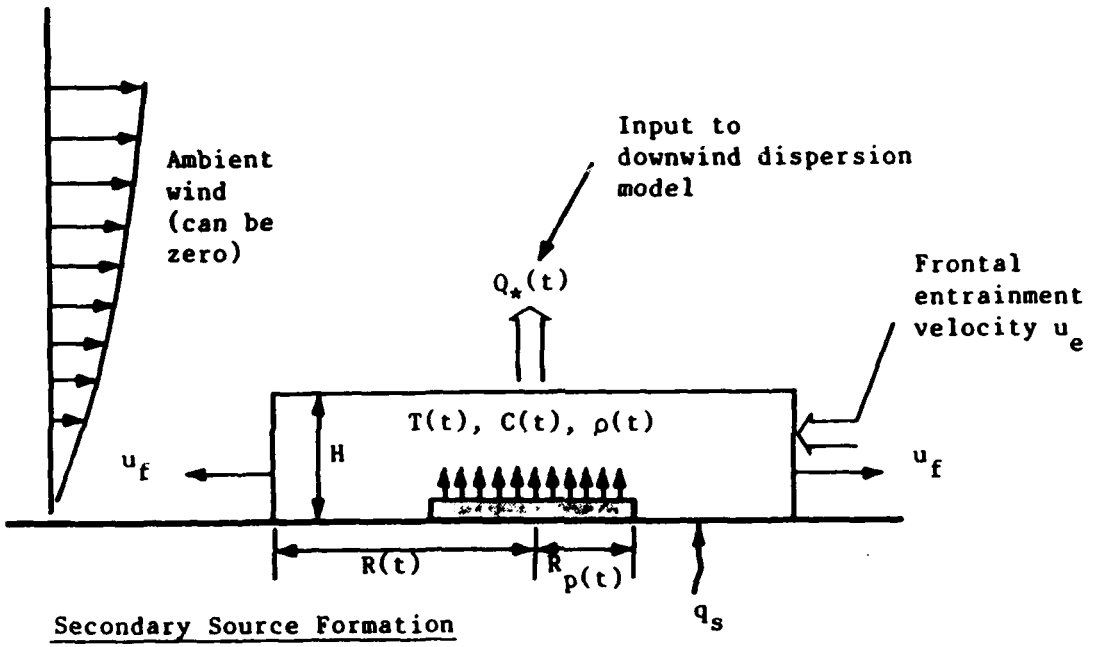

Figure 2. Schematic Diagram of DEGADIS.

$$C(x,y,z) = C_C(x) \exp\left[-\left(\frac{|y| - b(x)}{S_y(x)}\right)^2 - \left(\frac{z}{S_z(x)}\right)^{1+\alpha}\right], \quad |y| > b$$

$$C(x,y,z) = C_C(x) \exp\left[-\left(\frac{z}{S_z(x)}\right)^{1+\alpha}\right], \quad |y| \leq b$$

$$u_X = u_O\left(\frac{Z}{Z_O}\right)^{\alpha}$$

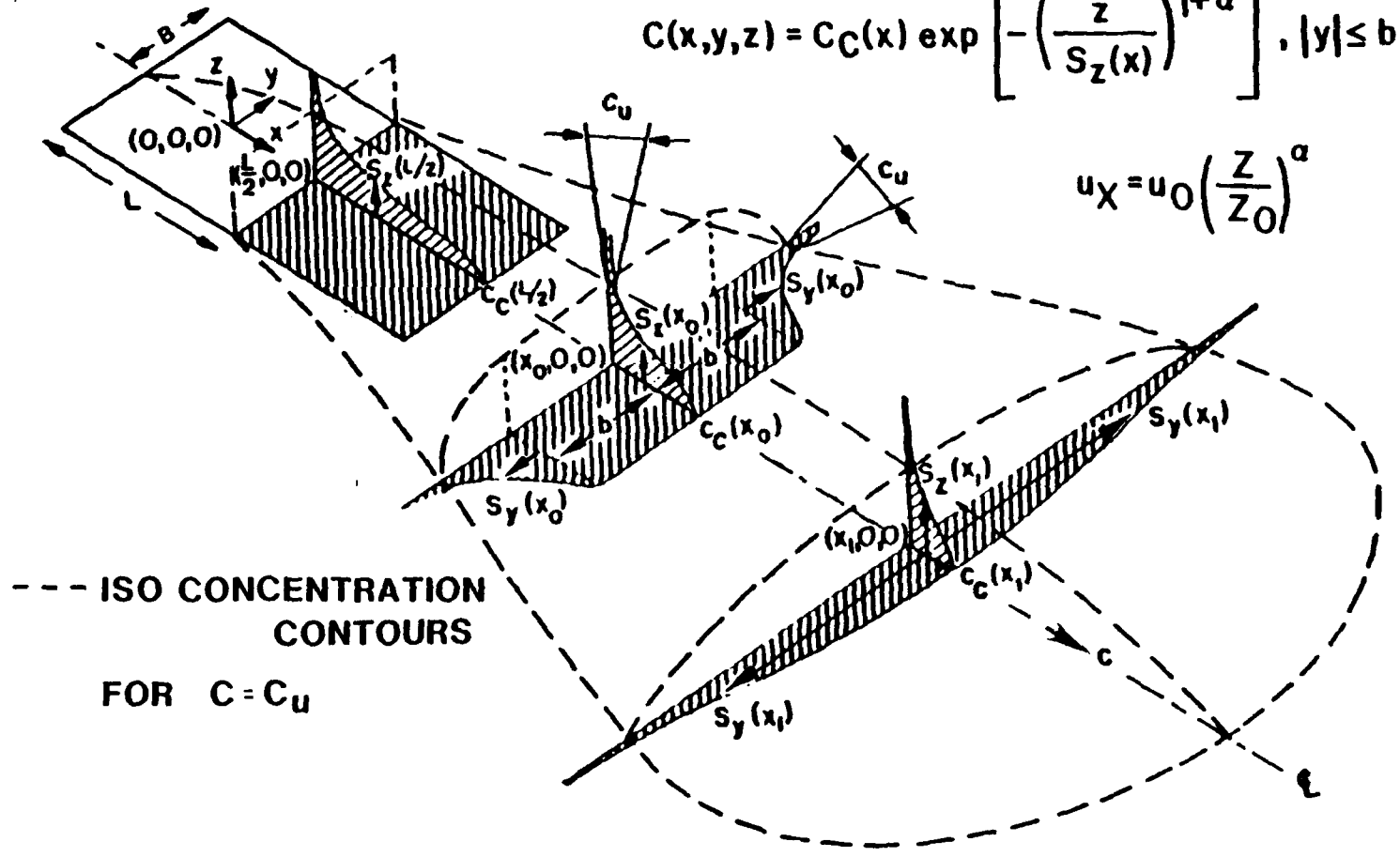

Figure 2. Schematic Diagram of DEGADIS (Concluded).

vertical mixing rate is based on laboratory-scale data for vertical mixing in stably density-stratified fluids reported by Kantha et al. (Reference 17), Lofquist (Reference 18), and McQuaid (Reference 19). The vertical dispersion parameters S_z and the horizontal dispersion parameter S_y determine the vertical and horizontal profiles, respectively. It should be noted that the rates of change of S_y and S_z approach the rates of change of σ_y and σ_z, respectively, as the density of the plume approaches the ambient density. A complete description of DEGADIS is included in Appendix B; a discussion of the sensitivity of DEGADIS to uncertainty in model input parameters not routinely available at operational USAF sites is included in Appendix C.

At present, DEGADIS does not have provisions for describing jet releases. However, it is characteristic of DEGADIS predictions that the distance to a given concentration level is not a strong function of the source area when the emission flux is greater than or equal to the maximum atmospheric takeup flux (within an order of magnitude). Using the arguments presented in Section IV, the diameter of the source used in the simulations was given by $D = Q/uH$ along with the assumed value of $H = 2$ meters for all releases. (Essentially identical values for c_c, S_y, S_z, and b were predicted using these values for D and 10D.)

In addition, the thermodynamics treatment in DEGADIS does not presently provide for phase-change heat effects (other than ambient humidity condensation) in the gas/air mixture. Therefore, aerosol phase change effects on the cloud density were accounted for by estimating the mixture density as a function of contaminant concentration using TRAUMA as discussed in Section II. This assumes that a given amount of pure released aerosol and ambient humid air are mixed until they reach equilibrium (adiabatic mixing). Note that because the mixture density as a function of concentration is approximated by adiabatic mixing, heat transfer is not included in the DEGADIS simulations of the DT releases herein.

Table 10 shows a comparison between the reported temperature associated with the maximum reported concentration and the adiabatic mixing temperature associated with the maximum reported concentration for the DT tests. The assumption of no heat transfer (or adiabatic mixing of the released aerosol with the ambient air) reproduces the reported temperature remark ably well. Furthermore, Table 10 shows the difference in the mixture

density associated with the difference in temperature to be insignificant. Therefore, the assumption of insignificant heat transfer is justifiable for the DT series. The validity of this assumption for the release of a given material is generally based on the competing effects of warming the contaminant mixture by mixing with (warm) air compared with warming by heat transfer; both of these effects are related to the windspeed. For high windspeeds, the rate of mixing is increased, thereby adding more energy to the mixture. Also for high windspeeds, the mean cloud advection speed is higher, implying that the travel time to a given distance is decreased, and shorter travel times provide less time for heat transfer to occur. It is straightforward to show that the mean advection time to a given distance should be proportional to $(T_{OBS} - T_{AM})$ where T_{OBS} is the observed temperature and T_{AM} is the adiabatic mixing temperature for the same concentration level. For lower windspeeds such as DT2 and DT4, the heat transfer processes were more important than for DT1 and DT3 which had higher windspeeds. Indeed, for calm conditions, heat transfer processes would be more important than the heat transfer processes observed in the DT series.

TABLE 10. COMPARISON OF THE TEMPERATURE ASSOCIATED WITH THE OBSERVED MAXIMUM CONCENTRATION AND THE ADIABATIC MIXING TEMPERATURE ASSOCIATED WITH THE MAXIMUM CONCENTRATION AT 800 METERS

	Measured Temperature at the Maximum Reported Concentration (°C)	Adiabatic Mixing Temperature at the Maximum Reported Concentration (°C)	Density Error in Assuming No Heat Transfer (%)
DT1	23.6	20.9	0.9
DT2	22.5	17.2	1.8
DT3	24.9	22.4	0.8
DT4	23.0	17.7	1.8

The exposure limits for ammonia (and other toxic materials) are generally based on exposure to a given concentration over a specified time

period; the short-term exposure limit (STEL, based on a 15-minute exposure) for ammonia established by the 1979 American Conference of Governmental Industrial Hygienists (ACGIH) is 35 parts per million (Reference 20). Therefore, it is necessary to be able to predict not only the maximum concentration, but also the average concentration over a period of time (for example, 15 minutes). A discussion of the implications to DEGADIS of the averaging time is included in Appendix D. In the DT series, the MSA nondispersive IR gas sensor response time was about 2 seconds, and the concentration data were smoothed using a 3-second sliding average (Reference 1). An averaging time of 3 seconds was used in the DEGADIS simulations for comparison with the data.

The Pasquill-Hanna Gaussian model results for the DT series are shown in Table 11 and compared with the concentration profile parameters at 800 meters as presented in Table 7. As indicated, the predicted values of σ_y are in reasonable agreement with the estimated values, but the predicted values of σ_z are much larger (by an average factor of about 6) than the estimated values. In Tables 12-15 and Figures 3-6, the model results are compared with maximum reported concentrations (for all time). (All model simulations were made for the ammonia release rate (Table 1) and the estimated ammonia mass rate at 800 meters (Table 2).) In Tables 12-15, the observed temperatures reported correspond in time with the maximum reported concentrations. The values of S_y and S_z are reported in Tables 12-15; the approximations $S_z \cong \sigma_z$ and $S_y \cong \sqrt{2}\sigma_y$ are used for comparison. As indicated, the predicted values of the maximum concentration are much smaller (by an average factor of about 6) than the maximum observed values.

TABLE 11. COMPARISON OF OBSERVED AND PREDICTED GAUSSIAN PROFILE PARAMETERS AT 800 METERS

	Estimated σ_y (m)	Predicted[a] σ_y (m)	Estimated σ_z (m)	Predicted[b] σ_z (m)
DT1	31.2	31.2	3.42	21.0
DT2	65.7	31.2	3.60	21.0
DT3	66.0	31.2	2.50	21.0
DT4	86.7	23.4	2.80	12.2

[a]From Hanna et al. (Reference 13) and corrected for averaging time
[b]From Pasquill and Smith (Reference 9)

TABLE 12. COMPARISON OF OBSERVED AND MODEL-PREDICTED CONCENTRATION PROFILE PARAMETERS FOR DT1

	at 800 m				at 3.5 km	at 5.5 km
	Maximum Concentration (Vol. %)	Temperature (°C)	S_z (m)	S_y (m)	Maximum Concentration (Vol. ppm)	Maximum Concentration (Vol. ppm)
Observed	1.12	23.6	3.78	43.8	670	150
Gaussian Plume Model						
(66.5 kg/s)	0.10	--	21[a]	44[b]	75	35
(81 kg/s)	0.12	--	21[a]	44[b]	92	43
DEGADIS						
(66.5 kg/s)	0.69	24.0	6.71	87.9	850	360
(81 kg/s)	0.83	23.0	6.06	90.5	1040	450

[a]For comparison, $S_z \cong \sigma_z$
[b]For comparison, $S_y \cong \sqrt{2}\sigma_y$

TABLE 13. COMPARISON OF OBSERVED AND MODEL-PREDICTED CONCENTRATION PROFILE PARAMETERS FOR DT2

	at 800 m				at 1.4 km
	Maximum Concentration (Vol. %)	Temperature (°C)	S_z (m)	S_y (m)	Maximum Concentration (Vol. ppm)
Observed	1.86	22.5	4.80	105	4000
Gaussian Plume Model					
(104.6 kg/s)	0.21	--	21[a]	44[b]	780
(117 kg/s)	0.24	--	21[a]	44[b]	870
DEGADIS					
(104.6 kg/s)	1.59	19.2	3.53	109	5600
(117 kg/s)	1.81	17.8	3.36	111	6200

[a]For comparison, $S_z \cong \sigma_z$
[b]For comparison, $S_y \cong \sqrt{2}\sigma_y$

TABLE 14. COMPARISON OF OBSERVED AND MODEL-PREDICTED CONCENTRATION PROFILE PARAMETERS FOR DT3

	at 800 m				at 2.8 km
	Maximum Concentration (Vol. %)	Temperature (°C)	S_z (m)	S_y (m)	Maximum Concentration (Vol. ppm)
Observed	1.62	24.9	2.66	106	1100
Gaussian Plume Model					
(56.0 kg/s)	0.08	--	21[a]	44[b]	96
(133 kg/s)	0.20	--	21[a]	44[b]	230
DEGADIS					
(56.0 kg/s)	0.61	29.5	7.30	84.7	1090
(133 kg/s)	1.37	24.2	4.82	97.3	2050

[a]For comparison, $S_z \cong \sigma_z$
[b]For comparison, $S_y \cong \sqrt{2}\sigma_y$

TABLE 15. COMPARISON OF OBSERVED AND MODEL-PREDICTED CONCENTRATION PROFILE PARAMETERS FOR DT4

	at 800 m				at 2.8 km
	Maximum Concentration (Vol. %)	Temperature (°C)	S_z (m)	S_y (m)	Maximum Concentration (Vol. ppm)
Observed	2.1	23.0	3.11	143.5	5100
Gaussian Plume Model					
(72.1 kg/s)	0.44	--	12[a]	33[b]	500
(108 kg/s)	0.65	--	12[a]	33[b]	750
DEGADIS					
(72.1 kg/s)	1.42	22.7	3.13	97.5	1900
(108 kg/s)	2.30	17.0	2.60	102	2600

[a]For comparison, $S_z \cong \sigma_z$
[b]For comparison, $S_y \cong \sqrt{2}\sigma_y$

DEGADIS predictions (using the approximations and assumptions described above) for the DT tests are shown in Tables 12-15 and Figures 3-6. The DEGADIS-predicted maximum concentration and vertical dispersion parameter S_z are generally consistent with the observed values at 800 meters. It should be noted that the maximum reported concentrations for the sensor locations past 1.4 kilometers may be significantly lower than the maximum concentration which occurred during the tests due to the wide spacing of these sensors. (Furthermore, the wind field may not have been constant to these long distances.)

The DEGADIS-predicted plume width (see Figure 2) is larger than the observed width due to the presence of the horizontally homogeneous central section even though the predicted and estimated values of S_y are in good agreement. For Test 4, the observed width to the 0.2 percent concentration level was 440 meters (Reference 21), while the DEGADIS-predicted width was 800 meters and the Gaussian plume model prediction was 60 meters to the same concentration level.

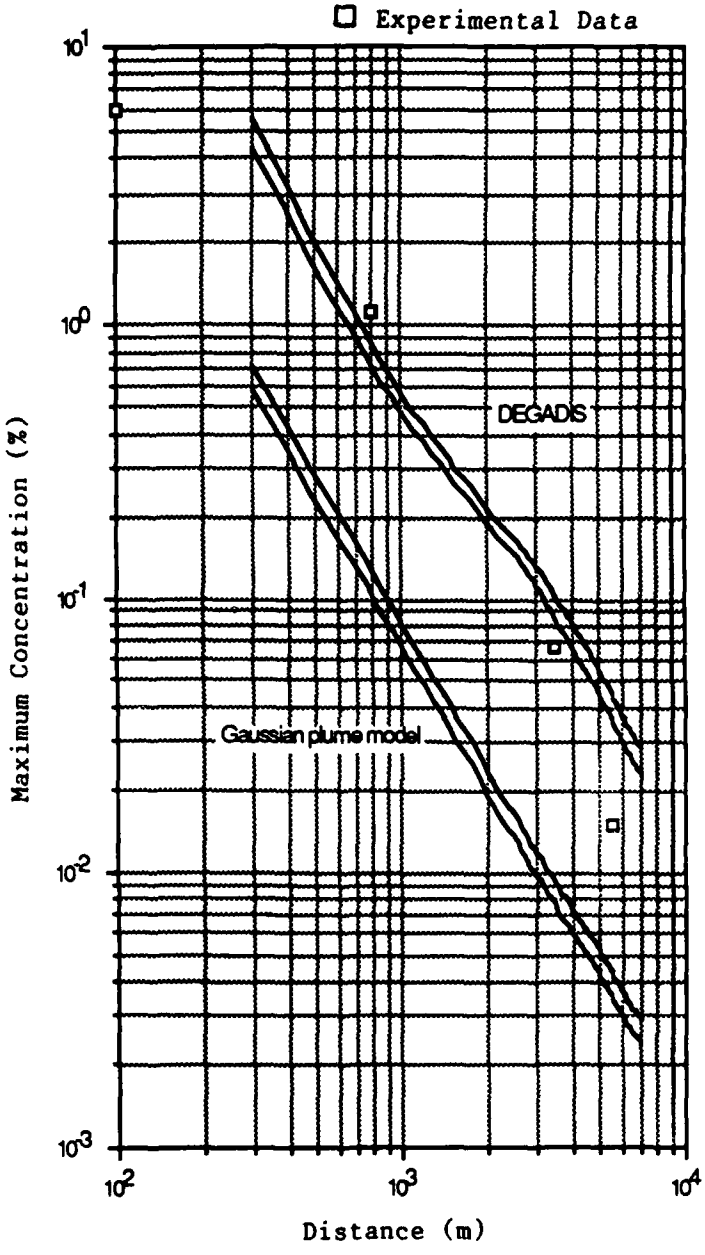

Figure 3. Maximum Observed Concentration and Maximum Predicted Concentrations using DEGADIS and the Pasquill-Hanna Gaussian Plume Model for DT1. (The upper line for each model was made using the ammonia mass release rate (Table 1), and the lower line for each model was made using the estimated ammonia mass rate at 800 meters (Table 2).)

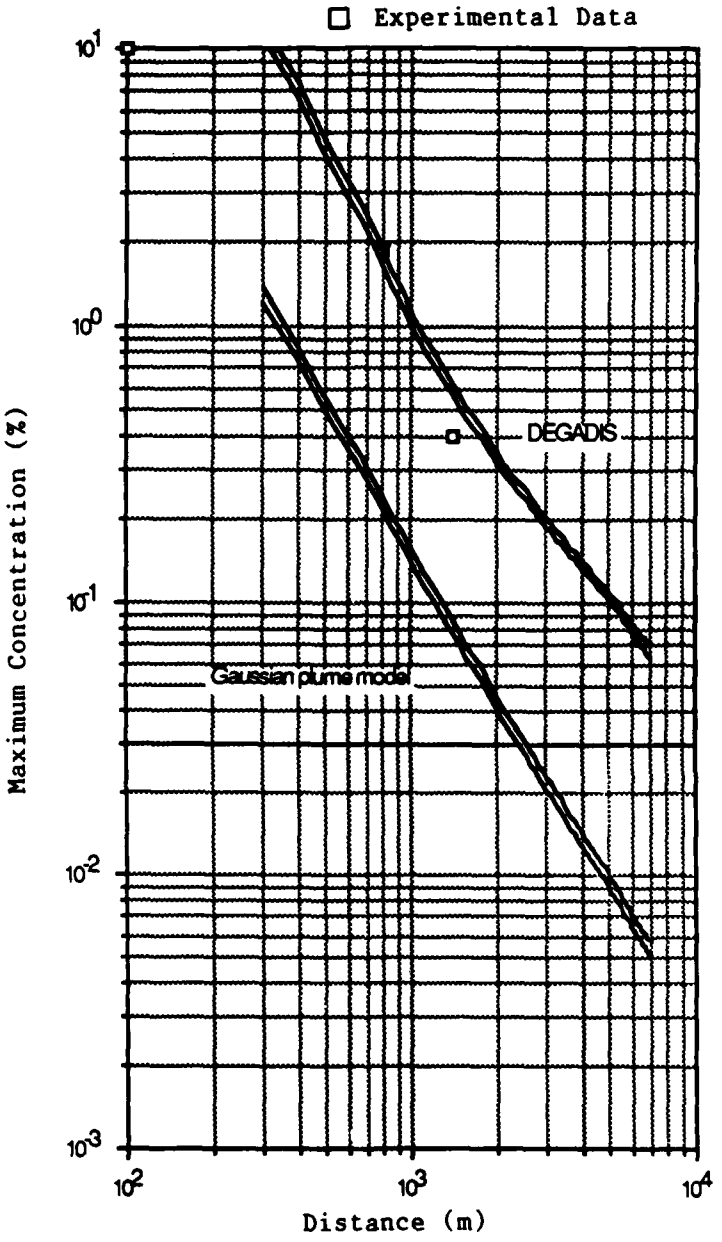

Figure 4. Maximum Observed Concentration and Maximum Predicted Concentrations using DEGADIS and the Pasquill-Hanna Gaussian Plume Model for DT2. (The upper line for each model was made using the ammonia mass release rate (Table 1), and the lower line for each model was made using the estimated ammonia mass rate at 800 meters (Table 2).)

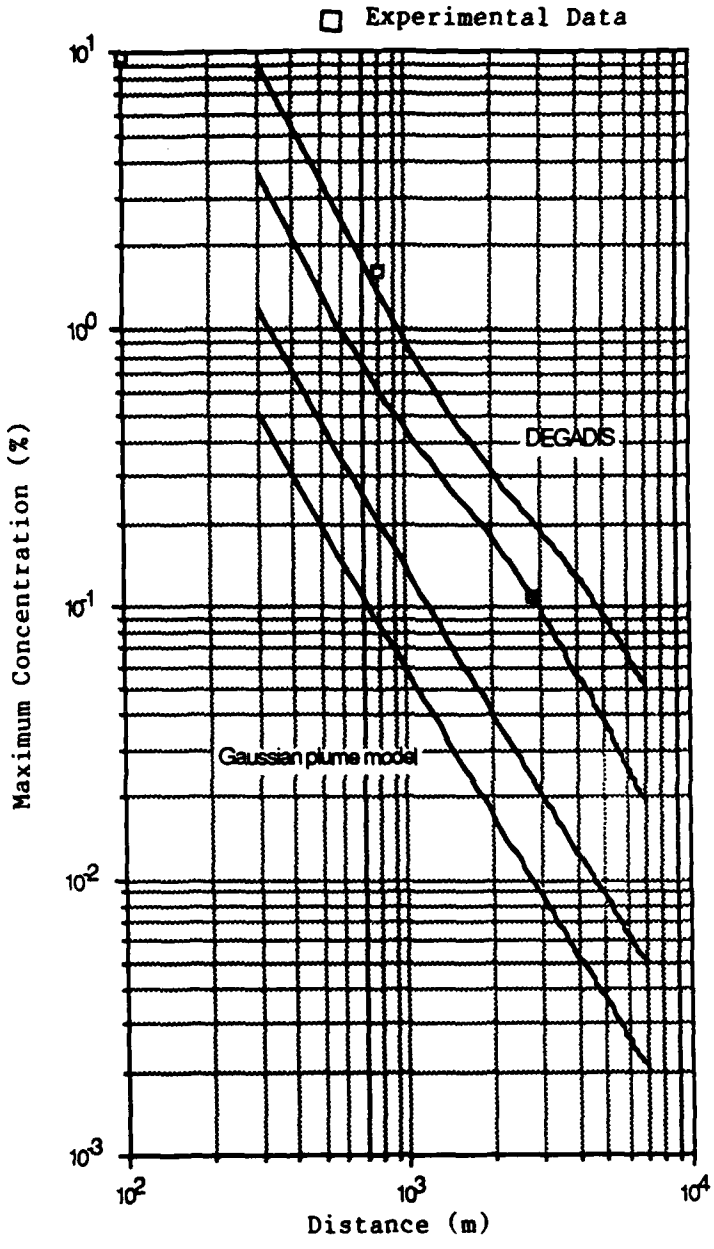

Figure 5. Maximum Observed Concentration and Maximum Predicted Concentrations using DEGADIS and the Pasquill-Hanna Gaussian Plume Model for DT3. (The upper line for each model was made using the ammonia mass release rate (Table 1), and the lower line for each model was made using the estimated ammonia mass rate at 800 meters (Table 2).)

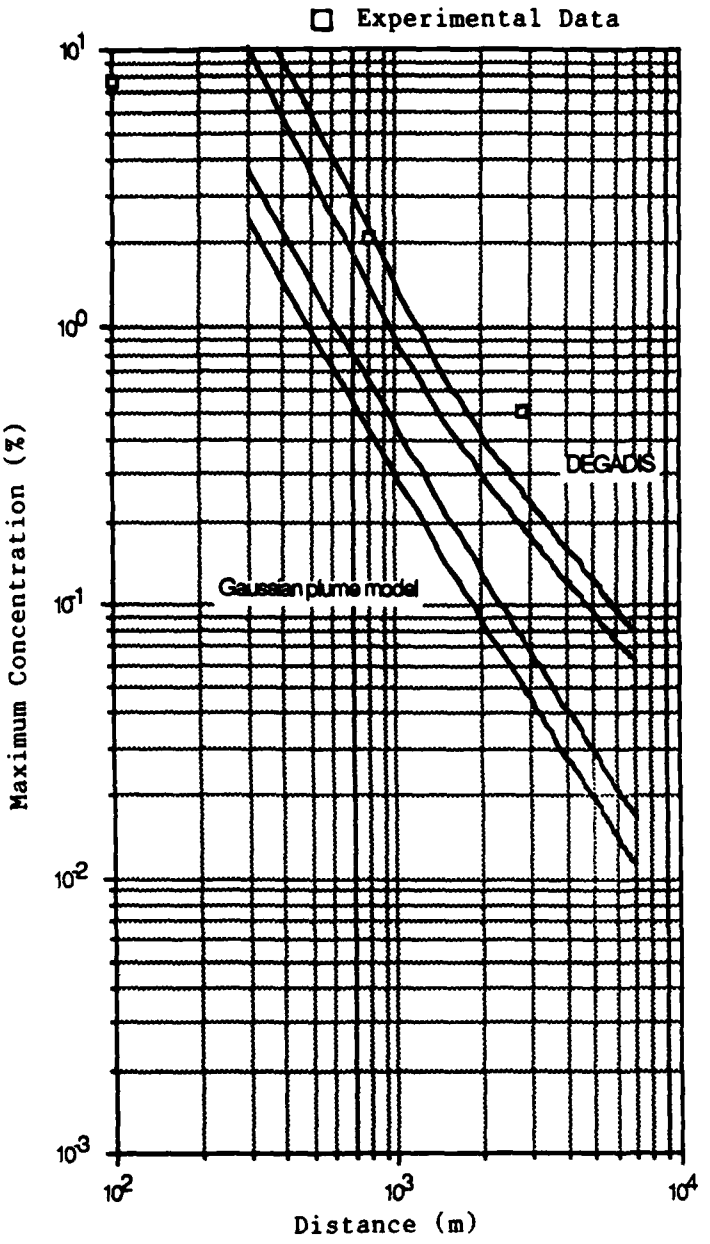

Figure 6. Maximum Observed Concentration and Maximum Predicted Concentrations using DEGADIS and the Pasquill-Hanna Gaussian Plume Model for DT4. (The upper line for each model was made using the ammonia mass release rate (Table 1), and the lower line for each model was made using the estimated ammonia mass rate at 800 meters (Table 2).)

SECTION VI

CONCLUSIONS AND RECOMMENDATIONS

Field-scale releases of pressurized liquid anhydrous ammonia (the Desert Tortoise (DT) series) were performed by Lawrence Livermore National Laboratories (LLNL) in 1983 for the U.S. Coast Guard, the Fertilizer Institute, and Environment Canada. Release rates for the four experiments ranged from 80 to 130 kilograms per second. Ammonia concentration measurements were taken at sensor arrays located 100 and 800 meters downwind of the release; in addition to these arrays, portable gas sensors were deployed from 1.4 to 5.5 kilometers downwind of the release. The data from these experiments were analyzed to determine the concentration profile parameters at the 800-meter array. These concentration profile parameters were compared with DEGADIS and the Pasquill-Hanna Gaussian plume model. The Pasquill-Hanna Gaussian plume model-predicted maximum concentrations were significantly lower (by an average factor of about 6) than the maximum reported concentrations; this disagreement is due to the overprediction of the vertical dispersion present during the tests. On the other hand, DEGADIS-predicted maximum concentrations were in reasonable agreement with the maximum reported concentrations. In contrast to the Gaussian plume model, DEGADIS accounts for the reduced vertical dispersion due to the stable density stratifications present in these releases.

A quantitative method of assessing the relative important of jet and nonjet dispersion processes was developed. When applied to the DT releases, the jet dispersion processes clearly dominated only one release (DT3) according to the developed criteria.

The effects of different averaging times on the DEGADIS predictions were discussed. For the DT series, a 3-second sliding average was used by LLNL to remove noise in the raw data; an averaging time of 3 seconds was used in the DEGADIS simulations.

Based on comparison of reported temperature corresponding to the maximum reported concentration and the adiabatic mixing temperature corresponding to the same maximum reported concentration, heat transfer was found to be insignificant in the DT series.

A computer code, TRAUMA, was used to determine the ammonia/air/water mixture density as a function of ammonia mole fraction for input to DEGADIS. Based on comparisons with TRAUMA and DEGADIS computations, it was found that assuming ideal solution liquid phase behavior adequately describe the ammonia/air/water mixture density for the DT release conditions. It was also found that assuming a pseudobinary of air/water and ammonia does not adequately describe the ammonia/air/water mixture density based on comparisons with DEGADIS.

Finally, a linear relationship between ammonia concentration and mixture density was used in DEGADIS; the endpoints were represented by the released ammonia aerosol and ambient air. Upon comparison, the DEGADIS-predicted distances using this simplified scheme were within about $\pm$20 percent of the DEGADIS-predicted distance to a given concentration level using the density specification from TRAUMA (Figure 1). This last simplification would be expected to be less valid as heat transfer from the ground to the cloud becomes more important. Where appropriate, this last simplification may be useful as a screening technique for preliminary hazard assessment.

REFERENCES

1. Goldwire, H.C., Jr., McRae, T.G., Johnson, G.W., Hipple, D.L., Koopman, R.P., McClure, J.W., Morris, L.K., and Cederwall, R.T., Desert Tortoise Series Data Report--1983 Pressurized Ammonia Spills, Lawrence Livermore National Laboratories Report UCID-20562, Livermore, California, December 1985.

2. Wheatley, C.J., A Theoretical Study of NH_3 Concentrations in Moist Air Arising from Accidental Release of Liquefied NH_3, Using the Computer Code TRAUMA, UK Atomic Energy Authority Report SRD R393, 1985.

3. Wheatley, C.J., "Factors Affecting Cloud Formation from Releases of Liquified Gases," paper presented at Institute of Chemical Engineers Symposium on Refinement of Estimates of the Consequences of Heavy Toxic Vapour Releases, January 1986.

4. Wheatley, C.J., A Theory of Heterogeneous Equilibrium Between Vapour and Liquid Phases of Binary Systems and Formulae for the Partial Pressures of HF and H_2O Vapour, UK Safety and Reliability Directorate Report SRD R357, 1986.

5. Wheatley, C.J., Discharge of Liquid Ammonia to Moist Atmospheres--Survey of Experimental Data and Model for Estimating Initial Conditions for Dispersion Calculations, UK Atomic Energy Authority Report SRD R410, 1986.

6. Wheatley, C.J., A User's Guide to TRAUMA, a Computer Code for Assessing the Consequences of Accidental Two-Phase Releases of NH_3 into Moist Air, UK Atomic Energy Authority Report SRD R394, 1986.

7. List, E.J., "Turbulent Jets and Plumes," Ann. Rev. Fluid Mech., 14, 1982, pp. 189-212.

8. Xiao-yun, Li, Leudens, H., and Ooms, G., "An Experimental Verification of a Theoretical Model for the Dispersion of a Stack Plume Heavier than Air," Atmospheric Environment, 20, 1986, pp. 1087-1094.

9. Pasquill, F. and Smith, F. B., Atmospheric Diffusion, 3rd edition, Halstead Press, New York, 1983.

10. Havens, J.A. and Spicer, T.O., Development of an Atmospheric Dispersion Model for Heavier-than-Air Gas Mixtures, Final Report to U.S. Coast Guard, Contract DT-CG-23-80-C-20029, May 1985.

11. Spicer, T.O. and Havens, J.A., Development of Vapor Dispersion Models for Nonneutrally Buoyant Gas Mixtures--Analysis of USAF/N_2O_4 Test Data, USAF Engineering and Services Laboratory, Final Report ESL-TR-86-24, September 1986.

12. Britter, R.E., "The Ground Level Extent of a Negatively Buoyant Plume in a Turbulent Boundary Layer," Atmospheric Environment, 14, 1980, pp. 779-785.

13. Hanna, S.R., Briggs, G.A., and Hosker, R.P., Jr., Handbook on Atmospheric Diffusion, U.S. DOE/TIC 11223, 1982.

14. Colenbrander, G.W., "A Mathematical Model for the Transient Behavior of Dense Vapor Clouds," paper presented at 3rd International Symposium on Loss Prevention and Safety Promotion in the Process Industries, Basel, Switzerland, 1980.

15. Colenbrander, G.W. and Puttock, J.S., "Dense Gas Dispersion Behavior: Experimental Observations and Model Developments," paper presented at International Symposium on Loss Prevention and Safety Promotion in the Process Industries, Harrogate, England, September, 1983.

16. van Ulden, A.P., "A New Bulk Model for Dense Gas Dispersion: Two-Dimensional Spread in Still Air," paper presented at I.U.T.A.M. Symposium on Atmospheric Dispersion of Heavy Gases and Small Particles, Delft University of Technology, The Netherlands, 29 August-2 September 1983.

17. Kantha, L.H., Phillips, O.M., and Azad, R.S., "On Turbulent Entrainment at a Stable Density Interface," Journal of Fluid Mechanics, 79, 1977, pp. 753-768.

18. Lofquist, Karl, "Flow and Stress Near an Interface Between Stratified Liquids," Physics of Fluids, 3, No. 2, March-April 1960.

19. McQuaid, James L., "Some Experiments on the Structure of Stably Stratified Shear Flows," Technical Paper P21, Safety in Mines Research Establishment, Sheffield, UK, 1976.

20. Braker, W. and Mossman, A.L., Matheson Gas Data Book, 6th ed., Matheson, Lyndhurst, NJ, 1980.

21. Goldwire, H.C., Jr., "Large-Scale Ammonia Spill Tests," Chemical Engineering Progress, April 1986, pp. 35-41.

APPENDIX A

DERIVATION OF THE RELEASE RICHARDSON NUMBER CRITERIA

The purpose of this appendix is to show the method used to determine whether a ground-level jet dominates a release or whether the other non-jet phases of a ground-level release (including the negative buoyancy-dominated dispersion phase, the stably stratified shear flow phase, and the passive dispersion phase) are the only important dispersion phases.

From Havens and Spicer (Reference A-1) and Spicer and Havens (Reference A-2), the criteria for determining which phase of the dispersion process dominates a particular ground-level release was based on water tunnel experiments reported by Britter (Reference A-3). In that set of experiments, a salt/water solution was released at floor level, and the lateral and upwind extent of the plume was recorded as a function of the buoyancy length scale used by Britter ($L_B = Qg(\rho_E - \rho_a)/(\rho_E u^3)$ where Q is the volumetric emission rate and u is the ambient velocity). Analysis of Britter's releases showed that the release was passive from the source when $L_B/D \lesssim 0.005$; the release was dominated by the negative buoyancy dispersion phase when $L_B/D \gtrsim 0.1$. Based on these observations, the following criteria of a release Richardson number were obtained:

If $Ri_c \gtrsim 30$	negative buoyancy-dominated phase	
If $1 \lesssim Ri_c \lesssim 30$	stably stratified shear flow phase	(A-1)
If $Ri_c \lesssim 1$	passive dispersion phase	

where $Ri_c = g(\rho_E - \rho_a)H/(\rho_a u_*^2)$. These values were obtained using the reported ratio $(u/u_*) = 16$ for the water flume. Note that the length scale corresponding to the depth of the layer is approximated by $H = Q/uD$ for these nonjet releases.

With the criteria of domination of a particular nonjet dispersion phase established, the question of whether a particular release is dominated by jet effects can now be determined. For this analysis, a release will be considered dominated by jet effects associated with the release if the rate of air entrainment due to the jet dominates the rate of air entrainment due to the dominant nonjet phase of the release.

When the release Richardson number is less than 1, the release will be dominated by the passive dispersion phase in the absence of jet effects. Cude (Reference A-4) and Wheatley (Reference A-5) report that for a passive

release, jet effects will dominate a particular release when $(V/u) \gtrsim 1$ where V is the velocity of the released material. This criterion can also be obtained by examining the rate of air entrainment as presented by Wheatley (Reference A-6)

$$\frac{dM_a}{dx} = \left[\frac{0.159}{2} \right] \left[\frac{2\pi R}{2} \right] V_j \rho_a \qquad \text{(A-2)}$$

which has been written for a jet released near ground level without drag on the bottom surface. The DEGADIS model's vertical rate of air entrainment per unit width for the stably stratified shear flow and passive dispersion phases is given by

$$\frac{d}{dx} (\rho_L u_L H_L) = \frac{\rho_a \delta_L k u_* (1 + \alpha)}{\phi(Ri_*)} \qquad \text{(A-3)}$$

where $\phi(Ri_*) \cong 0.88 + 0.099\ Ri_*$. Using an effective width of $2\pi R$, a typical value of $\alpha = 0.2$, $\delta_L = 2.1$, $k = 0.35$, and $(u/u_*) = 30$ (typical of atmospheric boundary layers), the above equations can be combined to show that jet effects dominate the rate of dispersion when

$$\frac{V}{u} \gtrsim 16/(19 + Ri_c) \qquad \text{(A-4)}$$

This criterion has the characteristic that as the density of the released fluid increases, the release is more readily dominated by jet effects (since the rate of air entrainment would decrease in the absence of the jet effects). Note that when $Ri_c \lesssim 1$ (i.e. a passive release), this criterion shows that the jet effects dominate the passive dispersion regime when $(V/u) \gtrsim 0.8$, which is consistent with the previously reported criterion.

If the negative buoyancy-dominated dispersion phase is considered, the ambient flow is no longer important in determining the rate of nonjet air entrainment. For this case, the relative importance of jet effects were evaluated using the criterion from Britter's data; the release velocity V was used in place of the ambient velocity in the buoyancy length scale. It can be shown that jet effects dominate the negative buoyancy-dominated phase when

$$\left[\frac{V}{u_*}\right]^2 \tilde{>} 10\ Ri_c \qquad \text{(A-5)}$$

This criterion has the characteristic that as the density of the released fluid increases, the release is less readily dominated by jet effects (since the rate of air entrainment would increase in the absence of the jet effects due to the entrainment associated with the gravity front).

The following procedure is then suggested for determining which dispersion phase is dominant from the start of a release:

(1) Calculate $Ri_c = g(\rho_E - \rho_a)H/(\rho_a u_*^2)$.

(2) Determine the dominant nonjet dispersion phase in the absence of a jet using Equation (A-1).

(3) Determine if ground-level jet effects dominate the dominant nonjet phase determined from (2) using the relationships summarized in Table A-1.

TABLE A-1. CRITERIA FOR DETERMINING WHETHER JET EFFECTS DOMINATE A GROUND-LEVEL RELEASE

Ground-level jet effects dominate:		
Negative buoyancy-dominated phase	when	$\left[\frac{V}{u_*}\right]^2 \tilde{>} 10\ Ri_c$
Stably stratified shear flow phase	when	$V/u \tilde{>} 16/(19 + Ri_c)$
Passive dispersion phase	when	$V/u \tilde{>} 0.8$

REFERENCES FOR APPENDIX A

A-1. Havens, J.A. and Spicer, T.O., Development of an Atmospheric Dispersion Model for Heavier-than-Air Gas Mixtures, Final Report to U.S. Coast Guard, Contract DT-CG-23-80-C-20029, May 1985.

A-2. Spicer, T.O. and Havens, J.A., Development of Vapor Dispersion Models for Nonneutrally Buoyant Gas Mixtures--Analysis of USAF/N_2O_4 Test Data, USAF Engineering and Services Laboratory, Final Report ESL-TR-86-24, September 1986.

A-3. Britter, R.E., "The Ground Level Extent of a Negatively Buoyant Plume in a Turbulent Boundary Layer," Atmospheric Environment, 14, 1980, pp. 779-785.

A-4. Cude, A.L., "Dispersion of Gases Vented to Atmosphere from Relief Valves," The Chemical Engineer, October 1974, pp. 629-636.

A-5. Wheatley, C.J., A Theoretical Study of NH_3 Concentrations in Moist Air Arising from Accidental Release of Liquefied NH_3, Using the Computer Code TRAUMA, UK Atomic Energy Authority Report SRD R393, 1985.

A-6. Wheatley, C.J., Discharge of Liquid Ammonia to Moist Atmospheres--Survey of Experimental Data and Model for Estimating Initial Conditions for Dispersion Calculations, UK Atomic Energy Authority Report SRD R410, 1986.

APPENDIX B
DESCRIPTION OF THE
DEGADIS DENSE GAS DISPERSION MODEL

The DEGADIS (DEnse GAs DISpersion) model was developed from research sponsored by the U.S. Coast Guard and the Gas Research Institute (Reference B-1). DEGADIS is an adaptation of the Shell HEGADAS model described by Colenbrander (Reference B-2) and Colenbrander and Puttock (Reference B-3). DEGADIS also incorporates some techniques used by van Ulden (Reference B-4).

If the primary source (gas) release rate exceeds the maximum atmospheric takeup rate, a denser-than-air gas blanket is formed over the primary source. This near-field, buoyancy-dominated regime is modeled using a lumped parameter model of a denser-than-air gas "secondary source" cloud which incorporates air entrainment at the gravity-spreading front using a frontal entrainment velocity. If the primary source release rate does not exceed the maximum atmospheric takeup rate, the released gas is taken up directly by the atmosphere and dispersed downwind. For either source condition, the downwind dispersion phase of the calculation assumes a power law concentration distribution in the vertical direction and a modified Gaussian profile in the horizontal direction with a power law specification for the wind profile (Figure B-1). The source model represents a spatially averaged concentration of gas present over the primary source, while the downwind dispersion phase of the calculation models an ensemble average of the concentration downwind of the source.

A. DENSER-THAN-AIR GAS SOURCE CLOUD FORMATION

A lumped parameter model of the formation of the denser-than-air gas source cloud or blanket, which may be formed from a primary source such as an evaporating liquid pool or otherwise specified ground-level emission source, or by an initially specified gas volume of prescribed dimensions for an instantaneous release, is illustrated in Figure B-1. The gas blanket is represented as a cylindrical gas volume which spreads laterally as a density-driven flow with entrainment from the top of the source blanket by wind shear and air entrainment into the advancing front edge. The source blanket will continue to grow over the primary source until

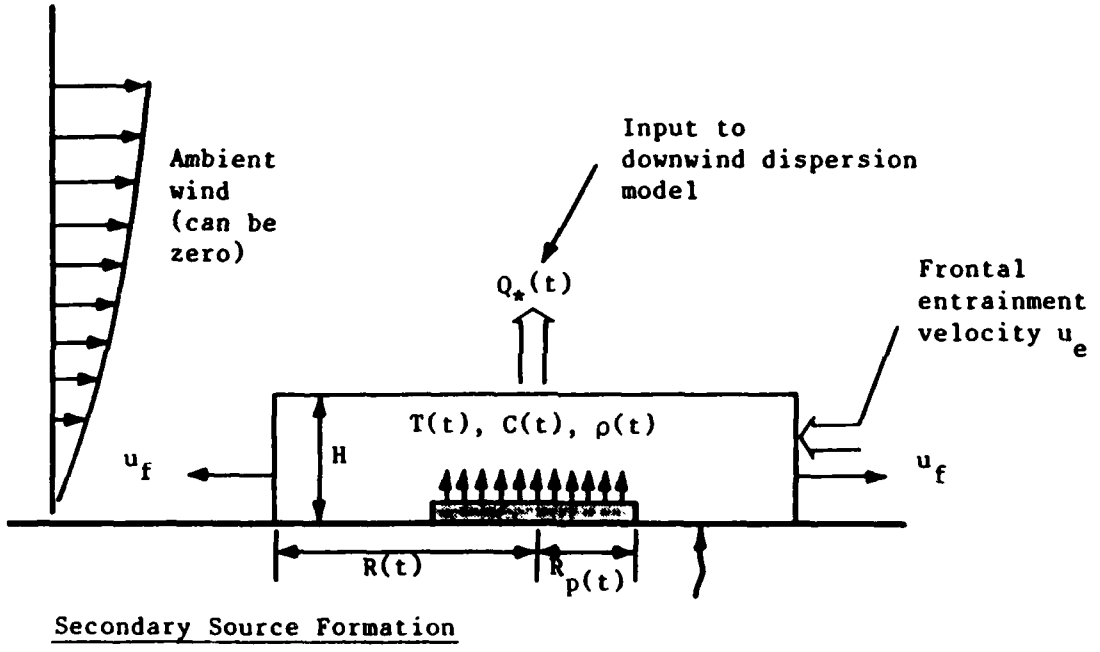

Figure B-1. Schematic Diagram of DEGADIS Dense Gas Dispersion Model.

$$C(x,y,z) = C_C(x) \exp\left[-\left(\frac{|y|-b(x)}{S_y(x)}\right)^2 - \left(\frac{z}{S_z(x)}\right)^{1+\alpha}\right], |y| > b$$

$$C(x,y,z) = C_C(x) \exp\left[-\left(\frac{z}{S_z(x)}\right)^{1+\alpha}\right], |y| \leq b$$

$$u_X = u_O\left(\frac{Z}{Z_O}\right)^{\alpha}$$

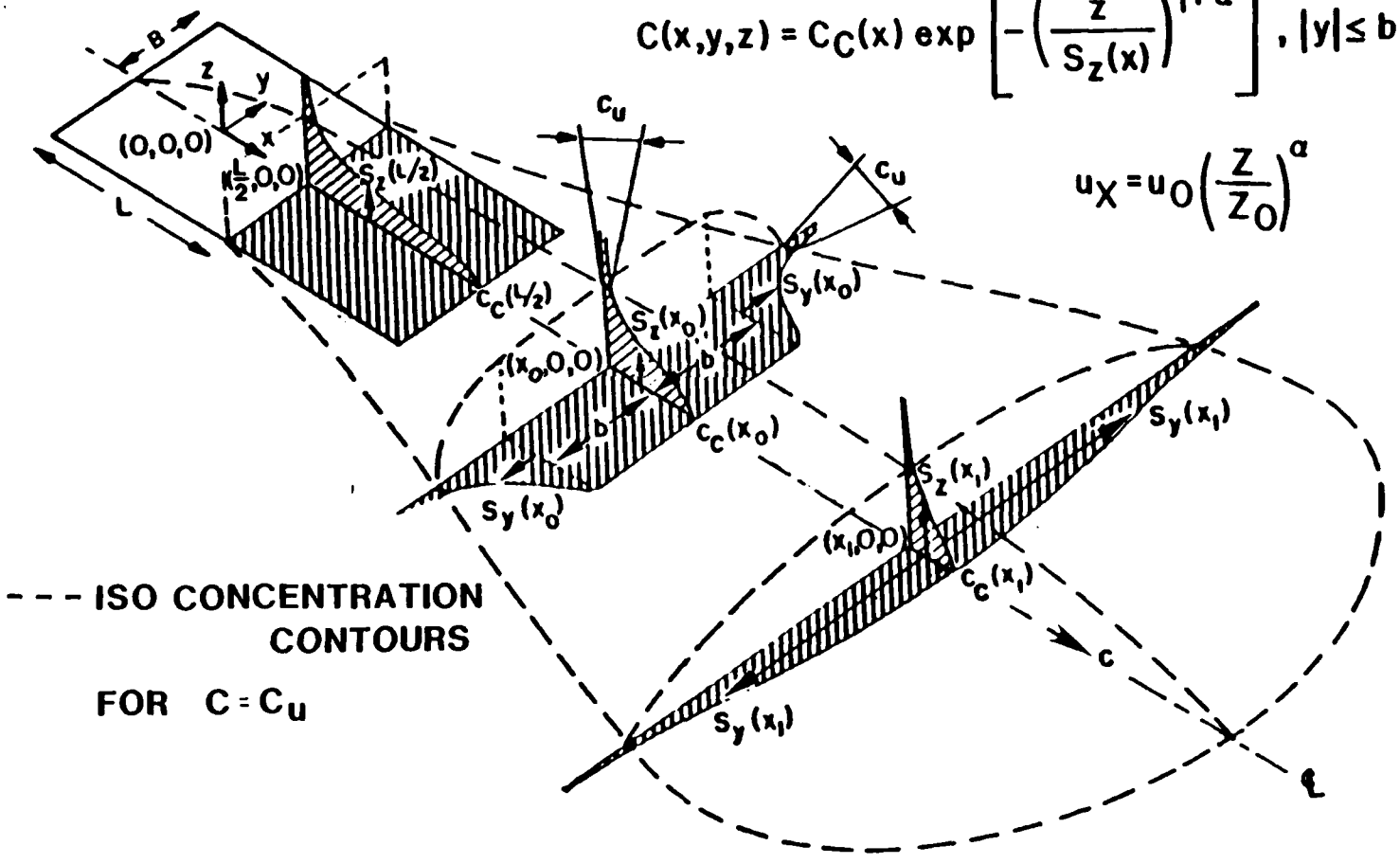

Figure B-1. Schematic Diagram of DEGADIS Dense Gas Dispersion Model (Concluded).

the atmospheric takeup rate from the top is matched by the air entrainment rate from the side and, if applicable, by the rate of gas addition from under the blanket. Of course, the blanket is not formed if the atmospheric takeup rate is greater than the evolution rate of the primary source. For application of the downwind calculation procedure, the blanket is modeled as being stationary over the center of the source (x = 0).

1. Secondary Source Blanket Extent for Ground-Level Releases

If a denser-than-air gas blanket is present, the (downwind) emission rate from the blanket is equal to the maximum atmospheric takeup rate. That is, for $E(t)/\pi R_p^2(t) > Q_{*max}$, a source blanket is formed over the primary source. The blanket frontal (spreading) velocity is modeled as

$$u_f = C_E \sqrt{g \left[\frac{\rho - \rho_a}{\rho_a}\right] H} \qquad \text{(B-1)}$$

where ρ is the average density of the source blanket. This gravity intrusion relationship is applicable only for $\rho > \rho_a$; the value of C_E used is 1.15 based on laboratory measurements of cloud spreading velocity (Reference B-1).

The blanket radius R as a function of time is determined by integrating $dR/dt = u_f$. When the total mass of the cloud is decreasing with time, the radius is assumed to decrease according to $(dR/dt)/R = (dH/dt)/H$ for ground-level sources. The radius of the blanket is constrained to be greater than or equal to the radius R_p of any primary (liquid) source present.

2. Secondary Source Blanket Extent for Instantaneous Releases

The gravity intrusion relationship (Equation (B-1)) will overpredict initial velocities for instantaneous, aboveground releases of a denser-than-air gas since no initial acceleration phase is included. In this case, the following procedure adapted from van Ulden (Reference B-4) is recommended.

For instantaneous gas releases, the radially symmetric cloud is considered to be composed of a tail section with height H_t and radius R_h and a head section with height H_h (Figure B-2). A momentum balance is used to account for the acceleration of the cloud from rest; the effect of ambient (wind) momentum is ignored. Although the following equations are derived assuming the primary source emission rate is zero, the resulting equations are assumed to model the secondary source cloud development when the primary source rate is nonzero. When the frontal velocity from the momentum balance is the same as Equation (B-1), the momentum balance is no longer applied and the frontal velocity is given by Equation (B-1).

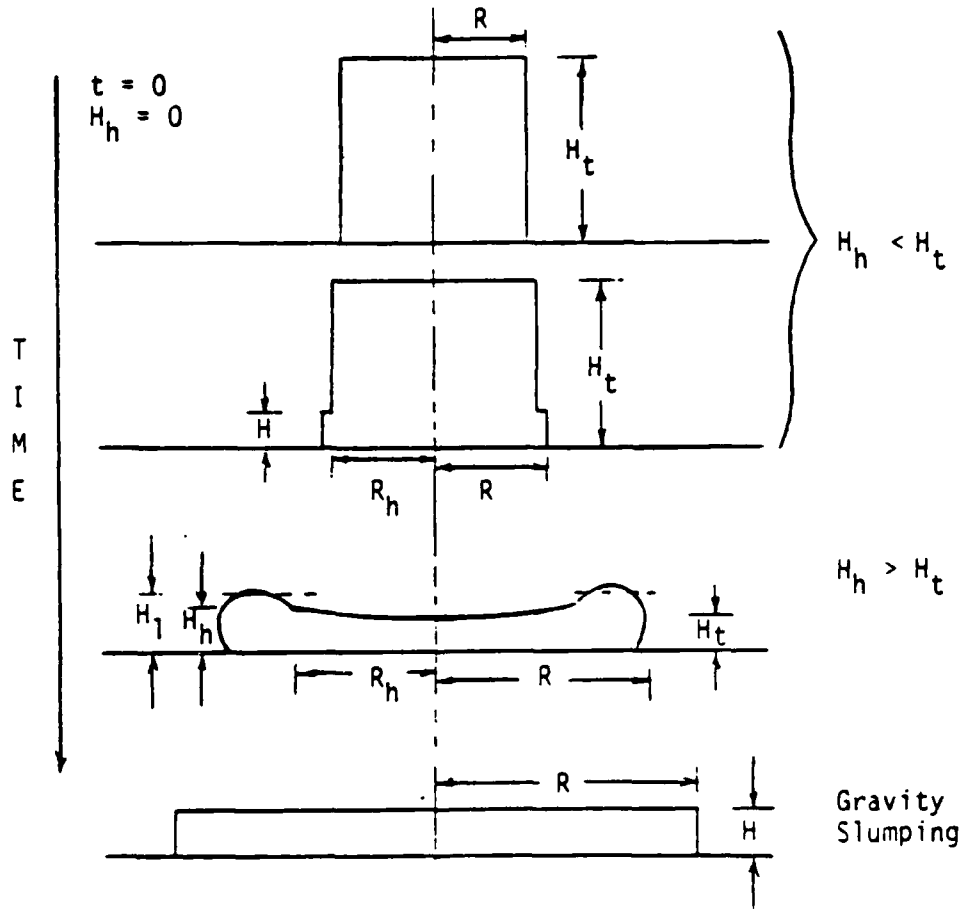

Figure B-2. Schematic Diagram of a Radially Spreading Cloud.

Three main forces act on the cloud: (1) a static pressure force (F_p), (2) a dynamic drag force (F_d), and (3) a force which accounts for the acceleration reaction of the ambient fluid, represented as a rate of virtual momentum change with respect to time ($-dP_v/dt$). Denoting the momentum of the head and tail as P_h and P_t, respectively, the momentum balance is

$$\frac{dP}{dt} = \frac{d}{dt}(P_h + P_t) = F_p + F_d - \frac{dP_v}{dt} \qquad \text{(B-2)}$$

or

$$\frac{d}{dt}(P_h + P_t + P_v) = F_p + F_d \qquad \text{(B-3)}$$

The terms in the momentum balance are evaluated differently for early times before a gravity current head has developed ($H_h < H_t$) and for times after the head has developed but the cloud is still accelerating (Figure B-2). Because the gravity current head develops so rapidly, the model equations describing the times after the gravity current head forms ($H_h \geq H_t$) are derived first. The model equations describing earlier times ($H_h < H_t$) use simplification of the equations for $H_h \geq H_t$.

a. Unsteady Gravity Current

When the cloud accelerates to the point that $H_h \geq H_t$ (Figures B-2, B-3), the frontal velocity is determined from the momentum balance (Equation (B-2)) as follows.

The static pressure force, obtained by integrating the static pressure over the boundary of the current, is

$$F_p = \left(\frac{1}{2} g\Delta\rho H_t \right) \left(2\pi R H_t \right) = \pi g \Delta\rho R H_t^2 \qquad \text{(B-4)}$$

Neglecting the shear stress at the bottom, the dynamic force on the current is the sum of the drag force on the head of the current and the lift forcethat arises due to asymmetry in the ambient flow around the head. The drag force is represented by

$$F_D = -\frac{d_v}{2} \rho_a u_f^2 \left(2\pi R_h a_v H_h \right) = -a_v d_v \pi R H_h \rho_a u_f^2 \qquad \text{(B-5)}$$

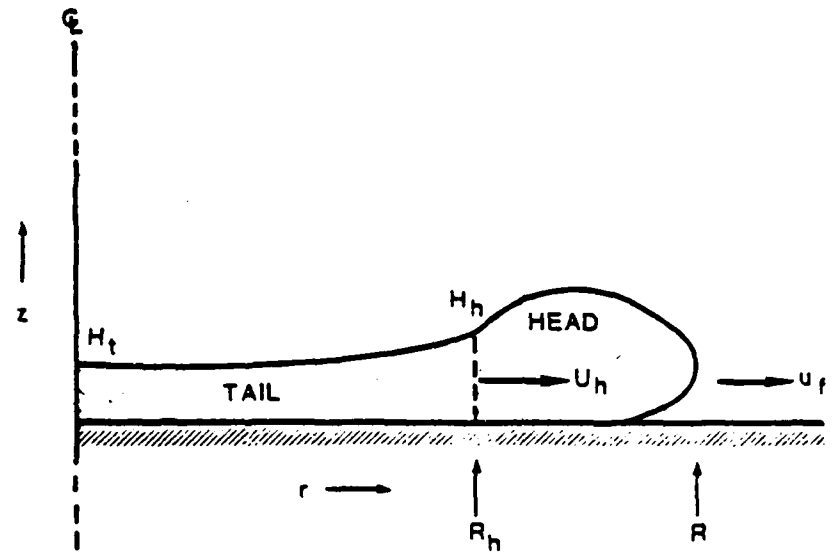

Figure B-3. The Unsteady Gravity Current (Reference B-4).

where d_v is an effective drag coefficient and the constant a_v is an empirical ratio of the average head depth H_1 to H_h ($a_v = H_1/H_h$).

The horizontal acceleration reaction ($-dP_v/dt$) is approximated by the reaction to an accelerating elliptical cylinder with an aspect ratio H/R (Reference B-5):

$$-\left(\frac{dP_v}{dt}\right)_R = -\frac{d}{dt}\left(k_1\rho_a\pi RH^2u_f\right) \tag{B-6}$$

and the vertical acceleration reaction is represented as

$$-\left(\frac{dP_v}{dt}\right)_z = -\frac{d}{dt}\left(k_2\rho_a\pi RH^2u_f\right) \tag{B-7}$$

where k_1 and k_2 are coefficients of order one. Using a single constant, Equations (B-6) and (B-7) give

$$-\frac{dP_v}{dt} = -e_v \pi \rho_a \frac{d(RH^2 u_f)}{dt} \tag{B-8}$$

Using Equations (B-4), (B-5), and (B-8), the momentum balance (Equation B-2)) becomes

$$\frac{dP}{dt} = \pi g \Delta\rho R H_t^2 - a_v d_v \pi \rho_a R H_h u_f^2 - e_v \pi \rho_a \frac{d(RH^2 u_f)}{dt} \tag{B-9}$$

Following van Ulden (Reference B-4, Reference B-6), it is assumed that the potential energy decrease due to slumping of the cloud is offset by the production of kinetic energy, which through the action of shear, is partly transformed to turbulent kinetic energy. Part of the turbulent kinetic energy is transformed back into potential energy due to entrainment of air by the cloud. This "buoyant destruction" of kinetic energy is assumed to be proportional to the rate of production of turbulent kinetic energy, and following Simpson and Britter (Reference B-7) it is assumed that the turbulent kinetic energy production rate scales as $\pi \rho_a H R u_f^3$. Then,

$$\frac{1}{2} g \Delta\rho H \frac{dV}{dt} = \epsilon \pi \rho_a H R u_f^3 \tag{B-10}$$

which can be written

$$\frac{dV}{dt} = \frac{\epsilon (2\pi RH) u_f}{\left[\frac{g\Delta\rho H}{\rho_a u_f^2}\right]} = \frac{\epsilon (2\pi RH) u_f}{Ri_f} \tag{B-11}$$

where ϵ is an empirically determined coefficient. Noting dV/dt represents the air entrainment rate,

$$\frac{\dot{M}_a}{\rho_a} = \epsilon (2\pi RH) u_f \Big/ \left[\frac{g\Delta\rho H}{\rho_a u_f^2}\right] \tag{B-12}$$

where $\dot{M}_a$ represents the air entrainment mass rate.

The volume integral

$$V = 2\pi \int_0^R h(r,t) r dr \tag{B-13}$$

where $h(r,t)$ is to be expressed in terms of H_h and H_t, and the momentum integral

$$P = 2\pi \int_0^R \rho u(r,t) h(r,t) r dr = P_t + P_h \tag{B-14}$$

are then approximated with separate analyses of the head and tail of the current.

In the tail of the current, the shallow water equations are assumed applicable. It is assumed that the shape of the current is quasi-stationary in time, and the layer-averaged density difference is assumed horizontally uniform. It follows that the volume and momentum of the tail are given by

$$V_t = \pi R_h^2 \left(H_t + H_h \right) / 2. \tag{B-15}$$

$$P_t = \frac{2}{5} \rho \left(\frac{2}{3} H_t + H_h \right) \pi R_h^3 \frac{u_f}{R} \tag{B-16}$$

A momentum balance for the head region, Figure B-4, assuming quasi-steady state, indicates that the static and dynamic pressure forces on the head should be balanced by the net flux of momentum due to flow into and out of the head. The static pressure and drag are, respectively

$$F_P = \left(\frac{1}{2} g \Delta\rho H_h \right) \left(2\pi R_h H_h \right) = \pi g \Delta\rho R_h H_h^2 \tag{B-17}$$

$$F_D = - d_v \left(\frac{1}{2} \rho_a u_f^2 \right) \left[2\pi R_h (a_v H_h) \right]$$

$$= - a_v d_v \rho_a u_f^2 \pi R_h H_h \tag{B-18}$$

Near the surface, the inward flow (u_4 in Figure B-4) carries momentum into the head, while the return flow (u_3 in Figure B-4) carries momentum out of

Figure B-4. The Head of a Steady Gravity Current (Reference B-4, Reference B-7).

the head. Assuming $u_3 \simeq u_4$, $H_4 \simeq 1/2\ H_h$, and $u_4 \simeq \delta_v u_f$, the momentum flux into the head is approximately

$$Q_h \simeq \delta_v^2 \rho_a u_f^2 \left[2\pi R_h H_h \right] \tag{B-19}$$

Upon rearranging, the momentum balance on the head gives

$$\frac{\rho_a u_f^2}{g\Delta\rho H_h} = 1./\left(a_v d_v - 2\delta_v^2 \right) = C_E^2 \tag{B-20}$$

when $\delta_v = 0.2$ and $d_v = 0.64$; Equation (B-20) then specifies the head velocity boundary condition. The volume of the head is determined by assuming that the head length scales with H_1. It follows that

$$R - R_h = b_v H_1 \tag{B-21}$$

where b_v is an empirical constant, and the volume of the head becomes

$$V_h = \pi a_v b_v (R + R_h) H_h^2 \tag{B-22}$$

If the layer-averaged velocity is assumed to increase linearly with r, it follows that

$$u_h = u_f \left(\frac{R_h}{R} \right) \tag{B-23}$$

and

$$P_h = \frac{2\pi}{3} \rho a_v \frac{u_f H_h}{R} \left[R^3 - R_h^3 \right] \tag{B-24}$$

Along with the definition of u_f,

$$\frac{dR}{dt} = u_f, \tag{B-25}$$

Equations (B-9), (B-11), (B-20), (B-21), (B-23), and (B-25) are solved to determine ρ, H_t, H_h, V, P_h, and P_t when $H_h > H_t$.

The constants a_v, b_v, d_v, e_v, and ϵ are assigned values 1.3, 1.2, 0.64, 20., and 0.59, respectively, based on analysis of the still-air denser-than-air gas release experiments of Havens and Spicer (Reference B-1).

b. Initial Gravity Current Development

To model the initial cloud shape, the tail and head height are considered constant with respect to radius. The momentum balance on the cloud is then given by

$$\frac{d}{dt} \left[P_h + P_t \right] = \pi g \Delta\rho \left[R_h H_t^2 + a_v b_v H_h^3 \right] - \pi a_v d_v \rho_a R H_h u_f^2 - \frac{dP_v}{dt} \tag{B-26}$$

where the first term on the right-hand side represents the static pressure force on the head and the second term represents the drag force on the bottom surface of the cloud. The third force is the acceleration reaction by the ambient fluid, represented by Equation (B-8).

The dimensions of the head are again given by

$$R_h = R - a_v b_v H_h \tag{B-27}$$

and

$$H_h = \left(\frac{u_f}{C_E} \right)^2 \Big/ [g\Delta\rho/\rho_a] \qquad \text{(B-28)}$$

When the height of the tail H_t is assumed uniform with respect to radius, it follows that

$$H_t = \left[\frac{M}{\rho} - \pi a_v^2 b_v (R + R_h) H_h^2 \right] \Big/ (\pi R_h^2) \qquad \text{(B-29)}$$

where M is the total mass of the cloud. The momentum of the head P_h and tail P_t are then

$$P_h = \frac{2}{3} \pi a_v \frac{\rho H_h (R^3 - R_h^3)}{R} u_f \qquad \text{(B-30)}$$

and

$$P_r = \frac{2}{3} \pi \frac{\rho H_t R_h^3}{R} u_f \qquad \text{(B-31)}$$

Equations (B-26) through (B-31) determine the momentum of the blanket as a function of time, and thus the frontal velocity u_f. The cloud accelerates from rest because $H_h = 0$ initially.

3. Material and Energy Balances

The balance on the total mass of gas in the source blanket ($M = \pi R^2 H\rho$) is

$$\frac{dM}{dt} = \frac{d}{dt} \left[\pi R^2 H\rho \right] = E(t) + \dot{M}_a + \dot{M}_{w,s} - \left(\frac{Q_{*max}}{w_c} \right) \left(\pi R^2 \right) \qquad \text{(B-32)}$$

where E(t) is the gas evolution rate from the primary (liquid) source. For spills over water, the water entrainment term ($\dot{M}_{w,s}$) is included in the source blanket description and is calculated from Equation (B-46), and the (humid) air entrainment rate (Equation (B-12)) is

$$\dot{M}_a = 2\pi RH(\epsilon u_f)\rho_a \Big/ \left(g\Delta\rho H/(\rho_a u_f^2) \right) \qquad \text{(B-33)}$$

The balance on the mass of contaminant in the source blanket ($M_c = w_c \pi R^2 H \rho$) is

$$\frac{dM_c}{dt} = \frac{d}{dt}\left[w_c \pi R^2 H \rho \right] = E(t) - Q_{*max}\,(\pi R^2) \qquad \text{(B-34)}$$

and the mass balance on the air in the source blanket ($M_a = w_a \pi R^2 H \rho$) is

$$\frac{dM_a}{dt} = \frac{d}{dt}\left[w_a \pi R^2 H \rho \right] = \frac{\dot{M}_a}{1 + H_a} - \left(\frac{Q_{*max}}{w_c} \right) w_a\,(\pi R^2) \qquad \text{(B-35)}$$

where the ambient humidity is H_a and the mass fraction of contaminant and air are $w_c = M_c/M$ and $w_a = M_a/M$, respectively.

The energy balance on the source blanket ($h\pi R^2 H \rho$) gives

$$\frac{d}{dt}\left[h \pi R^2 H \rho \right] = h_E E(t) + h_a \dot{M}_a + h_w \dot{M}_{w,s} - h \left(\frac{Q_{*max}}{w_c} \right) (\pi R^2) + \dot{Q}_s \qquad \text{(B-36)}$$

where h_E is the enthalpy of the emitted gas, h_a is the enthalpy of the ambient humid air, and h_w is the enthalpy of any water vapor entrained by the blanket if over water. There are three alternate submodels included for the heat transfer ($\dot{Q}_s$) from the surface to the cloud.

The simplest method for calculating the heat transfer between the substrate and the gas cloud is to specify a constant heat transfer coefficient for the heat transfer relation

$$\dot{Q}_s = q_s \left[\pi \left(R^2 - R_p^2 \right) \right] = h_0 \Delta T \left[\pi \left(R^2 - R_p^2 \right) \right] \qquad \text{(B-37)}$$

where $\dot{Q}_s$ is the rate of heat transfer to the cloud, q_s is the heat flux, and ΔT is the temperature difference. For the calculation of heat transfer over the source, the temperature difference is based on the average temperature of the blanket.

In the evaluation of the Burro and Coyote series of experiments, Koopman et al. (Reference B-8) proposed the following empirical heat transfer coefficient relationship for heat transfer between a cold LNG cloud and the ground

$$h_0 = V_H \rho C_p \tag{B-38}$$

where the value of V_H was estimated to be 0.0125 m/s. This constant can be varied in the model.

From the heat transfer coefficient descriptions for heat transfer from a flat plate, the following relationships can be applied. For natural convection, the heat transfer coefficient is estimated using the Nusselt (Nu), Grashoff (Gr), and Schmidt (Sc) numbers (Reference B-9) from

$$Nu = 0.14\ (Gr\ Sc)^{1/3} \tag{B-39}$$

Or

$$h_n = 0.14 \left[\frac{g \rho^2 C_p^3 \mu}{T\ Pr^2} \Delta T \right]^{1/3} \tag{B-40}$$

where h_n is the heat transfer coefficient due to natural convection and Pr is the Prandtl number. To simplify the calculations, the parameter group

$$\left[Pr^{-2} \left(C_p MW \right)^3 \left(\frac{\mu}{MW\ T} \right) \right]^{1/3} \tag{B-41}$$

is estimated to be 60 in mks units. The actual value of the group is 47.25, 58.5, and 73.4 for air, methane, and propane, respectively. Equation (B-40) becomes

$$h_n = 18 \left[\left(\frac{\rho}{MW} \right)^2 \Delta T \right]^{1/3} \tag{B-42}$$

where the density ρ, molecular weight MW, and temperature difference ΔT are based on the average composition of the gas blanket.

For forced convection, the Colburn analogy (Reference B-10) is applied to a flat plate using the Stanton number for heat transfer St_H and the Prandtl number as

$$St_H \, Pr^{2/3} = \frac{c_f}{2} = \left(\frac{u_*}{\bar{u}} \right)^2 \tag{B-43}$$

Or

$$h_f = (\bar{u}\rho C_p) \, Pr^{-2/3} \left(\frac{u_*}{\bar{u}} \right)^2 \tag{B-44}$$

where h_f is the heat transfer coefficient due to forced convection. If the velocity is evaluated at $z = H/2$ and Pr is estimated to be 0.741,

$$h_f = \left[1.22 \, \frac{u_*^2}{u_0} \left(\frac{2z_0}{H} \right)^{\alpha} \right] \rho C_p \tag{B-45}$$

If $H/2 < z_R$, then the velocity is evaluated at $z = z_R$.

The overall heat transfer coefficient is then the maximum of the forced and natural coefficients, i.e. $h_0 = \max(h_f, h_n)$. The heat flux and transfer rate are then estimated by Equation (B-37).

If the gas blanket is formed over water, water will be transferred from the surface to the cloud by a partial pressure driving force associated with the temperature difference between the surface and the gas blanket. The rate of mass transfer of water is

$$\dot{M}_{w,s} = \frac{F_0}{p} \left(p^*_{w,s} - p_{w,c} \right) \left[\pi \left(R^2 - R_p^2 \right) \right] \tag{B-46}$$

where F_0 is the overall mass transfer coefficient. The driving force is the difference of the vapor pressure of water at the surface temperature $p^*_{w,s}$ and the partial pressure of water in the cloud, $p_{w,c}$. (The water partial pressure in the cloud is the minimum of: (1) the water mole fraction times the ambient pressure; or (2) the water vapor pressure at the cloud temperature ($p^*_{w,c}$).) The natural convection coefficient is based on the heat transfer coefficient and the analogy between the Sherwood number

(Sh) and the Nusselt number (Nu) suggested by Bird et al. (Reference B-11)

$$Sh = Nu = 0.14\ (Gr\ Sc)^{1/3} = \frac{F_n L}{\mathcal{D}} \left(\frac{MW}{\rho} \right) \tag{B-47}$$

If the Schmidt number is taken as 0.6, and $\left(\frac{\mu}{T\ MW} \right)$ is estimated to be 2.2×10^{-9} in mks units,

$$F_n = 9.9 \times 10^{-3} \left[\left(\frac{\rho}{MW} \right)^2 \Delta T \right]^{1/3} \tag{B-48}$$

For forced convection, Treybal (Reference B-10) suggests that the Stanton number for mass transfer St_M and the Stanton number for heat transfer St_H are related by

$$St_M = St_H \left(\frac{Pr}{Sc} \right)^{2/3} = 1.15\ St_H \tag{B-49}$$

Or,

$$F_f = \frac{20.7\ h_0}{MW\ C_p} \tag{B-50}$$

The overall mass transfer coefficient F_0 is calculated as the larger of the natural and forced convection coefficients.

For the case when the primary (liquid) source emission rate E(t) is larger than the atmospheric takeup rate $Q_{*max}\pi R_p^2$, Equations (B-32), (B-34), (B-35), and (B-36) are integrated for the mass, concentration, and enthalpy of the gas blanket along with an appropriate equation of state (i.e. relationship between enthalpy and temperature and between temperature and density).

For the case when the emission rate is not sufficient to form a gas blanket, the flux of contaminant is not determined by the maximum atmospheric takeup rate. Consider the boundary layer formed by the emission of gas into the atmosphere above the primary source. If the source is modeled to have a uniform width 2b and entrain no air along the sides of the layer, the balance on the total material ($\rho_L u_L H_L$) in a differential slice of the layer is

$$\frac{d}{dx} \left[\rho_L u_L H_L \right] = \rho_a w_e + \left(\frac{Q_*}{w_c} \right) \tag{B-51}$$

where w_e is the vertical rate of of air entrainment into the layer given by Equation (B-83), ρ_L is the average density of the slice, and Q_*/w_c is the total flux of gas from the primary (liquid) source. The balance on the mass flow rate of contaminant ($w_c \rho_L u_L H_L$) at any ($x - x_{up}$) is

$$c_{c,L} u_L H_L = Q_* (x - x_{up}) \tag{B-52}$$

With an equation of state to relate $c_{c,L}$ and ρ_L, Equation (B-51) is integrated from the upwind edge of the source ($x = x_{up}$) to the downwind edge ($x = L + x_{up}$).

In order to generate the initial conditions for the downwind dispersion calculations, the maximum concentration c_c and the vertical dispersion parameter S_z are needed. Since Equations (B-51) and (B-52) are written for a vertically averaged layer, consider the vertical average of the power law distribution. The height of the layer H_L is the height to some concentration level, say 10 percent of the maximum. Although strictly a function of α, this value is modeled by

$$H_L = \delta_L H_{EFF} \tag{B-53}$$

where H_{EFF} is the effective height defined by Equation (B-79) and δ_L is 2.15. The vertically averaged concentration $c_{c,L}$ can be defined by

$$c_{c,L} H_L = \int_0^\infty c \, dz \tag{B-54}$$

And similarly, the effective transport velocity u_L is defined by

$$c_{c,L} u_L H_L = \int_0^\infty c u_x \, dz \tag{B-55}$$

With Equation (B-53) and defining relations for H_{EFF} and u_{EFF} (Equations (B-79) and (B-93), respectively), it follows that

$$c_c = \delta_L c_{c,L} \tag{B-56}$$

$$u_L H_L = \delta_L \left(\frac{u_0 z_0}{1 + \alpha} \right) \left(\frac{S_z}{z_0} \right)^{1+\alpha} \tag{B-57}$$

and

$$\delta_L w_e' = w_e \tag{B-58}$$

where w_e' is given by Equation (B-83).

4. Maximum Atmospheric Takeup Rate

The maximum atmospheric takeup rate will be the largest takeup rate which satisfies Equations (B-51) and (B-52). As well, the maximum concentration of contaminant in the power law profile at the downwind edge of the source will be the source contaminant concentration $(c_c)_s$. If Equations (B-51) and (B-52) are combined along with the assumption of adiabatic mixing of ideal gases with the same constant molal heat capacity (i.e. $\left[\frac{\rho - \rho_a}{c_c}\right] = \gamma$ = constant), the maximum takeup flux is modeled by

$$Q_{*max} = (c_c)_s \frac{ku_*(1 + \alpha)}{\hat{\phi}} \left[\frac{\delta_L}{\delta_L - 1}\right] \tag{B-59}$$

where

$$\frac{1}{\hat{\phi}} = \frac{1}{L}\int_0^L \frac{dx}{\phi(Ri_*)} \tag{B-60}$$

where $\phi(Ri_*)$ is given in Equation (B-76) for $\rho > \rho_a$.

An upper bound of the atmospheric takeup flux can be characterized by the condition where the source begins to spread as a gravity intrusion against the approach flow. In water flume experiments, Britter (Reference B-12) measured the upstream and lateral extent of a steady-state plume from a circular source as a function of Ri_*. A significant upstream spread was obtained for $Ri_* > 32$, and lateral spreading at the center of the source was insignificant for $Ri_* < 8$. The presence of any significant lateral spreading represents a lower bound on the conditions of the maximum takeup flux.

The integral of Equation (B-60) is calculated using a local Richardson number of

$$Ri_*(x) = \zeta(x - x_{up})^{\frac{1}{1+\alpha}} \tag{B-61}$$

where

$$\zeta = g\left[\frac{\rho - \rho_a}{\rho_a}\right]\frac{z_0}{u_*^2}\frac{\Gamma\left(\frac{1}{1+\alpha}\right)}{1+\alpha}\left[\frac{ku_*(1+\alpha)}{\phi_c}\left[\frac{1+\alpha}{u_0 z_0}\right]\left[\frac{\delta_L}{\delta_L - 1}\right]\right]^{\frac{1}{1+\alpha}} \tag{B-62}$$

and ϕ_c is 3.1 (corresponding to $Ri_* = 20(8 < Ri_* < 32)$). Using this $Ri_*(x)$, Equation (B-60) is

$$\frac{1}{\hat{\phi}} = \frac{1}{L}\int_0^L \frac{dx}{0.88 + 0.099\,\zeta^{1.04}\,x^{\frac{1.04}{1+\alpha}}}$$

To simplify the numerical problem, the integral is approximated as

$$\frac{1}{\hat{\phi}} = \frac{1}{0.099\,L\,\zeta^{1.04}}\ln\left[\frac{0.88 + 0.099\,\zeta^{1.04}\,L^{\left(\frac{1.04}{1+\alpha}\right)}}{0.88}\right] \tag{B-63}$$

which then specifies the maximum atmospheric takeup flux.

5. Transient Denser-than-Air Gas Release Simulation

If a steady-state spill is being simulated, the transient source calculation is carried out until the source characteristics are no longer varying significantly with time. The maximum centerline concentration c_c, the horizontal and vertical dispersion parameters S_y and S_z, the half width b, and if necessary, the enthalpy h are used as initial conditions for the downwind calculation specified in a transient spill.

If a transient spill is being simulated, the spill is modeled as a series of pseudo-steady-state releases. Consider a series of observers traveling with the wind over the transient gas source described above; each observer originates from the point which corresponds with the maximum upwind extent of the gas blanket ($x = -R_{max}$). The desired observer

velocity is the average transport velocity of the gas u_{EFF} from Equation (B-93); however, the value of u_{EFF} will differ from observer to observer with the consequence that some observers may be overtaken by others. For a neutrally buoyant cloud, u_{EFF} becomes a function of downwind distance alone which circumvents this problem. With this functionality, Colenbrander (Reference B-2) models the observer velocity as

$$u_i(x) = \frac{u_0}{\Gamma\left(\frac{1}{1+\alpha}\right)} \left(\frac{S_{z_{0m}}}{z_0} \right)^{\alpha} \left[\frac{x + R_{max}}{\frac{\sqrt{\pi}}{2} R_m + R_{max}} \right]^{\alpha/(1+\alpha)} \tag{B-64}$$

where $S_{z_{0m}}$ is the value of S_{z_0} when the averaged source rate ($\pi R^2 Q_*$) is a maximum and the subscript i denotes observer i. Noting that $u_i(x) = dx_i/dt$, observer position and velocity as functions of time are determined.

A pseudo-steady-state approximation of the transient source is obtained as each observer passes over the source. If t_{up_i} and t_{dn_i} denote the times when observer i encounters the upwind and downwind edges of the source, respectively, then the source fetch seen by observer i is:

$$L_i = x_{up_i} - x_{dn_i} \tag{B-65}$$

The width of the source $2B_i'(t)$ is defined by

$$B_i'^2(t) = R^2(t) - x_i^2(t) \tag{B-66}$$

Then the gas source area seen by observer i is

$$2L_i b_i = 2 \int_{t_{up_i}}^{t_{dn_i}} B_i' u_i dt \tag{B-67}$$

where $2b_i$ is the average width.

The takeup rate of contaminant $2(Q_* Lb)_i$ is calculated as

$$2(Q_* Lb)_i = 2 \int_{t_{up_i}}^{t_{dn_i}} Q_* B_i' u_i dt \tag{B-68}$$

The total mass flux rate from the source is

$$2(\rho_L u_L H_L b)_i = 2 \int_{t_{up_i}}^{t_{dn_i}} \left[\rho_a w_e' + \left(\frac{Q_*}{w_c} \right) \right] B_i' u_i dt \tag{B-69}$$

With these equations, the average composition of the layer can be determined at each $x - x_{up}$ over the source. With the enthalpy of the layer given by

$$2(h_L \rho_L u_L H_L b)_i = 2 \int_{t_{up_i}}^{t_{dn_i}} h \left(\frac{Q_*}{w_c} \right) B_i' u_i dt \tag{B-70}$$

(due to the choice of the reference temperature as the ambient temperature) and with a suitable equation of state relating enthalpy, temperature, and density, the source can be averaged for each observer. After the average composition of the layer is determined at the downwind edge, an adiabatic mixing calculation is performed between this gas and the ambient air. This calculation represents the function between density and concentration for the remainder of the calculation if the calculation is adiabatic; it represents the adiabatic mixing condition if heat transfer is included in the downwind calculation.

For each of several observers released successively from $x = -R_{max}$, the observed dimensions L and b, the downwind edge of the source x_{dn}, the average vertical dispersion coefficient S_z, the average takeup flux Q_*, the centerline concentration c_c, and if applicable, the average enthalpy h_L can be determined for each observer. With these input values, a steady-state calculation is made for each observer. The distribution parameters for any specified time t_s are determined by locating the position of the series of observers at time t_s, i.e. $x_i(t_s)$. The corresponding concentration distribution is then computed from the assumed profiles.

B. STEADY-STATE DOWNWIND DISPERSION

The model treats dispersion of gas entrained into the wind field from an idealized, rectangularly shaped source of width 2b and length L. The circular source cloud is represented as an equivalent area rectangle ($\pi R^2 = 2bL$) with equivalent fetch ($L = 2R$). Similarity forms for the concentration profiles are assumed which represent the plume as being composed of a horizontally homogeneous section with Gaussian concentration profile edges as follows:

$$c(x,y,z) = c_c(x) \exp\left[- \left(\frac{|y| - b(x)}{S_y(x)} \right)^2 - \left(\frac{z}{S_z(x)} \right)^{1+\alpha} \right] \quad \text{for } |y| > b$$

$$= c_c(x) \exp\left[- \left(\frac{z}{S_z(x)} \right)^{1+\alpha} \right] \quad \text{for } |y| \leq b \qquad \text{(B-71)}$$

A power law wind velocity profile is assumed

$$u_x = u_0 \left(\frac{z}{z_0} \right)^{\alpha} \qquad \text{(B-72)}$$

where the value of α is determined by a weighted least-squares fit of the logarithmic profile

$$u_x = \frac{u_*}{k} \left[\ln\left(\frac{z + z_R}{z_R} \right) - \psi\left(\frac{z}{\lambda} \right) \right] \qquad \text{(B-73)}$$

Functional forms for ψ and typical values of α are given in Table B-1 for different Pasquill stability categories. With these profiles, the parameters of Equation (B-71) are constrained by ordinary differential equations.

1. Vertical Dispersion

The vertical dispersion parameter S_z is determined by requiring that it satisfy the diffusion equation

TABLE B-1. TYPICAL ATMOSPHERIC BOUNDARY LAYER STABILITY AND WIND PROFILE CONCENTRATIONS

Pasquill Stability Category	Monin-Obukhov Length (λ) as a Function of Surface Roughness z_R(m)[1]	Typical Power Law Exponents α in Eq. (B-72)	Corrections to Logarithmic Profiles as Given by Businger et al. (Reference 20) ψ in Eq. (B-73)
A	$-11.4\ z_R^{0.10}$	0.108	$\psi = 2\ln\left[\frac{1+a}{2}\right] + \ln\left[\frac{1+a^2}{2}\right] - 2\tan^{-1}(a) + \frac{\pi}{a}$, with $a = (1-15(z/\lambda))^{1/4}$
B	$-26.0\ z_R^{0.17}$	0.112	
C	$-123\ z_R^{0.30}$	0.120	
D	∞	0.142	$\psi = 0$
E	$123\ z_R^{0.30}$	0.203	$\psi = -4.7(z/\lambda)$
F	$26.0\ z_R^{0.17}$	0.253	

[1] Curve fit of data from Pasquill (Reference 17).

$$u_x \frac{\partial c}{\partial x} = \frac{\partial}{\partial z} K_z \frac{\partial c}{\partial z} \tag{B-74}$$

with the vertical turbulent diffusivity given by

$$K_z = \frac{k u_* z}{\phi(Ri_*)} \tag{B-75}$$

The function $\phi(Ri_*)$ is a curve fit of laboratory-scale data for vertical mixing in stably density-stratified fluid flows reported by Kantha et al. (Reference B-2), Lofquist (Reference B-14), and McQuaid (Reference B-15) for $Ri_* > 0$. For $Ri_* < 0$, the function $\phi(Ri_*)$ is taken from Colenbrander and Puttock (Reference B-3) and has been modified so the passive limit of the two functions agree as follows:

$$\begin{aligned} \phi(Ri_*) &= 0.88 + 0.099\, Ri_*^{1.04} && Ri_* \geq 0 \\ &= 0.88/(1 + 0.65\, |Ri_*|^{0.6}) && Ri_* < 0 \end{aligned} \tag{B-76}$$

The friction velocity is calculated using Equation (B-73) from a known velocity u_0 at a specific height z_0. Combining the assumed similarity forms for concentration and velocity, Equations (B-71), (B-72), (B-74), and (B-75) give

$$\frac{d}{dx}\left[\left(\frac{u_0 z_0}{1+\alpha}\right)\left(\frac{S_z}{z_0}\right)^{1+\alpha}\right] = \frac{k u_* (1+\alpha)}{\phi(Ri_*)} \tag{B-77}$$

where the Richardson number Ri_* is computed as

$$Ri_* = g\left(\frac{\rho - \rho_a}{\rho_a}\right)\frac{H_{EFF}}{u_*^2} \tag{B-78}$$

and the effective cloud depth is defined as

$$H_{EFF} = \frac{1}{c_c}\int_0^\infty c\,dz = \Gamma\left(\frac{1}{1+\alpha}\right)\frac{S_z}{1+\alpha} \tag{B-79}$$

Equation (B-77) can be viewed as a volumetric balance on a differential slice of material downwind of the source. For a mass balance over the same slice,

$$\frac{d}{dx}\left(\rho_L u_L H_L \right) = \rho_a w_e \tag{B-80}$$

which is the same result as Equation (B-51) without the source term. With Equations (B-57) and (B-58), this becomes

$$\frac{d}{dx}\left(\rho_L u_{EFF} H_{EFF} \right) = \rho_a w_e' \tag{B-81}$$

Using the assumption of adiabatic mixing of ideal gases with the same constant molal heat capacity (i.e. $\frac{\rho - \rho_a}{c_c}$ = constant) along with the contaminant material balance, the mass balance becomes

$$\frac{d}{dx}\left(u_{EFF} H_{EFF} \right) = w_e' \tag{B-82}$$

which leads to

$$w_e' = \frac{w_e}{\delta_L} = \frac{k u_* (1 + \alpha)}{\phi(Ri_*)} \tag{B-83}$$

Equations (B-81) and (B-83) are combined to give

$$\frac{d}{dx}\left(\rho_L u_{EFF} H_{EFF} \right) = \frac{\rho_a k u_* (1 + \alpha)}{\phi(Ri_*)} \tag{B-84}$$

Furthermore, Equation (B-84) is assumed to apply when $(\rho - \rho_a)/c_c$ is not constant.

When heat transfer from the surface is present, vertical mixing will be enhanced by the convection turbulence due to heat transfer. Zeman and Tennekes (Reference B-16) model the resulting vertical turbulent velocity as

$$\frac{w}{u_*} = \left[1 + \frac{1}{4}\left(\frac{w_*}{u_*} \right)^2 \right]^{1/2} \tag{B-85}$$

where w_* is the convective scale velocity described as

$$\left(\frac{w_*}{u_*} \right)^2 = \left[\frac{gh}{u_* \bar{u}} \frac{\left(T_s - T_{c,L} \right)}{T_{c,L}} \right]^{2/3} \tag{B-86}$$

If $\bar{u}$ is is evaluated at H_{EFF},

$$\frac{w}{u_*} = \left(1 + \frac{1}{4} Ri_T^{2/3} \right)^{1/2} \tag{B-87}$$

where

$$Ri_T = g \left(\frac{T_s - T_{c,L}}{T_{c,L}} \right) \frac{H_{EFF}}{u_* u_0} \left(\frac{z_0}{H_{EFF}} \right)^{\alpha} \tag{B-88}$$

and $T_{c,L}$ is the temperature obtained from the energy balance of Equations (B-102) and (B-103). Equation (B-84) is modified to account for this enhanced mixing by

$$\frac{d}{dx} \left(\rho_L u_{EFF} H_{EFF} \right) = \frac{\rho_a kw(1 + \alpha)}{\phi(Ri'_*)} \tag{B-89}$$

where $Ri'_* = Ri_* \left(\frac{u_*}{w} \right)^2$.

Although derived for two-dimensional dispersion, this is extended for application to a denser-than-air gas plume which spreads laterally as a density intrusion:

$$\frac{d}{dx} \left(\rho_L u_{EFF} H_{EFF} B_{EFF} \right) = \frac{\rho_a kw(1 + \alpha)}{\phi(Ri'_*)} B_{EFF} \tag{B-90}$$

where the plume effective half width is defined by

$$B_{EFF} = b + \frac{\sqrt{\pi}}{2} S_y \tag{B-91}$$

and determined using the gravity intrusion relation

$$\frac{dB_{EFF}}{dt} = C_E \left[g \left(\frac{\rho - \rho_a}{\rho_a} \right) H_{EFF} \right]^{1/2} \tag{B-92}$$

The average transport velocity in the plume is defined by

$$u_{EFF} = \frac{\int_0^\infty cu_x dz}{\int_0^\infty c dz} = u_0 \left(\frac{S_z}{z_0} \right)^\alpha \Big/ \Gamma \left(\frac{1}{1+\alpha} \right) \tag{B-93}$$

and the lateral spread of the cloud is modeled by

$$\frac{dB_{EFF}}{dx} = \frac{1}{u_{EFF}} \frac{dB_{EFF}}{dt}$$

$$= C_E \left[\frac{g z_0 \Gamma^3 \left(\frac{1}{1+\alpha} \right)}{u_0^2 (1+\alpha)} \right]^{1/2} \left[\frac{\rho - \rho_a}{\rho_a} \right]^{1/2} \left(\frac{S_z}{z_0} \right)^{\left(\frac{1}{2} - \alpha \right)} \tag{B-94}$$

2. Horizontal Dispersion

The crosswind similarity parameter $S_y(x)$ is also determined by requiring that it satisfy the diffusion equation

$$u_x \frac{\partial c}{\partial x} = \frac{\partial}{\partial y} \left[K_y \frac{\partial c}{\partial y} \right] \tag{B-95}$$

with the horizontal turbulent diffusivity given by

$$K_y = K_0 u_x B_{EFF}^{\gamma_1} \tag{B-96}$$

When $b = 0$, $S_y = \sqrt{2}\,\sigma_y$, where σ_y is the similarity parameter correlated by Pasquill (Reference B-16) in the form $\sigma_y = \delta x^\beta$. Furthermore, Equations (B-95) and (B-96) require that

$$\sigma_y \frac{d\sigma_y}{dx} = K_0 B_{EFF}^{\gamma_1} \tag{B-97}$$

where $\gamma_1 = 2 - 1/\beta$ and $K_0 = \frac{2\beta}{\pi} (\delta\sqrt{\pi/2})^{1/\beta}$. Then,

$$S_y \frac{dS_y}{dx} = \frac{4\beta}{\pi} B_{EFF}^2 \left[\frac{\delta\sqrt{\pi/2}}{B_{EFF}} \right]^{1/\beta} \tag{B-98}$$

where Equation (B-98) is also assumed applicable for determining S_y when b is not zero.

At the downwind distance x_t where b = 0, the crosswind concentration profile is assumed Gaussian with S_y given by

$$S_y = \sqrt{2}\ \delta(x + x_v)^{\beta} \tag{B-99}$$

where x_v is a virtual source distance determined as

$$S_y(x_t) = \sqrt{2}\ \delta(x_t + x_v)^{\beta} \tag{B-100}$$

The gravity spreading calculation is terminated for $x > x_t$.

For a steady plume, the centerline concentration c_c is determined from the material balance

$$E = \int_0^{\infty} \int_{-\infty}^{\infty} cu_x dydz = 2c_c \left(\frac{u_0 z_0}{1 + \alpha} \right) \left(\frac{S_z}{z_0} \right)^{1+\alpha} B_{EFF} \tag{B-101}$$

where E is the plume source strength.

3. Energy Balance

For some simulations of cryogenic gas releases, heat transfer to the plume in the downwind dispersion calculation may be important, particularly in low wind conditions. The source calculation determines a gas/air mixture initial condition for the downwind dispersion problem. Air entrained into the plume is assumed to mix adiabatically. Heat transfer to the plume downwind of the source adds additional heat. This added heat per unit mass D_h is determined by an energy balance on a uniform cross section as

$$\frac{d}{dx} \left[D_h \rho_L u_{EFF} H_{EFF} \right] = q_s / \delta_L \tag{B-102}$$

where q_s is determined by Equation (B-37) along with the desired method of calculating h_0. Equation (B-102) is applied when b = 0 and is extended to

$$\frac{d}{dx} \left[D_h \rho_L u_{EFF} H_{EFF} B_{EFF} \right] = q_s B_{EFF} / \delta_L \tag{B-103}$$

when $b > 0$. Since the average density of the layer ρ_L cannot be determined until the temperature (i.e. D_h) is known, a trial and error procedure is required.

Equations (B-77), (B-78), (B-79), (B-87)-(B-91), (B-94), and (B-98)-(B-103) are combined with an equation of state relating cloud density to gas concentration and temperature and are solved simultaneously to predict S_z, S_y, c_c, and b as functions of downwind distance beginning at the downwind edge of the gas source.

C. CORRECTION FOR ALONG-WIND DISPERSION

Following Colenbrander (Reference B-2), an adjustment to c_c is applied to account for dispersion parallel to the wind direction. The calculated centerline concentration $c_c(x)$ is considered to have resulted from the release of successive planar puffs of gas ($c_c(x)\Delta x$) without any dispersion in the x-direction. If it is assumed that each puff diffuses in the x-direction as the puff moves downwind independently of any other puff and that the dispersion is one-dimensional and Gaussian, the x-direction concentration dependence is given by

$$c_c'(x;x_{p_i}) = \frac{c_c(x_{p_i})\Delta x_i}{\sqrt{2\pi}\,\sigma_x} \exp\left[-\frac{1}{2}\left[\frac{x - x_{p_i}}{\sigma_x}\right]^2\right] \qquad \text{(B-104)}$$

where x_{p_i} denotes the position of the puff center due to observer i.

After Beals (Reference B-18), the x-direction dispersion coefficient σ_x is assumed to be a function of distance from the downwind edge of the gas source ($X = x - x_0$) and atmospheric stability given by

$$\begin{aligned} \sigma_x(X) &= 0.02\,X^{1.22} && \text{unstable, } x \geq 130 \text{ m} \\ &= 0.04\,X^{1.14} && \text{neutral, } x \geq 100 \text{ m} \\ &= 0.17\,X^{0.97} && \text{stable, } x \geq 50 \text{ m} \end{aligned} \qquad \text{(B-105)}$$

where ($X = x - x_0$) and σ_x are in meters. The concentration at x is then determined by superposition, i.e., the contribution to c_c at a given x from neighboring puffs is added to give an x-direction corrected value of c_c'. For N observers,

$$c_c'(x) = \sum_{i=1}^{N} \frac{c_c(x_{p_i})}{\sqrt{2\pi}\,\sigma_x} \exp\left[-\frac{1}{2}\left[\frac{x - x_{p_i}}{\sigma_x} \right]^2 \right] \Delta x_i \qquad \text{(B-106)}$$

and for large N,

$$c_c'(x) = \frac{1}{\sqrt{2\pi}} \int_0^{\infty} \frac{c_c(\xi)}{\sigma_x(\xi - \xi_0)} \exp\left[-\frac{1}{2}\left[\frac{x - \xi}{\sigma_x(\xi - \xi_0)} \right]^2 \right] d\xi \qquad \text{(B-107)}$$

The corrected centerline concentration c_c' is used in the assumed profiles in place of c_c, along with the distribution parameters S_y, S_z, and b.

D. DEGADIS MODEL INPUTS AND OUTPUTS

As implemented under VAX/VMS*, DEGADIS requires three areas of input information:

- simulation definition
- numerical parameters
- VAX/VMS command procedure for execution

DEGADISIN is the interactive input module which generates the simulation definition from user responses. An example input session is included in Section D.3. The numerical parameters (convergence criteria, initial increments, etc.) are supplied to DEGADIS through a series of input files. Although these numerical parameters are easily changed, the user should need to change these only rarely with the exception of the time sort parameters. The VAX/VMS command procedure used to execute DEGADIS is generated in DEGADISIN by default. Additional information can be found in Havens and Spicer (Reference B-1).

1. VAX/VMS Command Procedure

The VAX/VMS command procedure generated by DEGADISIN controls the execution of images for the simulation. Image execution follows one of two paths, either for a transient release or for a steady-state release.

---

*VAX and VMS are registered trademarks of Digital Equipment Corporation.

DEGADISIN will automatically generate the appropriate command procedure. DEGADISIN requires a simulation name be specified. The simulation name must be a valid VAX/VMS file name without a file extension and is designated herein as RUNNAME. DEGADIS will use this file name with standard extensions for input, interprocess communication, and output.

2. Simulation Definition

DEGADISIN is an interactive method of simulation definition where the user specifies information about the ambient wind field, the properties of the released gas, and some details of the release. A summary of required input information is included in Figure B-5.

The ambient wind field is characterized by a known velocity u_0 at a given height z_0, a surface roughness z_R, and the Pasquill stability class. The Pasquill stability class along with the desired averaging time are used to estimate values of the lateral similarity parameter coefficients δ and β (References B-17 and B-19 and Appendix D), values of the along-wind similarity coefficients (Reference B-18), and the Monin-Obukhov length λ used by Businger et al. (Reference B-20) in their logarithmic velocity profile function. The Monin-Obukhov length is then used to calculate the friction velocity u_*. Once these parameters have been estimated using the Pasquill stability class, the user has the option of interactively changing any of these to better describe the simulation. In addition to these specifications, the ambient temperature, pressure, and humidity must be specified.

The properties of air and the released gas are used to evaluate the mixture density as a function of temperature and composition. The desired released gas properties include the molecular weight MW_c, the storage temperature (normal boiling point for cryogenic gases) T_0, the vapor phase density at the storage temperature and ambient pressure ρ_0, and two constants q_1 and p_1 which describe the heat capacity according to the equation

$$C_{p_c}(T) = (MW_c)^{-1} \left[3.33 \times 10^4 + q_1 \left[\frac{T^{p_1} - T_0^{p_1}}{T - T_0} \right] \right] \qquad \text{(B-108)}$$

where $C_{p_c}(T)$ is the mean heat capacity (J/kg K) at temperature T. Note that a constant heat capacity with respect to temperature can be

DECADISIN

Variable	Symbol	Units	Comments
TITLE:			Text title block 4 lines of 80 spaces
U0	u_0	m/s	Reference velocity
Z0	z_0	m	Reference height
ZR	z_R	m	Roughness length
DELTA	δ	$m^{1-\beta}$	Lateral similarity coefficient
BETA	β	N/A	Lateral similarity power
ML	λ	m	Monin-Obukhov length
SIGX_COEFF			Along-wind similarity coefficient
SIGX_POW		N/A	Along-wind similarity power
SIGX_MIN_DIST		m	Minimum distance to apply along-wind dispersion correction
TAMB	T	K	Ambient temperature
PAMB	p	atm	Ambient pressure

Figure B-5. Summary of Simulation Definition Input Information for DEGADIS.

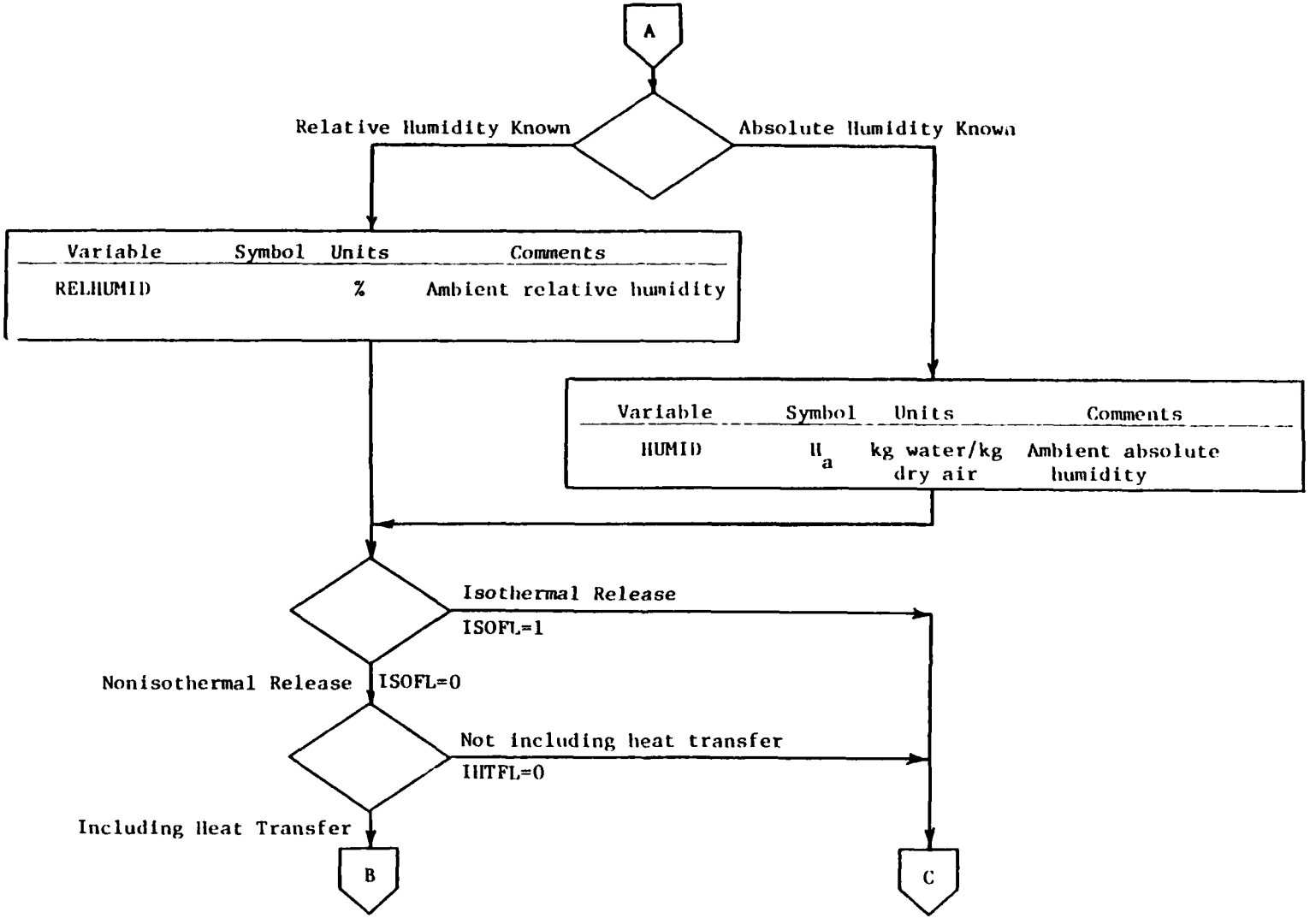

Figure B-5. Summary of Simulation Definition Input Information for DEGADIS (Continued).

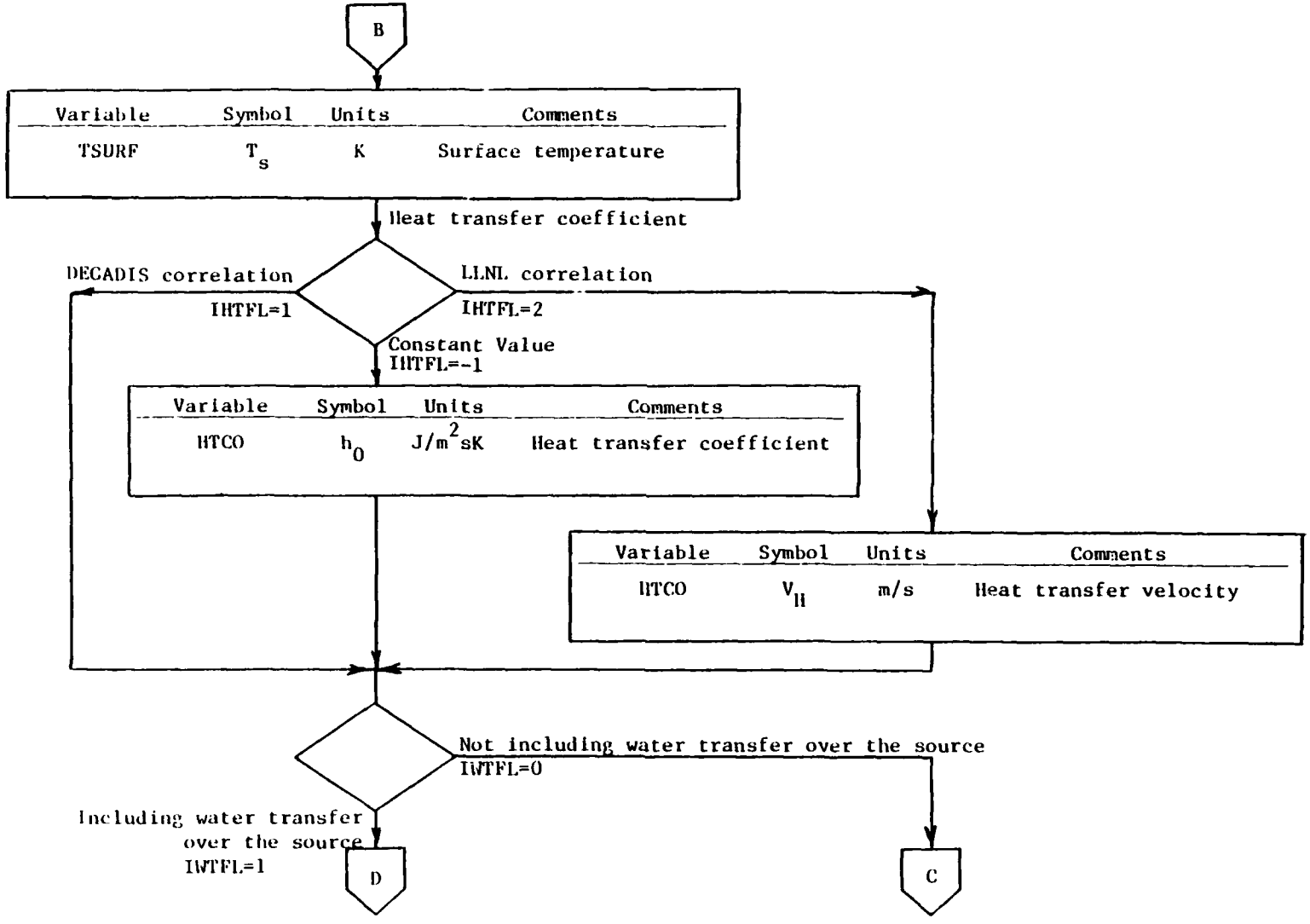

Figure B-5. Summary of Simulation Definition Input Information for DEGADIS (Continued).

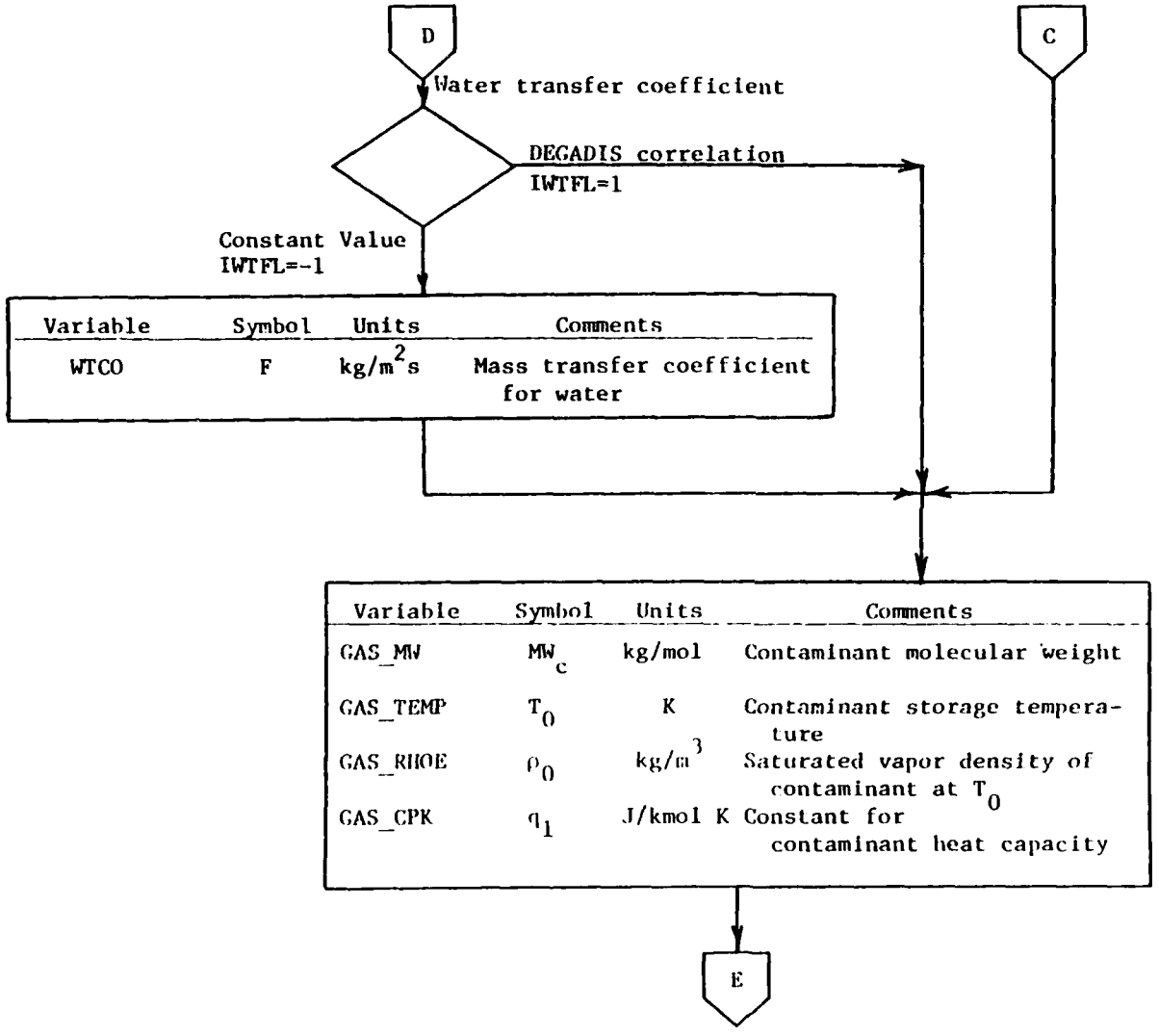

Figure B-5. Summary of Simulation Definition Input Information for DEGADIS (Continued).

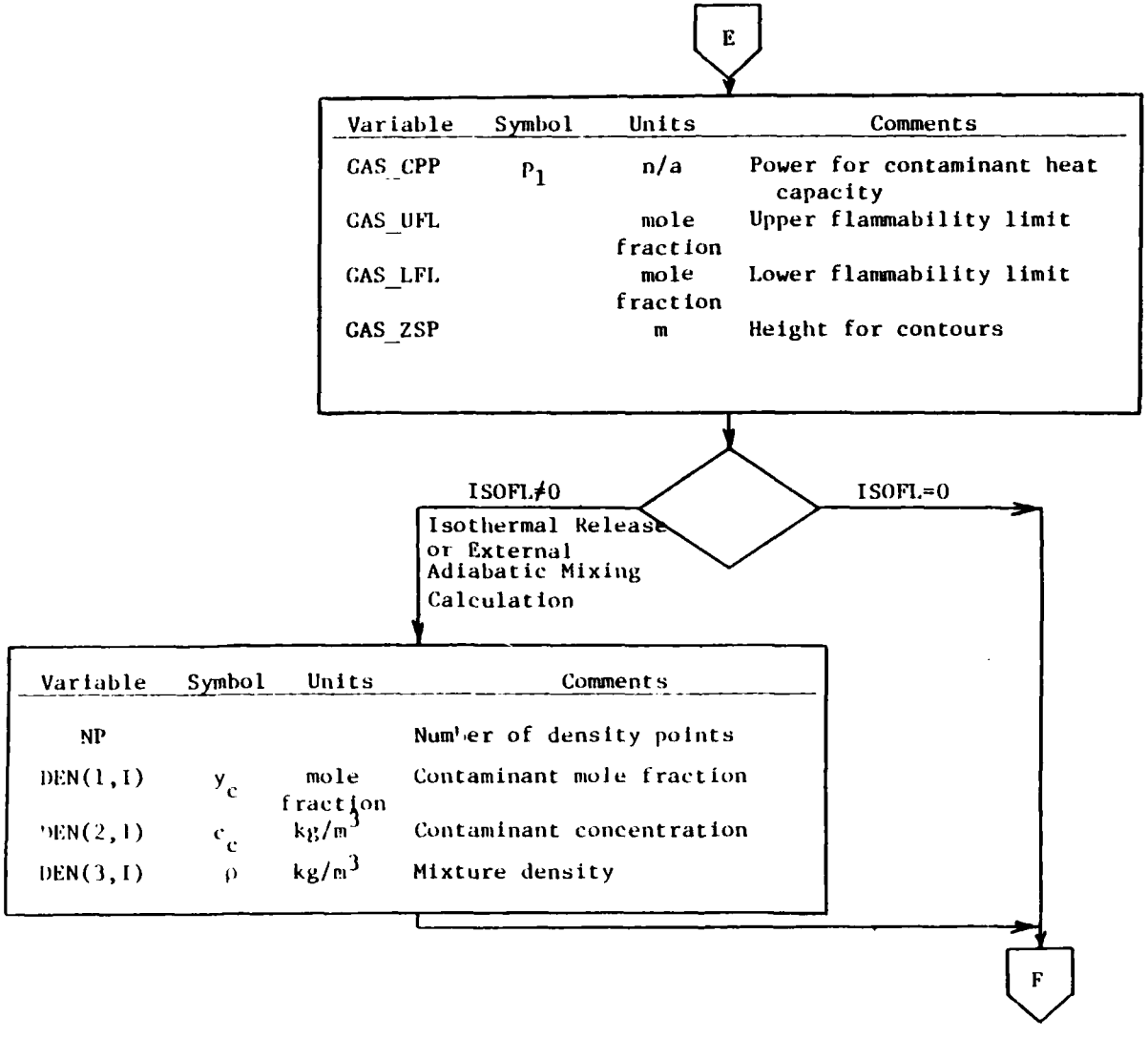

Figure B-5. Summary of Simulation Definition Input Information for DEGADIS (Continued).

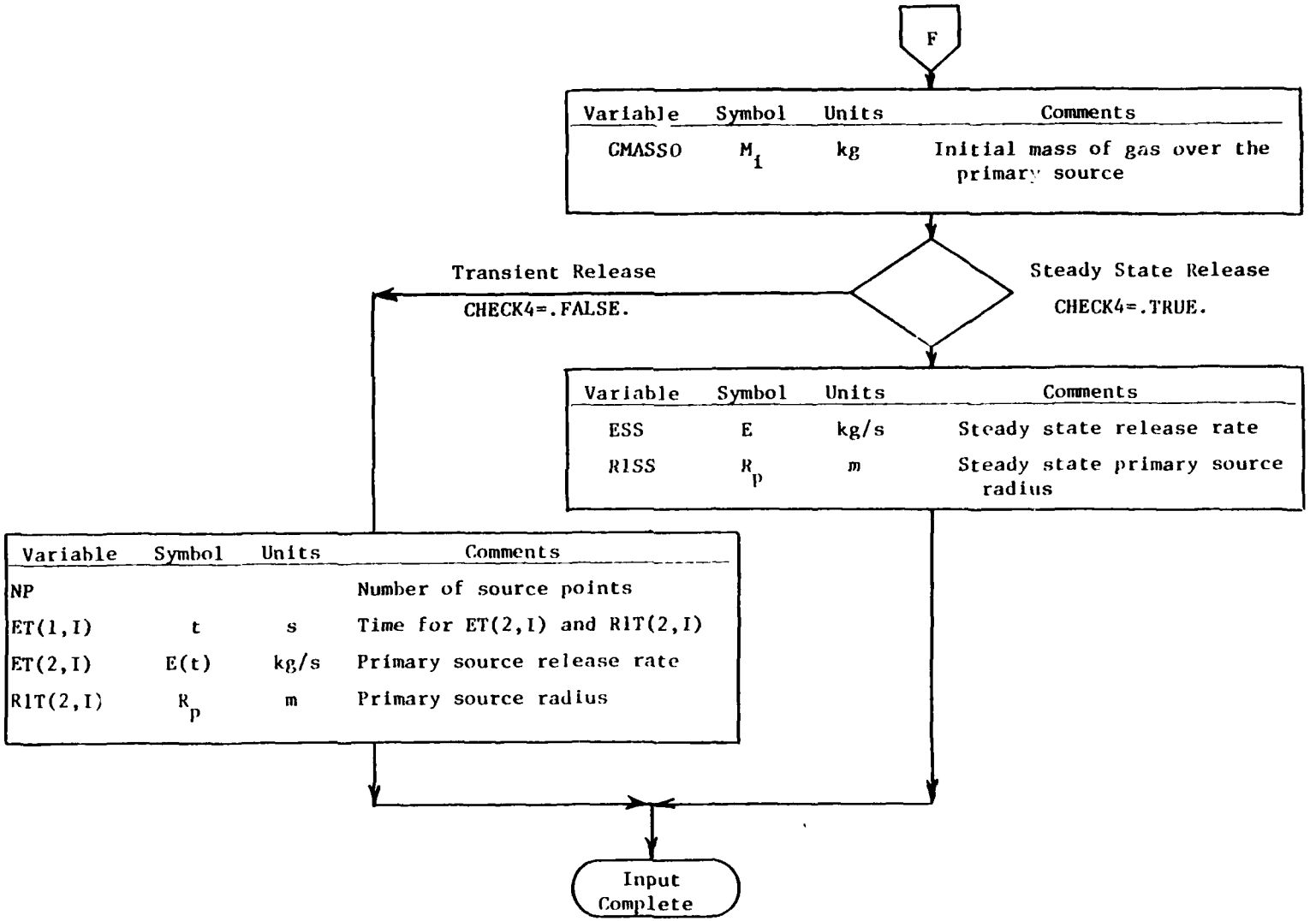

Figure B-5. Summary of Simulation Definition Input Information for DEGADIS (Concluded).

obtained by setting $p_1 = 1.0$ and choosing the appropriate value for q_1. Representative gas properties for liquefied natural gas (LNG) as methane, liquefied petroleum gas (LPG) as propane, pure unreacted NO_2, pure unreacted N_2O_4, and ammonia (NH_3) are included in DEGADISIN. Also included are the lower and upper flammability limits (LFL and UFL, respectively), for LNG and LPG.

The user may also choose to calculate the mixture density as a function of composition using some other method. This mixture density is entered in the program as if the release were isothermal; for each composition, the program requests the contaminant mole fraction, the contaminant concentration, and the mixture density. For ease of input, these values may be entered from a file made available to DEGADISIN.

In specifying the details of the release, the user must choose to simulate the release as transient or steady-state. For both release types, the area source is assumed circular. The source radius and emission rate must be specified for a steady-state release only once, while these must be specified as a function of time for transient releases (either interactively or by file). For transient releases, the user must specify the initial amount of gas present over the source (in order to simulate, for example, instantaneous releases such as the Thorney Island Trials).

Figure B-5 summarizes the simulation information gathered by DEGADISIN contained in the RUNNAME file with extension INP. The structure of RUNNAME.INP is illustrated in Figure B-6. At this point, RUNNAME.INP may be edited to correct any misinformation entered during the input session. Note that care must be exercised when editing RUNNAME.INP due to the fact that information contained in the file can be different depending on the answered questions (e.g. steady-state versus transient simulation).

```
Desert Tortoise 4.  Pressurized ammonia release by LLNL.
Released mass rate of 108 kg/s; source radius from assumed H.

   4.990000        5.830000       3.0000000E-03
     5
  5.3000000E-02  0.8940000        45.20000
  0.1700000      0.9700000        50.00000
   306.3800      0.8910000       8.1456132E-03
    1   306.3800
    0  0.0000000E+00
    0  0.0000000E+00
NH3
   17.00000        306.3800        3.722660
   3930.000        1.000000
  2.0000000E-02  2.0000000E-03  0.5000000
    20
  0.0000000E+00  0.0000000E+00   1.025059      0.0000000E+00   306.3800
  3.1000000E-02  2.0116368E-02   1.089491      0.0000000E+00   306.3800
  4.2000000E-02  2.7710385E-02   1.102633      0.0000000E+00   306.3800
  6.1000000E-02  4.1382639E-02   1.124741      0.0000000E+00   306.3800
  7.9000000E-02  5.5295185E-02   1.151617      0.0000000E+00   306.3800
  0.1400000      0.1126337       1.289311      0.0000000E+00   306.3800
  0.1590000      0.1339750       1.339125      0.0000000E+00   306.3800
  0.1730000      0.1503675       1.372819      0.0000000E+00   306.3800
  0.1850000      0.1644708       1.396704      0.0000000E+00   306.3800
  0.1980000      0.1795058       1.416039      0.0000000E+00   306.3800
  0.2150000      0.1988646       1.433694      0.0000000E+00   306.3800
  0.4260000      0.4822193       1.587227      0.0000000E+00   306.3800
  0.5400000      0.6960659       1.704466      0.0000000E+00   306.3800
  0.6400000      0.9445107       1.848052      0.0000000E+00   306.3800
  0.7270000       1.235210       2.024047      0.0000000E+00   306.3800
  0.8020000       1.577622       2.240009      0.0000000E+00   306.3800
  0.8660000       1.983670       2.505674      0.0000000E+00   306.3800
  0.9200000       2.468807       2.833904      0.0000000E+00   306.3800
  0.9640000       3.038278       3.231240      0.0000000E+00   306.3800
   1.000000       3.722663       3.722663      0.0000000E+00   306.3800
  3.7000000E-03
  0.0000000E+00
    4
  0.0000000E+00   108.0000        1.450000
   6023.000       108.0000        1.450000
   6024.000      0.0000000E+00  0.0000000E+00
   6025.000      0.0000000E+00  0.0000000E+00
 F F F F T F
22-SEP-1987 17:07:11.02
   108.0000        2.900000        1.138827
```

Figure B-6. DT4.INP Listing.

(The reverse of this page is blank.)

3. Example Input Sessions

The input procedures for simulation of the transient release and the steady-state release are very similar. Therefore, only the specification of a steady-state release (DT4) has been included. In the point by-point discussion of the input procedure, note the following:

(*) The file name specification RUNNAME must satisfy system restrictions.

(*) A line terminator (normally a carriage return) must end every line entered by the user.

(*) When DEGADISIN requests the user to choose an option, all acceptable responses are a single character (capital or lower case). The default responses are denoted by a capital letter inside angle brackets (e.g. <N>). When applicable, a menu of acceptable responses is included inside parentheses.

(*) For numerical responses, a comma, space, tab, or line terminator (carriage return) may separate the numbers.

(*) When a file is used as input (i.e., for the density or transient source input), DEGADISIN reads the same information from the file which would be entered at the terminal in the same order and in the same format.

NOTES ON STEADY-STATE SIMULATION OF DESERT TORTOISE 4

(1) Begin the input procedure by execution of DEGADISIN.

(2) The file name specification must follow system restrictions. The DEGADIS model uses this file name along with various file extensions for input and output.

(3) The Title Block is used to carry any desired comments such as information on the specification of certain parameters.

(4) The wind field parameters include the wind velocity (m/s) at a specified height (m) and the surface roughness (m).

(5) The Pasquill stability class is used to generate estimates of other atmospheric parameters which follow.

(6) The current settings of pertinent atmospheric parameters are displayed in this list. If any of these are to be changed, the first letter of the parameter to be changed is entered. The value of the Monin-Obukhov length is to be changed. Note that the default--indicated by <N>--is No for no changes.

```
(1)$ RUN SYS$DEGADIS:DEGADISIN

                DEnse GAs DISpersion Model input module.

(2)Enter the simulation name : [DIR]RUNNAME DT4
      INPUT MODULE -- DEGADIS MODEL

      **********************************
      Enter Title Block -- up to 4 lines of 80 characters
      To stop, type "//"
(3)Desert Tortoise 4.  Pressurized ammonia release by LLNL.
Released mass rate of 108 kg/s; source radius from assumed H.
//
(4)    ENTER WIND PARAMETERS -- U0 (m/s), Z0 (m), and ZR(m)
      U0 -- Wind velocity at reference height Z0
      ZR -- Surface Roughness
4.99,5.83,0.003

(5)    Enter the Pasquill stability class: (A,B,C,D,E,F) <D> E

(6)The values for the atmospheric parameters are set as follows:
DELTA:                          0.0530
BETA:                           0.8940
Monin-Obukhov length:          21.1038 m
Sigma X Coefficient:            0.1700
Sigma X Power:                  0.9700
Sigma X Minimum Distance:      50.0000 m
Do you wish to change any of these?
(No,Delta,Beta,Length,Coefficient,Power,Minimum) <N> L
```

(7) The value of the Monin-Obukhov length is indicated to be infinite (which is the default value for a Pasquill D stability). Any value of the Monin-Obukhov length can be specified, but an infinite value is a special case which can be obtained for any Pasquill stability class by setting the Monin-Obukhov length to 0. The desired Monin-Obukhov length is entered.

(8) The ambient temperature and pressure are entered.

(9) DEGADISIN calculates the ambient air density for the given input parameters.

(10) If the release is isothermal, respond "Y." A positive response causes DEGADISIN to ask for a list of concentration, density, and mole fraction points for the gas mixture. The default response is negative. For the Desert Tortoise series, the simulations were made using the list of concentration, mole fraction, and density so that the behavior of the ammonia aerosol could be simulated. Note that this option does not mean that the ammonia aerosol was always at the same temperature.

(11) Enter the three-letter designation of the diffusing gas. The properties of LNG as methane, LPG as propane, pure NO_2 (without reaction), pure N_2O_4 (without reaction), and ammonia (NH_3) are included as LNG, LPG, NO2, N2O, and NH3, resectively.

(7) Note: For infinity, ML = 0.0
Enter the desired Monin-Obukhov length: (m) 45.2

The values for the atmospheric parameters are set as follows:

DELTA:	0.0530
BETA:	0.8940
Monin-Obukhov length:	45.2000 m
Sigma X Coefficient:	0.1700
Sigma X Power:	0.9700
Sigma X Minimum Distance:	50.0000 m

Do you wish to change any of these?
(No,Delta,Beta,Length,Coefficient,Power,Minimum) <N>

(8) Enter the ambient temperature(C) and pressure(atm): 33.23,0.891

The ambient humidity can be entered as Relative or Absolute.
Enter either R or A <R or a>:
Enter the relative humidity (%): 21.3

(9) Ambient Air density is 1.0215 kg/m**3

(10) Is this an Isothermal spill? <y or N> Y

(11) Enter the code name of the diffusing species: NH3

(12) A list of the properties for the specified gas (if available) is given. If any of the parameters are to be changed, the first letter of the parameter to be changed in the list is given to the prompt. Note that for NH_3, the storage temperature is assumed to be the ambient temperature, and the vapor density is calculated by the ideal gas equation of state. For this simulation, it was necessary to change the vapor density to account for the aerosol.

(13) The gas property list is displayed again. The default response is no change.

(14) Since this is an isothermal simulation, the density and concentration must be specified as a function of mole fraction.

(12) The characteristics for the gas are set as follows:

Molecular weight:	17.00
Storage temperature [K]:	306.38
Density at storage temperature, PAMB [kg/m**3]:	0.60254
Mean Heat capacity constant	3930.0
Mean Heat capacity power	1.0000
Upper Flammability Limit [mole frac]	2.00000E-02
Lower Flammability Limit [mole frac]	2.00000E-03
Height of Flammability Limit [m]	0.50000

Do you wish to change any of these? (No,Mole,Temp,Den,Heat,Power,Upper,Lower,Z) <N> D
Enter the desired Density at Storage Temperature and ambient pressure: 3.72266

(13) The characteristics for the gas are set as follows:

Molecular weight:	17.00
Storage temperature [K]:	306.38
Density at storage temperature, PAMB [kg/m**3]:	3.7227
Mean Heat capacity constant	3930.0
Mean Heat capacity power	1.0000
Upper Flammability Limit [mole frac]	2.00000E-02
Lower Flammability Limit [mole frac]	2.00000E-03
Height of Flammability Limit [m]	0.50000

Do you wish to change any of these? (No,Mole,Temp,Den,Heat,Power,Upper,Lower,Z) <N>

(14) The density is determined as a function of concentration
by a listing of ordered triples supplied by the user.
Use the following form:

```
first point      -- pure air  y=0.0,Cc=0.,RHOG=RHOA=1.02152 kg/m**3
     .
     .
     .
last point       -- pure gas  y=1.0,Cc=RHOE,RHOG=RHOE
```

(15) A file may be used to enter the density information. In the file, the first line should have the number of data triples. Each subsequent line should contain a mole fraction, concentration, and density for the gas mixture. The file DT4.TRAUMA was generated using TRAUMA for the ammonia aerosol.

(16) The lowest concentration of interest is the concentration at which the calculations are stopped.

(17) If a steady-state release is to be simulated, type "Y" to the prompt. For a steady simulation, the steady-state mass evolution rate (kg/s) and primary source extent (m) are required.

(18) A note about the numerical parameter files is included. These files contain various constant values used in the programs to which the user has access without recompiling the programs. Access is granted as a convenience.

(19) DEGADISIN will generate a command procedure suitable for running the model under VMS.

(20) If so desired, DEGADISIN will initiate the command procedure under VMS. If not, the program returns to the operating system.

(15) Do you have an input file for the Density function? [y or N] Y
Enter the file name: [DIR]FILE_NAME.EXT DT4.TRAUMA

(16) The suggested LOWEST CONCENTRATION OF INTEREST (gas_lfl/2.)
is 3.72266E-03 kg/m**3. Enter the desired value: 0.0037

Specification of source rate and extent.

(17) Is this a Steady state simulation? <y or N> Y

Enter the desired evolution rate [=] kg/sec : 108.
Enter the desired source radius [=] m : 1.45

(18) In addition to the information just obtained, DEGADIS
requires a series of numerical parameter files which use
the same name as [DIR]RUNNAME given above.

For convenience, example parameter files are included for
each step. They are:
EXAMPLE.ER1 and
EXAMPLE.ER2
Note that each of these files can be edited during the course of the
simulation if a parameter proves to be out of specification.

(19) Do you want a command file to be generated to execute the procedure? <Y or n>
The command file will be generated under the file name:
DT4.com

(20) Do you wish to initiate this procedure? <y or N>
$

The generated INP file for DT4 is shown in Figure B-6. If necessary, the user may edit the INP file before beginning the simulation.

4. Example Simulation Output

After proper completion of the model, DT4.LIS contains the output listing for the steady-state release. A point-by-point discussion of the output follows.

(1) The date and time DEGADISIN was run are included.

********** U O A _ D E G A D I S M O D E L O U T P U T - -

********** ********** 22-SEP-1987 16:28:57.04 ****

(1) Data input on 20-AUG-1987 17:12:04.15
Source program run on 22-SEP 1987 16:28:57.04

****
*
* NOTE:
* -----
*
* > All Calculations are limited to circular liquid sources.
*
****

QR

(2) The input information gathered by DEGADISIN is repeated to assist in documentation of the simulations. Included here are the Title Block and the atmospheric conditions.

(2) TITLE BLOCK

Desert Tortoise 4. Pressurized ammonia release by LLNL.
Released mass rate of 108 kg/s; source radius from assumed H.

Wind velocity at reference height		4.99	m/s
Reference height		5.83	m
Surface roughness length		3.000E-03	m
Pasquill Stability class		E	
Monin Obukhov length		45.2	m
Gaussian distribution constants	Delta	0.05300	m
	Beta	0.89400	
Wind velocity power law constant	Alpha	0.19220	
Friction velocity		0.21354	m/s
Ambient Temperature		306.38	K
Ambient Pressure		0.891	atm
Ambient Absolute Humidity		8.146E-03	kg/kg BDA
Ambient Relative Humidity		21.30	%

Input: Mole fraction	CONCENTRATION OF C kg/m**3	GAS DENSITY kg/m**3
0.00000	0.00000	1.02506
0.03100	0.02012	1.08949
0.04200	0.02771	1.10263
0.06100	0.04138	1.12474
0.07900	0.05530	1.15162
0.14000	0.11263	1.28931

(3) Continuing with the input information, the contaminant gas properties are output.

(4) The specification of the mass evolution rate and source radius are output. For a steady-state release, there is no initial mass in the cloud, and the source strength and source radius are held constant for an arbitrarily large period of time.

(5) Finally, certain numerical parameters and calculation flags are displayed. Some of these are set in DEGADISIN while others are set in the numerical parameter files.

Specified Gas Properties:

(3)

Molecular weight:	17.000	
Storage temperature:	306.38	K
Density at storage temperature and ambient pressure:	3.7227	kg/m**3
Mean heat capacity constant:	3930.0	
Mean heat capacity power:	1.0000	
Upper mole fraction contour:	2.00000E-02	
Lower mole fraction contour:	2.00000E-03	
Height for isopleths:	1.0000	m

Source input data points

(4) Initial mass in cloud: 0.00000E+00

TIME	SOURCE STRENGTH	SOURCE RADIUS
s	kg/s	m
0.00000E+00	108.00	1.4500
6023.0	108.00	1.4500
6024.0	0.00000E+00	0.00000E+00
6025.0	0.00000E+00	0.00000E+00

(5) Calculation procedure for ALPHA: 1

Entrainment prescription for PHI: 3

Layer thickness ratio used for average depth: 2.1500

Air entrainment coefficient used: 0.590

Gravity slumping velocity coefficient used: 1.150

Isothermal calculation

Heat transfer not included

Water transfer not included

(6) A summary of the calculated secondary source parameters is included. The secondary source gas radius and height are output as functions of time along with other secondary parameters including the source mass flux (Qstar), the vertical concentration distribution parameter at the downwind edge (SZ(x = L/2.)), the contaminant mole fraction (Mole frac C), the gas mixture density (Density), and the Richardson number based on the cloud spreading velocity (Rich No.).

(6)

CALCULATED SOURCE PARAMETERS

Time sec	Gas Radius m	Height m	Qstar kg/m^^2/s	SZ(x=L/2.) m	Mole frac C	Density kg/m^^3	Rich No.
0.000000E+00	1.45000	1.100000E-05	0.201836	8.472245E-02	1.00000	3.72266	0.756144
2.000000E-02	1.47243	8.521862E-02	0.198798	8.564490E-02	0.997634	3.69036	0.756144
4.000000E-02	1.51321	0.165024	0.193530	8.731551E-02	0.993474	3.63358	0.756144
6.000000E-02	1.56446	0.238127	0.187285	8.943314E-02	0.988365	3.56384	0.756144
8.000000E-02	1.62307	0.304430	0.180609	9.188325E-02	0.982673	3.48613	0.756144
0.160000	1.89965	0.509132	0.154720	0.103289	0.957605	3.17349	0.756144
0.240000	2.20745	0.633237	0.134019	0.114301	0.933180	2.95292	0.756144
0.320000	2.52418	0.712099	0.118050	0.124969	0.911034	2.77940	0.756144
0.480000	3.15711	0.789551	9.595145E-02	0.143468	0.874436	2.55695	0.756144
0.640000	3.77398	0.816624	8.153981E-02	0.158879	0.845747	2.42160	0.756144
0.960000	4.95224	0.821833	6.394785E-02	0.184619	0.804115	2.24879	0.756144
1.28000	6.06431	0.797867	5.344478E-02	0.203670	0.774954	2.16213	0.756144
1.92000	8.13911	0.745157	4.139437E-02	0.233999	0.736374	2.05104	0.756144
2.56000	10.0636	0.694296	3.448758E-02	0.256131	0.711394	1.99248	0.756144
3.20000	11.8802	0.648887	2.993524E-02	0.273299	0.693880	1.95705	0.756144
3.84000	13.6106	0.610069	2.669493E-02	0.287681	0.680925	1.93084	0.756144
4.48000	15.2693	0.576355	2.425545E-02	0.299986	0.670999	1.91076	0.756144
5.12000	16.8671	0.546634	2.234361E-02	0.310677	0.663219	1.89502	0.756144
6.40000	19.9099	0.496128	1.952284E-02	0.328386	0.652067	1.87246	0.756144
7.68000	22.7842	0.454249	1.752759E-02	0.342448	0.644863	1.85789	0.756144
8.96000	25.5197	0.418501	1.603339E-02	0.353813	0.640294	1.84865	0.756144
10.2400	28.1375	0.387014	1.486140E-02	0.362707	0.637617	1.84463	0.756144
12.8000	33.0770	0.334427	1.315472E-02	0.376258	0.636246	1.84266	0.756144
15.3600	37.6824	0.291694	1.197572E-02	0.385758	0.638563	1.84599	0.756144
17.9200	42.0048	0.255547	1.111050E-02	0.391704	0.643492	1.85512	0.756144
20.4800	46.0814	0.224279	1.045218E-02	0.394781	0.650456	1.86920	0.756144
25.6000	53.5897	0.172770	9.545507E-03	0.395138	0.669231	1.90719	0.756144
30.7200	58.4443	0.141302	9.207259E-03	0.388275	0.692412	1.95408	0.756144
40.9600	57.7949	0.134216	9.776789E-03	0.366989	0.730592	2.03439	0.756144
56.3200	57.2132	0.126926	1.024356E-02	0.345192	0.763648	2.12957	0.756144
66.5600	56.9783	0.124287	1.043536E-02	0.337636	0.776252	2.16587	0.756144
76.8000	56.8113	0.122591	1.056540E-02	0.335192	0.784426	2.18940	0.756144

(6)

CALCULATED SOURCE PARAMETERS

Time sec	Gas Radius m	Height m	Qstar kg/m^^2/s	SZ(x=L/2.) m	Mole frac C	Density kg/m^^3	Rich No.
0.000000E+00	1.45000	1.100000E-05	0.201836	8.472245E-02	1.00000	3.72266	0.756144
2.000000E-02	1.47243	8.521862E-02	0.198798	8.564490E-02	0.997634	3.69036	0.756144
4.000000E-02	1.51321	0.165024	0.193530	8.731551E-02	0.993474	3.63358	0.756144
6.000000E-02	1.56446	0.238127	0.187285	8.943314E-02	0.988365	3.56384	0.756144
8.000000E-02	1.62307	0.304430	0.180609	9.188325E-02	0.982673	3.48613	0.756144
0.160000	1.89965	0.509132	0.154720	0.103289	0.957605	3.17349	0.756144
0.240000	2.20745	0.633237	0.134019	0.114301	0.933180	2.95292	0.756144
0.320000	2.52418	0.712099	0.118050	0.124969	0.911034	2.77940	0.756144
0.480000	3.15711	0.789551	9.595145E-02	0.143468	0.874436	2.55695	0.756144
0.640000	3.77398	0.816624	8.153981E-02	0.158879	0.845747	2.42160	0.756144
0.960000	4.95224	0.821833	6.394785E-02	0.184619	0.804115	2.24879	0.756144
1.28000	6.06431	0.797867	5.344478E-02	0.203670	0.774954	2.16213	0.756144
1.92000	8.13911	0.745157	4.139437E-02	0.233999	0.736374	2.05104	0.756144
2.56000	10.0636	0.694296	3.448758E-02	0.256131	0.711394	1.99248	0.756144
3.20000	11.8802	0.648887	2.993524E-02	0.273299	0.693880	1.95705	0.756144
3.84000	13.6106	0.610069	2.669493E-02	0.287681	0.680925	1.93084	0.756144
4.48000	15.2693	0.576355	2.425545E-02	0.299986	0.670999	1.91076	0.756144
5.12000	16.8671	0.546634	2.234361E-02	0.310677	0.663219	1.89502	0.756144
6.40000	19.9099	0.496128	1.952284E-02	0.328386	0.652067	1.87246	0.756144
7.68000	22.7842	0.454249	1.752759E-02	0.342448	0.644863	1.85789	0.756144
8.96000	25.5197	0.418501	1.603339E-02	0.353813	0.640294	1.84865	0.756144
10.2400	28.1375	0.387014	1.486140E-02	0.362707	0.637617	1.84463	0.756144
12.8000	33.0770	0.334427	1.315472E-02	0.376258	0.636246	1.84266	0.756144
15.3600	37.6824	0.291694	1.197572E-02	0.385758	0.638563	1.84599	0.756144
17.9200	42.0048	0.255547	1.111050E-02	0.391704	0.643492	1.85512	0.756144
20.4800	46.0814	0.224279	1.045218E-02	0.394781	0.650456	1.86920	0.756144
25.6000	53.5897	0.172770	9.545507E-03	0.395138	0.669231	1.90719	0.756144
30.7200	58.4443	0.141302	9.207259E-03	0.388275	0.692412	1.95408	0.756144
40.9600	57.7949	0.134216	9.776789E-03	0.366989	0.730592	2.03439	0.756144
56.3200	57.2132	0.126926	1.024356E-02	0.345192	0.763648	2.12957	0.756144
66.5600	56.9783	0.124287	1.043536E-02	0.337636	0.776252	2.16587	0.756144
76.8000	56.8113	0.122591	1.056540E-02	0.335192	0.784426	2.18940	0.756144

(7) For a steady-state release, the source calculations are terminated after the calculated parameters are no longer changing as a function of time. A summary of the steady-state secondary source is included.

(8) The downwind portion of the calculation is included. The distance downwind of the source is given in the first column. Columns 2 through 5 contain the mole fraction, contaminant concentration, mixture density, and mixture temperature on the centerline of the gas cloud at ground level. Columns 6 through 8 contain the contour shape parameters b (Half Width), S_z, and S_y. Finally, columns 9 and 10 contain the width from the centerline to the indicated concentration levels at the indicated height. Note that the output is prematurely terminated. Output actually continues until the centerline, ground-level concentration drops below the lowest concentration of interest.

(7) Source strength [kg/s] : 108.00 Equivalent Primary source radius [m] : 1.0253
Equivalent Primary source length [m] : 2.9000 Equivalent Primary source width [m] : 1.1388

Secondary source concentration [kg/m**3] : 1.4936 Secondary source SZ [m] : 0.33519

Contaminant flux rate: 8.36555E-03

Secondary source mass fractions... contaminant: 0.682186 air: 0.31525
Enthalpy: 0.00000E+00 Density: 2.1894
Secondary source length [m] : 113.62 Secondary source half-width [m] : 44.619

(8)

Distance (m)	Mole Fraction	Concentration (kg/m**3)	Density (kg/m**3)	Temperature (K)	Half Width (m)	Sz (m)	Sy (m)	Width at z= 0.200 mole% (m)	Width at z= 2.00 (m)
56.8	0.785	1.49	2.19	306.	44.6	0.335	1.814E-06	44.6	44.6
61.6	0.771	1.43	2.14	306.	45.1	0.324	3.94	52.1	48.8
66.4	0.756	1.36	2.10	306.	47.4	0.316	5.68	57.3	52.2
76.0	0.723	1.22	2.02	306.	52.5	0.309	8.30	66.4	58.4
82.4	0.699	1.13	1.96	306.	56.0	0.310	9.78	72.1	62.4
95.2	0.647	0.967	1.86	306.	62.8	0.317	12.4	83.2	70.5
108.	0.590	0.815	1.77	306.	69.5	0.333	14.8	94.0	79.1
121.	0.537	0.691	1.70	306.	76.0	0.352	17.1	105.	88.1
134.	0.486	0.589	1.65	306.	82.3	0.374	19.2	115.	97.0
146.	0.440	0.507	1.60	306.	88.5	0.397	21.3	125.	106.
159.	0.399	0.440	1.56	306.	94.6	0.421	23.3	135.	114.
172.	0.361	0.384	1.53	306.	101.	0.448	25.3	145.	123.
185.	0.326	0.334	1.51	306.	107.	0.478	27.2	155.	132.
198.	0.293	0.292	1.48	306.	113.	0.511	29.0	165.	140.
210.	0.265	0.256	1.46	306.	119.	0.544	30.9	174.	148.
223.	0.240	0.227	1.45	306.	125.	0.576	32.7	184.	157.
236.	0.219	0.204	1.44	306.	131.	0.607	34.5	193.	164.
249.	0.201	0.184	1.42	306.	137.	0.636	36.3	202.	172.
262.	0.186	0.167	1.40	306.	143.	0.665	38.1	212.	180.
274.	0.174	0.152	1.38	306.	149.	0.695	39.9	221.	187.
287.	0.162	0.138	1.35	306.	155.	0.726	41.6	229.	194.
300.	0.152	0.127	1.32	306.	160.	0.759	43.3	238.	201.
313.	0.143	0.116	1.30	306.	166.	0.794	45.0	246.	208.
326.	0.134	0.107	1.28	306.	171.	0.829	46.7	254.	214.

5. Model Limitations and Cautions

DEGADIS model application should be limited to the description of atmospheric dispersion of denser-than-air gas releases at ground level onto flat, unobstructed terrain or water. Application to releases from sources above ground level (e.g. overflow from dikes) would be expected to give conservative predictions of the downwind hazard zones, but this has not been verified.

The dispersion of a denser-than-air gas by the action of the wind assumes the maintenance of a wind velocity profile in the gas cloud or plume whose characteristics are determined by the approach wind flow (upwind of the release). The treatment of vertical momentum transfer invokes the assumption of of a logarithmic vertical velocity profile, which is in turn curve-fitted to a power law vertical velocity profile. DEGADIS also uses similarity forms for the vertical profile of gas concentration in the cloud, and the vertical profile is dependent on the power law exponent α used in the representation of the velocity profile. The vertical velocity profile, which is directly related to the air entrainment velocity into the cloud, is dependent on the factors which determine the structure of the atmospheric boundary surface layer, wind speed, surface roughness, and atmospheric stability. Consequently, the representations of the vertical velocity and concentration profiles in DEGADIS are subject to similar limitations as in other descriptions of the surface layer. Table B-2 indicates typical recommended surface roughness values. Table B-1 indicates logarithmic wind velocity profile corrections for different atmospheric stabilities, along with typical values of the wind profile power law exponent α determined in DEGADIS.

Demonstration of the model has been primarily directed to the prediction of hazard extent defined by gas concentrations in the hydrocarbon flammable limit range (~1 to 20 percent). Based on the simulations of field experiments presented in Havens and Spicer (Reference B-1), the ratio of observed distance to calculated distance for a given time-averaged concentration level (OBS/PRE) ranged from 0.73 to 0.96 for the 5 percent level 9 out of 10 times (i.e., 90 percent confidence interval). For the 2.5 percent level, (OBS/PRE) ranged from 0.82 to 1.03 for a 90 percent confidence interval. For the 1 percent level, (OBS/PRE) ranged from 0.95 to 1.24 for a 90 percent confidence interval. If for a

TABLE B-2. REPRESENTATIVE VALUES OF SURFACE ROUGHNESS FOR A UNIFORM DISTRIBUTION OF THESE TYPES OF GROUND COVER (REFERENCE B-21)

	Surface Roughness (m)	Height of Ground Cover (m)
Ice	0.00001	
Smooth mud flats	0.00001	
Smooth snow on short grass	0.00005	
Snow	0.00005 to 0.0001	
Sand	0.0003	
Smooth desert	0.0003	
Snow surface, natural prairie	0.001	
Soils	0.001 to 0.01	
Short grass	0.003 to 0.01	0.02 to 0.1
Mown grass	0.002	0.015
	0.007	0.03
Long grass	0.04 to 0.10	0.25 to 1.
Agricultural crops	0.04 to 0.20	~0.40 to 2.
Orchards	0.50 to 1.	~5. to 10.
Deciduous forests	1. to 6.	~10. to 60.
Coniferous forests	1. to 6.	~10. to 60.

given release scenario the calculated distance to the 2.5 percent average concentration level was 120 meters, the distance to the 2.5 percent average concentration for 9 out of 10 realizations of the same release would be expected to range between 98 meters and 124 meters.

REFERENCES FOR APPENDIX B

B-1. Havens, J.A. and Spicer, T.O., Development of an Atmospheric Dispersion Model for Heavier-than-Air Gas Mixtures," Final Report to U.S. Coast Guard, Contract DT-CG-23-80-C-20029, DC, May 1985.

B-2. Colenbrander, G.W., "A Mathematical Model for the Transient Behavior of Dense Vapor Clouds," paper presented at the 3rd International Symposium on Loss Prevention and Safety Promotion in the Process Industries, Basel, Switzerland, 1980.

B-3. Colenbrander, G.W. and Puttock, J.S., "Dense Gas Dispersion Behavior: Experimental Observations and Model Developments," paper presented at the 4th International Symposium on Loss Prevention and Safety Promotion in the Process Industries, Harrogate, England, September 1983.

B-4. van Ulden, A.P., "The Unsteady Gravity Spread of a Dense Cloud in a Calm Environment," paper presented at the 10th International Technical Meeting on Air Pollution Modeling and its Applications, NATO-CCMS, Rome, Italy, October 1979.

B-5. Batchelor, G.K., An Introduction to Fluid Dynamics, Cambridge University Press, Cambridge, UK, 1967.

B-6. van Ulden, A.P., "A New Bulk Model for Dense Gas Dispersion: Two-Dimensional Spread in Still Air," paper presented at the I.U.T.A.M. Symposium on Atmospheric Dispersion of Heavy Gases and Small Particles, Delft University of Technology, The Netherlands, 29 August-2 September 1983.

B-7. Simpson, J.E. and Britter, R.E., "The Dynamics of the Head of a Gravity Current Advancing over a Horizontal Surface," Journal of Fluid Mechanics, 94, Part 3, 1979.

B-8. Koopman, R.P. et al., Description and Analysis of Burro Series 40-m^3 LNG Spill Experiments," Lawrence Livermore National Laboratories Report UCRL-53186, Livermore, California, August 1981.

B-9. McAdams, W.H., Heat Transmission, McGraw-Hill, New York, 1954.

B-10. Treybal, R.E., Mass Transfer Operations, 3rd edition, McGraw-Hill, New York, 1980.

B-11. Bird, R.B., Stewart, W.E., and Lightfoot, E.N., Transport Phenomena, John Wiley and Sons, New York, 1960.

B-12. Britter, R.E., "The Ground Level Extent of a Negatively Buoyant Plume in a Turbulent Boundary Layer," Atmospheric Environment, 14, 1980.

B-13. Kantha, H.L., Phillips, O.M., and Azad, R.S., "On Turbulent Entrainment at a Stable Density Interface," Journal of Fluid Mechanics, 79, pp. 753-768, 1977.

B-14. Lofquist, Karl, "Flow and Stress Near an Interface Between Stratified Liquids," Physics of Fluids, 3, No. 2, March-April 1960.

B-15. McQuaid, James, Some Experiments on the Structure of Stably Stratified Shear Flows, Technical Paper P21, Safety in Mines Research Establishment, Sheffield, UK, 1976.

B-16. Zeman, O. and Tennekes, H., "Parameterization of the Turbulent Energy Budget at the top of the Daytime Atmospheric Boundary Layer," Journal of the Atmospheric Sciences, January 1977.

B-17. Pasquill, F., Atmospheric Diffusion, 2nd edition, Halstead Press, New York, 1974.

B-18. Beals, G.A., A Guide to Local Dispersion of Air Pollutants, Air Weather Service Technical Report 214, April, 1971.

B-19. Spicer, T.O., Using Different Time-Averaging Periods in DEGADIS, Report to the Exxon Education Foundation, Fayetteville, Arkansas, June 1987.

B-20. Businger, J.A., Wyngaard, J.C., Izumi, Y., and Bradley, E.F., "Flux-Profile Relationships in the Atmospheric Surface Layer," Journal of the Atmospheric Sciences, 28, March 1971.

B-21. Pielke, R.A., Mesoscale Meteorological Modeling, Academic Press, Orlando, 1984.

APPENDIX C

DISCUSSION OF THE SENSITIVITY OF DEGADIS TO UNCERTAINTY IN INPUT PARAMETERS NOT ROUTINELY AVAILABLE AT OPERATIONAL USAF SITES

The purpose of this appendix is to point out the effect of uncertainties in DEGADIS input parameters on the output of DEGADIS. The scope of this investigation is aimed at input parameters which are not normally available at operational USAF sites. For this analysis, the following data are assumed to be available:

- windspeed at a given elevation (assumed to be near 10 meters)
- ambient temperature, pressure, and humidity

(The ambient humidity is assumed to be available from the dewpoint temperature.) In addition to the above information, DEGADIS requires further information to define a simulation as follows:

- Pasquill stability category
- surface roughness
- initial contaminant density
- contaminant release rate

The release conditions of Desert Tortoise 4 (DT4) will be used to illustrate the effect of uncertainties in each of these. For comparison purposes, the DT4 conditions are the same as those in the body of this report with two exceptions. The first is the Monin-Obukhov length. Because LLNL measured the on-site velocity and temperature profiles, an estimate of the Monin-Obukhov length was available. This estimate was used in the simulations for comparison with the available data. Since the Monin-Obukhov length is not a parameter which is normally available and since DEGADIS can estimate the Monin-Obukhov length from the Pasquill stability category and the surface roughness, the Monin-Obukhov length will be estimated by DEGADIS (as outlined in Table B-1). The second is the mixture density specification as a function of contaminant concentration. For releases where heat transfer is not important, assuming a linear relationship between contaminant concentration (in kg/m^3) and mixture density may be adequate for hazard assessment as shown by comparison of DEGADIS predictions using the conditions of DT4 (Section III). (If heat transfer is important, the effect of heat transfer would be expected to

enhance dispersion so that a simulation which ignores heat transfer would be expected to be conservative.) For all comparisons, a linear relationship is assumed between contaminant concentration and mixture density.

The Pasquill stability category and site surface roughness are needed in addition to the normally available information outlined above to complete the description of the ambient meteorological conditions of the release. The Pasquill stability and surface roughness are used to estimate the power law wind profile parameters (α), the Monin-Obukhov length (λ), and the coefficients for the lateral and along-wind dispersion parameters (σ_y and σ_x). The parameter λ determines the shape of the ambient velocity profile (Equation B-73) and is used to estimate u_* and α. The parameter α is used in the vertical concentration profile and the vertical velocity profile. The σ_y coefficients are used in the determination of S_y; the σ_x coefficients are only used in transient simulations for the x-direction dispersion correction.

There are several methods which can be used to estimate the Pasquill stability category. An estimate of the Pasquill stability category from the cloud cover and wind speed can be obtained as shown in Table C-1 (Reference C-1 or C-2). If information on the horizontal wind direction is available, σ_θ can be estimated from the maximum deviation in the horizontal wind direction ($3\sigma_\theta \simeq$ maximum deviation); the corresponding stability categories are shown in Table C-2 (Reference C-1 or C-2).

A comparison of DT4 simulations using D, E, and F stabilities is shown in Figure C-1. A shown, the DEGADIS-predicted concentrations at a given distance for each stability class are within a factor of two for concentrations greater than about 1000 ppm.

The site surface roughness is normally determined by analysis of the velocity profile measured under a given set of circumstances for a specific site. Estimates of the surface roughness for a site are normally considered to be only a function of the ground cover; representative values for homogeneous surfaces are shown in Table C-3. As a first approximation, the surface roughness can be estimated as one-fifth to one-tenth of the terrain height for homogeneous terrain. For urban and suburban areas, Lettau (Reference C-3) suggests $z_R = hA^*/2A'$ for a uniform distribution of buildings where h is the building height, A^* is the area normal to the mean

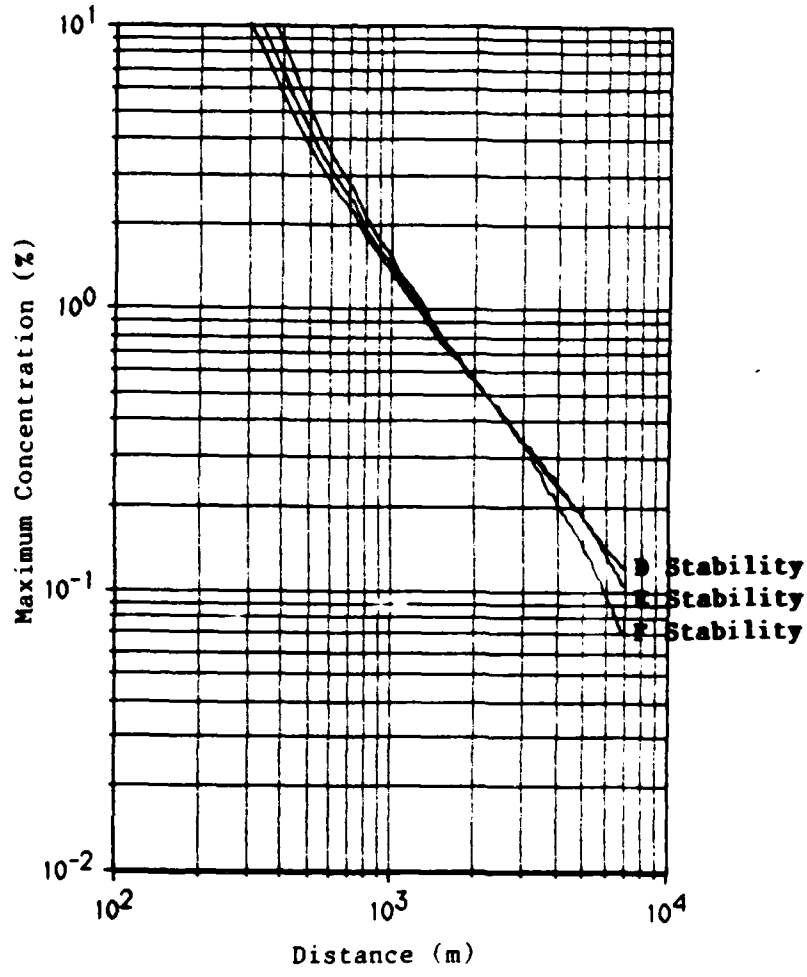

Figure C-1. Comparison of DEGADIS-Predicted Maximum Concentration as a Function of Distance for D, E, and F Pasquill Stabilities for the Test Case.

TABLE C-1. PASQUILL STABILITY CATEGORY AS A FUNCTION OF WINDSPEED AND CLOUD COVER (REFERENCE C-1 AND REFERENCE C-2)

Surface Windspeed (m/s)	Daytime Insolation			Night	
	Strong[a]	Moderate[b]	Slight[c]	Thin Overcast or >4/8 Low Cloud	<3/8 Cloud
<2	A	A-B	B		
2-3	A-B	B	C	E	F
3-5	B	B-C	C	D	E
5-6	C	C-D	D	D	D
>6	C	D	D	D	D

[a] >600 W/m^2
[b] 600 to 300 W/m^2
[c] <300 W/m^2

TABLE C-2. PASQUILL STABILITY CATEGORY AS A FUNCTION OF HORIZONTAL WIND DIRECTION FLUCTUATION (FROM REFERENCE C-1 AND REFERENCE C-2)

Pasquill Stability Category	σ_θ (at 10 m)
A	25
B	20
C	15
D	10
E	5
F	2.5

TABLE C-3. REPRESENTATIVE VALUES OF SURFACE ROUGHNESS FOR A UNIFORM DISTRIBUTION OF THESE TYPES OF GROUND COVER (REFERENCE C-4)

	Surface Roughness (m)	Height of Ground Cover (m)
Ice	0.00001	
Smooth mud flats	0.00001	
Smooth snow on short grass	0.00005	
Snow	0.00005 to 0.0001	
Sand	0.0003	
Smooth desert	0.0003	
Snow surface, natural prairie	0.001	
Soils	0.001 to 0.01	
Short grass	0.003 to 0.01	0.02 to 0.1
Mown grass	0.002	0.015
	0.007	0.03
Long grass	0.04 to 0.10	0.25 to 1.
Agricultural crops	0.04 to 0.20	~0.40 to 2.
Orchards	0.50 to 1.	~5. to 10.
Deciduous forests	1. to 6.	~10. to 60.
Coniferous forests	1. to 6.	~10. to 60.

wind direction, and A' is the building lot area. Of course, the area downwind of the source may be characterized by distinct terrain types having different surface roughnesses; for such conditions, separate calculations using the minimum and maximum roughnesses will act as upper and lower bounds for the simulation. It should be noted that DEGADIS is based on the assumption of dispersion on unobstructed, flat terrain. When the surface roughness used in DEGADIS becomes a significant fraction of the depth of the dispersing layer, the underlying assumptions in DEGADIS may no longer be satisfied.

A comparison of DT4 simulations using surface roughnesses of 0.3, 0.03, and 0.003 meters is shown in Figure C-2. As shown the DEGADIS-predicted concentrations at a given distance are reduced by a factor of about two for each order of magnitude increase in surface roughness.

For releases of materials which are not significantly colder than the ambient temperature (say, greater than about 200 K), the most important property of the released gas is the initial gas density and the density of the contaminant/air mixture as a function of contaminant concentration. For releases where heat transfer is not important, assuming a linear relationship between contaminant concentration (in kg/m^3) and mixture density may be adequate for hazard assessment. (If heat transfer is important, the effect of heat transfer would be expected to enhance dispersion so that a simulation which ignores heat transfer would be expected to be conservative.)

A comparison of DT4 simulations using different initial contaminant densities ranging from 20 percent below (2.98 kg/m^3) to 20 percent above (4.47 kg/m^3) the original initial contaminant density (3.72 kg/m^3) showed that the DEGADIS-predicted concentration as a function of distance was essentially unchanged. A DT4 simulation using an initial contaminant density of 1.86 kg/m^3 showed a variation of about 20 percent in the DEGADIS-predicted maximum concentration at a given distance. Note that this density is still much greater than the ambient air density (1.02 kg/m^3).

The last category to be examined is the release method of the material. For ground-level releases, two considerations are important including the rate of release and the diameter of release. As pointed out herein, the DT simulations were found to be insensitive to the choice of the source diameter. Furthermore, the effect of the source rate can be seen by comparing the simulations for each test for the two mass rates simulated (the released mass rate and the mass rate passing the 800-meter sensor array). As shown in these steady-state simulations, the concentration at a given distance for a given set of release conditions is proportional to the contaminant evolution rate. This is the same behavior shown by the steady-state Gaussian plume model.

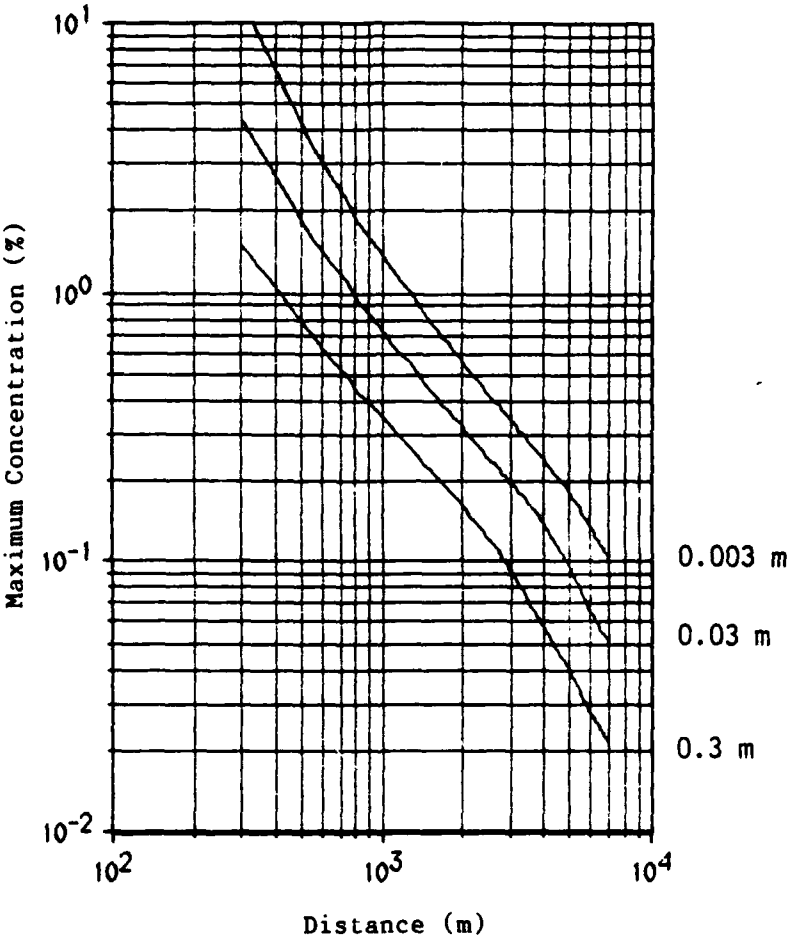

Figure C-2. Comparison of DEGADIS-Predicted Maximum Concentration as a Function of Distance for Surface Roughnesses of 0.3, 0.03, and 0.003 m for the Test Case.

From the above analysis, the inputs which have the largest effect on the DEGADIS-predicted distance to a given concentration level are the source evolution rate, surface roughness, and the Pasquill stability class for steady-state simulations. In addition, the initial contaminant density appears to be insignificant as long as it is above some threshold value.

REFERENCES FOR APPENDIX C

C-1. Gifford, F.A., "Turbulent Diffusion-Typing Schemes: A Review," Nuclear Safety, 17, 1976, p. 71.

C-2. Hanna, S.R., Briggs, G.A., Hosker, R.P., Jr., Handbook on Atmospheric Diffusion, U.S. DOE/TIC 11223, 1982.

C-3. Lettau, H.H., "Note on Aerodynamic Roughness Parameter Estimation on the Basis of Roughness Element Description," Journal of Applied Meteorology, 8, 1969, pp. 828-832.

C-4. Pielke, R.A., Mesoscale Meteorological Modeling, Academic Press, Orlando, 1984.

APPENDIX D

USING DIFFERENT TIME-AVERAGING PERIODS IN DEGADIS

Because of the nature of the exposure of individuals to airborne toxic materials, it is necessary to be able to predict the exposure to a given compound over a specified time period. Estimation of the maximum downwind concentration for a given averaging time using DEGADIS has been addressed by Spicer (Reference D-1); the following is a summary of that work. Although the effect of averaging time on the maximum downwind concentration for steady releases is still open to some question, the most important effect will be assumed to be the result of plume meander for modeling purposes. For transient releases, the most important effect will be assumed to be the duration of the release in addition to the mechanism of plume meander. (If, for example, the duration of the release is much shorter than the averaging time, then the time-averaged concentration will be reduced.) In the following, the implications of the averaging time on the Gaussian plume model are discussed, and a way of using different averaging times in DEGADIS for risk assessment purposes is presented.

The effect of averaging time on the maximum downwind concentration for steady releases is generally recognized as being a result of plume meander. The plume from a steady release of a passive gas would be expected to move downwind and meander with the ambient wind. At any point in time, the centerline of the plume would not necessarily correspond with the mean wind direction. After averaging the plume boundaries over some time period, the centerline of the plume should more closely correspond with the mean wind direction. This behavior is reflected in the values of the dispersion parameters used in the Gaussian plume model; Turner (Reference D-2) and Beals (Reference D-3) report different dispersion parameters for 10-minute average plume behavior and instantaneous or puff behavior. (It should be noted that estimates of puff coefficients are usually derived from observations of continuous releases which are analyzed as though the plume is a continuous train of superimposed puffs (Reference D-4).) Because of plume meander, the lateral Gaussian dispersion parameter σ_y depends on the averaging time, while the value of σ_z is essentially unaffected by the averaging time (Reference D-2). Several investigators have also looked at

the effect of averaging time by examining the ratio of maximum concentrations for different averaging times for continuous releases; the usual form of the function specified is

$$c_{max}(x;t_1)/c_{max}(x;t_2)^p = (t_2/t_1) \qquad \text{(D-1)}$$

where $c_{max}(x;t_1)$ is the maximum concentration associated with averaging time t_1, $c_{max}(x;t_2)$ is the maximum concentration associated with averaging time t_2, and p is some power. Turner (Reference D-2) proposed that $0.17 \leq p \leq 0.20$ based on reports by Stewart, Gale, and Crooks (Reference D-5) and Cramer (Reference D-6) (among others) for averaging times from about 3 seconds to about half an hour. Herman (Reference D-7) estimated p to be 0.5 ± 0.2 for averaging times from 1 hour to 1 year. These findings are in essential agreement with Hino (Reference D-8) who found that $p = 0.2$ for averaging times less than 10 minutes, and $p = 0.5$ for times greater than 10 minutes (with some dependence on the atmospheric stability). Of course, if the value of σ_z is independent of averaging time as proposed by Beals (Reference D-3), Equation (D-1) can be restated as

$$\sigma_y(x;t_1)/\sigma_y(x;t_2) = (t_1/t_2)^p \qquad \text{(D-2)}$$

where $\sigma_y(x;t_1)$ and $\sigma_y(x;t_2)$ are the values of σ_y associated with the averaging times t_1 and t_2, respectively. Obviously, Equation (D-2) will not be appropriate if the averaging time is taken to be zero (i.e., for a puff). However, Equation (D-2) can be solved for an effective averaging time associated with a puff value of σ_y. Using the values reported by Turner (Reference D-2), if the puff and 10-minute plume values for σ_y for D stability are used in Equation (D-2), the effective averaging time for the puff coefficient is about 20 seconds. This result indicates that the width of a steady-state plume would not be expected to vary significantly due to meander over any given ~20 second period. (Note that the last statement would not be approporiate if made about the maximum concentration.)

Puff values of σ_y reported by Turner (Reference D-2) and Beals (Reference D-3) are given for the general stability categories stable, neutral, and unstable. If all of the puff σ_y values are assigned the same minimum averaging time of 20 seconds, the puff σ_y values for the stable category approximately correspond to F stability, and the puff σ_y values

for the unstable category approximately correspond to B stability. If the value of σ_y is parameterized as

$$\sigma_y = \delta x^{\beta} \qquad \text{(D-3)}$$

where σ_y and x are in meters, then the value of β can be approximated as being the same for the plume and puff values. (Seinfeld (Reference D-4) used $\beta = 0.894$ for the plume σ_y values.) Using the same power β, the parameterizations for plume and puff σ_y values are shown in Table D-1.

TABLE D-1. COEFFICIENT δ IN GAUSSIAN DISPERSION MODEL FOR USE IN $\sigma_y = \delta x^{\beta}$ WITH $\beta = 0.894$ AND σ_y AND x IN METERS

Averaging Time	Stability Class					
	A	B	C	D	E	F
10 min	0.443	0.324	0.216	0.141	0.105	0.071
20 s or less	0.224	0.164	0.109	0.071	0.053	0.036

In the steady downwind dispersion phase of DEGADIS, Equation (D-3) is implemented to determine the lateral dispersion parameter S_y as a function of distance. (When the central horizontally-homogeneous section disappears ($b = 0$), $\sigma_y = S_y/\sqrt{2}$.) Due to the assumed profile of the area release in DEGADIS, the initial value of S_y is zero. Downwind of the source, the growth of S_y satisfies the diffusion equation and a lateral dispersion coefficient consistent with the specification of σ_y given by Equation (D-3). The rate of growth of the effective plume half-width B_{eff} is determined by lateral gravity spreading when b is nonzero. (The value of b is actually determined by $b = B_{eff} - \sqrt{\pi}\, S_y/2$.) At some distance downwind of the source (x_t), b goes to zero, then, $B_{eff} = \sqrt{\pi}\, S_y/2$; the effective plume width is, thereafter, determined using Equation (D-3), the value of

$S_y(x_t)$, and a virtual source distance (x_v) determined from $S_y(x_t) = \sqrt{2}\ \delta\ (x_t - x_v)^{\beta}$. Since the lateral gravity spreading is treated as being independent of the plume meander, the only consideration of averaging time for the steady DEGADIS downwind dispersion phase is the appropriate choice of the constants to be used in Equation (D-3). In DEGADIS, the default value for β is 0.894; the default value for δ is chosen based on an averaging time of 20 seconds or less.

For transient releases, DEGADIS uses an observer scheme to analyze the release. (A release is considered transient when the release duration is less than the time required for the gas to travel to the position of interest. When considering the effect of averaging time, a release is also considered transient when the release duration is less than the averaging time.) A series of observers which travel with the (approximate) mean advection velocity of the gas are released upwind of the source and travel downwind. As each observer travels over the source, time averages of the pertinent source parameters are determined. With this averaged source, a steady downwind dispersion phase calculation is performed for each observer. Since the (approximate) observer velocity is known, the observer position as a function of time can then be determined, and then, concentration as a function of distance and time can be determined. For transient releases, it is necessary to average the predicted concentration over time with the integral

$$c(x,y,z,t;t_{av}) = \frac{1}{t_{av}} \int_{t-t_{av}}^{t} c(x,y,z,t)\ dt \qquad \text{(D-4)}$$

where t_{av} is the averaging time.

The following methodology is recommended for using different averaging times in DEGADIS:

(1) To account for the effect of plume meander on time-averaged concentration, the appropriate value of δ from Table D-1 should be used in the simulation whether the release can be considered steady or not.

(2) If the release cannot be considered steady due to either consideration outlined above, then the release must be simulated as a transient release and the resulting concentrations averaged as in Equation (D-4).

REFERENCES FOR APPENDIX D

D-1. Spicer, T.O., Using Different Time Averaging Periods in DEGADIS, Report to the Exxon Education Foundation, June 1987.

D-2. Turner, D.B., Workbook of Atmospheric Dispersion Estimates, USEPA 999-AP-26, U.S. Environmental Protection Agency, Washington DC, 1970.

D-3. Beals, G.A., A Guide to Local Dispersion of Air Pollutants, Air Weather Service Technical Report 214, April 1971.

D-4. Seinfeld, J.H., "Atmospheric Diffusion Theory," Advances in Chemical Engineering, 12, 1983, pp. 209-299.

D-5. Stewart, N.G., Gale, H.J., and Crooks, R. N., "The Atmospheric Diffusion of Gases Discharged from the Chimney of the Howell Reactor BEPO," Int. J. Air Poll., 1, 1958, pp. 87-102.

D-6. Cramer, H.E., "Engineering Estimates of Atmospheric Dispersal Capacity," Amer. Ind. Hyg. Assoc. J., 20, 1959, pp. 183-189.

D-7. Herman, M.N., "Estimating Long-Term Ground Level Concentrations of SO_2 from Short-Term Peak Data," JAPCA, 30, 1980, pp. 676-678.

D-8. Hino, Mikio, "Maximum Ground-Level Concentration and Sampling Time," Atmospheric Environment, 2, 1968, pp. 149-165.

(The reverse of this page is blank.)